AN ABSTRACT OF THE THESIS OF

Farroh Seifkhani for the degree of Master of Science in Electrical and Computer Engineering presented on February 8, 1991 .

Title: Investigation, Analysis and Design of the Linear Brushless Doubly-Fed Machine.

Abstract approved: _____
Alan K. Wallace

This thesis covers the efforts of the design, analysis, characteristics, and construction of a Linear Brushless Doubly-Fed Machine (LBDFM), as well as the results of the investigations and comparison with its actual prototype.

In recent years, attempts to develop new means of high-speed, efficient transportation have led to considerable world-wide interest in high-speed trains. This concern has generated interests in the linear induction motor which has been considered as one of the more appropriate propulsion systems for Super-High-Speed Trains (SHST). Research and experiments on linear induction motors are being actively pursued in a number of countries. Linear induction motors are

generally applicable for the production of motion in a straight line, eliminating the need for gears and other mechanisms for conversion of rotational motion to linear motion.

The idea of investigation and construction of the linear brushless doubly-fed motor was first propounded at Oregon State University, because of potential applications as Variable-Speed Transportation (VST) system. The perceived advantages of a LBDFM over other LIM's are significant reduction of cost and maintenance requirements.

The cost of this machine itself is expected to be similar to that of a conventional LIM. However, it is believed that the rating of the power converter required for control of the traveling magnetic wave in the air gap is a fraction of the machine rating. The constructional design of the machine is such that the primary contains two 3-phase windings. One of these 3-phase systems is connected directly to the utility grid; the second 3-phase system, with a different number of poles, is connected to a power electronic converter which has the capability of providing adjustable frequency and amplitude of voltage or current. The speed of the traveling magnetic field can be varied simply by controlling the output frequency of the power electronic converter. The design of the actual machine is such that the two

3-phase systems laid in the primary of the machine are magnetically decoupled from each other because of the difference in pole number of the two systems, (e.g. 6-pole and 2-pole for the test prototype machine in our research lab). The other degree of freedom that this machine provides, is the operation of the machine under two distinct speeds by implementing the pole change technique. This mode of operation can give only discrete changes in speed, however, it provides efficient running at those speeds with a minimum of control mechanism. On the other hand, it is anticipated that the LBDFM with two actively fed windings will produce a continuously adjustable speed over a wide range. Hence, LBDFM will be superior if it can be designed to function effectively.

Investigation, Analysis and Design of the Linear Brushless Doubly-Fed Machine

by

Farroh Seifkhani

A THESIS

submitted to

Oregon State University

in partial fulfillment of
the requirements for the
degree of

Master of Science

Completed February 8, 1991
Commencement June 1991

APPROVED:

Redacted for Privacy

Professor of Electrical and Computer Engineering in charge of major

Redacted for Privacy

Head of the Department of Electrical and Computer Engineering

Redacted for Privacy

Dean of Graduate School

Date of thesis presentation February 8, 1991

Typed by researcher for Farroh Seifkhani

ACKNOWLEDGEMENTS

I wish to acknowledge and express my gratitude to the individuals who helped the work described here possible.

Thanks to my major professor Dr. Alan K. Wallace for the great deal of valuable input he provided me, his trust in my development of this thesis, and his confidence in allowing me freedom to proceed as I thought best.

My sincere appreciation to professor Rene Spee for his guidance and his help in editing this thesis.

I would like to thank my other committee members, professor John L. Saugen and professor James Coakley for taking their time to serve on my committee.

I also would like to add a special note to thank Mike Rugh for the excellent job he did on implementing the laboratory machine windings, Charles Meitle for his great work on installation of the prototype's frame, Patrick Rochelle my old friend and office-mate for his very valuable comments and discussions on developing the

computer programs, Ashok Ramchandran and Mehdi Safavi for their help on the testing of the laboratory machine which appears in chapter 7.

Finally, I would like to thank my father Hassan, mother Mahin, for their moral support, and my lovely brother Hooshang and his great patience and support through the many lonely hours during the preparation of this thesis.

TABLE OF CONTENTS

LIST OF FIGURES

LIST OF TABLES

Investigation, Analysis and Design

of the

Linear Brushless Doubly-Fed Machine

1. INTRODUCTION

Virtually, for any rotating electric machine, there exists a linear motion version. However, there are no rotary versions for certain linear motion machine. All types of linear motion electric machines can be labeled as Linear Motion Electromagnetic Systems (LMESs), wherein the motion of one member with respect to other members of the device is horizontal and/or vertical. Generally, LME systems have found application merely to function as motors, except for few specific purposes where linear systems can be used to function as generators.

It is a general principle that the topological features of an electric machine are modified to develop a linear motion version machine from its rotary counterpart. However, the operating characteristics, as well as the design and analysis of the new machine, are subject to considerable change. Thus, because of the topological changes in the magnetic circuit of a machine, new electromagnetic phenomena play roles which cannot be expressed by conventional rotary machine theories. Consequently, established methods of analysis

have to be modified and/or new theories have to be developed. This thesis deals with some method and analysis procedures which were used to develop a physical test prototype machine in the Energy Group research laboratory at Oregon State University to observe the performance of the device. Before proceeding to the analytical discussions and design criteria, it is worthwhile to discuss briefly and understand the basic differences, advantages, and disadvantages of transforming the rotary machine to its linear version.

1.1. The Basic Differences Between Linear and Rotary Motors

A linear motor is not necessarily the best device to provide applications involving linear motions. Linear motors are still in a stage of infancy of development, even though they are approaching a century of existence. One of the reasons for this large time span between invention and development is that they have larger airgaps which results in lower efficiencies. Despite this disadvantage, it may be more reliable and quieter than its rotary counterpart when used to produce motion in a straight line. Rotary motors require gear mechanisms, and in consequence can be heavier and more expensive as an overall system. In addition, rotary drives are completely dependent on friction between the road or rail surface and the driven wheel. Linear

systems realize their thrust via a magnetic field. As a consequence, they produce controllable motion independent of climatic conditions such as ice and rain.

A linear motor can be visualized in simple terms by unrolling a rotary motor as illustrated in Figure 1.1.1. Alternatively, if we imagine

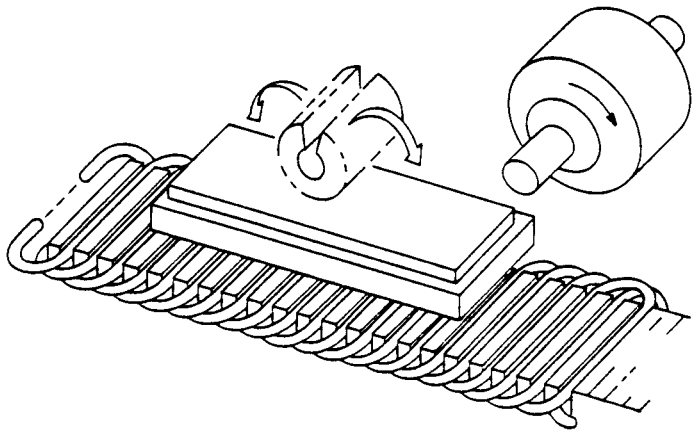

Fig. 1.1.1 Visualization of a linear machine

cutting the stator of an electric machine and flattening it from the center outward, we can envision a primary of a linear motor. If we lay a flat metallic plate on this already flattened motor, we have a linear electric motor which can be either double or single-sided. Comparing linear induction motors with their rotating versions, the linear induction motor has an open air gap with an entry end and an exit end while the rotating induction motor has a closed air gap. It is the

open-endedness of the air gap that gives rise to some unique characteristics of the linear induction motor. Other constructional features, such as large air gap length and a secondary conductive sheet, are not peculiar to the linear induction motor, but add complexity to the design and analysis. There are some rotating induction machines whose air gap is large and have a secondary conductive sheet such as the " drag-cup " servo motor. Thus, problems arising from a larger air gap and secondary conductive sheet are common both to some rotating and linear motors. Mostly, the research activities on linear induction motors has been focused on problems arising from a larger air gap or the secondary conductive sheet. More recently analyses of the problems arising from open air gap have been published including numerous articles on the problems of the end-effect which will be addressed in the ensuing chapter. This phenomena is rather complex and difficult to analyze, also, its influence in low speed applications is not significant [1-2].

2. ANALYSIS & SPECIFICATIONS OF THE LBDFM

Principally, the methods of analysis for the rotary version of the brushless doubly-fed machine, under investigation in the Department of Electrical and Computer Engineering at Oregon State University, are applicable to its linear motion counterpart. Unfortunately due to the end effect phenomenon, analysis of a Linear BDFM is much more complicated than its rotary version . In the conventional round-rotor induction motor the behavior of the machine need be calculated only over a pole pitch or a pole pair. The solution for the remaining pole pitches then simply can be obtained by using symmetry. The symmetry argument may not always be utilized for a linear machine since the poles at entrance, center, and exit are different. Therefore, a more detailed analysis may be required to appropriately describe the behavior of a linear machine. Among the numerous papers devoted to the modeling of conventional singly-fed linear induction machine, the works of Yamamura [2] and Dukowitz [3] are probably the most precise formulations because they find explicit solutions of the air gap magnetic fields for a machine with finite stator iron length in two and three dimensions using Fourier Transforms. Nevertheless, the models used have a number of limitations. First, steady-state operation with

balance sinusoidal stator currents is generally assumed. Hence, the solution cannot be readily extended to the study for a transient condition which is essential for any high horse-power applications in order be able to examine fault studies, unbalanced operation, stability analysis, and effect of non-ideal electronic power supplies. For a regular linear induction motor, transient analysis requires large number of independent equations (of the order of 40 or more) which must be solved to reasonably approach the solution. Also, "*space harmonics*" effects need to be considered. Hence, physical interpretation of the results becomes difficult.

It is necessary to point out that the LBDFM has been designed such that two distinct windings with different number of poles, p and q, are located in the primary. Consequently, the traveling waveforms due to each of the 3-phase systems have the distinct synchronous speeds of n_1 and n_2. It is assumed also that each set of 3-phase windings in the primary occupies all the slots of the primary core. Therefore, each slot of the primary core is filled with the copper of p and q windings. The amount of copper used for each set of 3-phase windings can be estimated based on the desired horsepower expected from each set. Hence, field analysis can be applied to each 3-phase

system separately. The overall mmf of the machine, therefore, can be obtained by superimposing each field distribution in the air gap, assuming that a linear relationship exists.

To briefly point out the field analysis, described in reference [1], a model of idealized linear induction motor is assumed which assumes an infinite magnetic thickness in the secondary.

2.1 Field Analysis

Figure 2.1.1 presents the primary in region 1, the air gap in region 2, and the infinite thick secondary in region 3. In practice, the

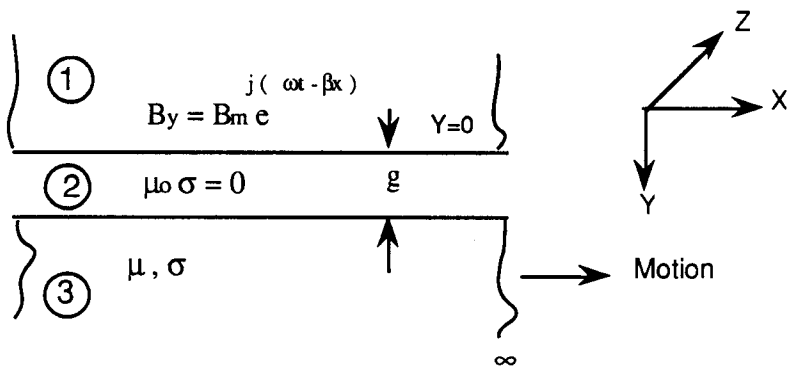

Fig. 2.1.1 Presentation of primary, airgap, and secondary.

excitation windings are located in the slotted primary structure. For

analysis, the structure is assumed to be smooth in order to allow the representation of the machine excitation to be made as a current sheet of negligible thickness and finite width. A few assumptions are made to simplify the analysis. First, source voltage or current varies sinusoidally with time and the ideal distribution of the primary winding assumes a sinusoidal distribution of the fields. Second, variations in the Z direction are ignored and as all currents are assumed to flow in the Z direction, the field problem reduces to a two dimensional one. Third, both primary and secondary are made of laminated iron to ensure that conductivity in the z direction is negligible. With all these assumptions and the use of Maxwell's equations, the time-average value of the thrust can be given as [1] :

$$F_x = \frac{\sigma B_m^2 s n_s \lambda L}{4 |\Delta|^2 Re(\alpha)} \qquad (2.1)$$

where;

σ = Conductivity of the secondary.

B_m = Maximum air gap flux density.

s = Slip.

n_S = Synchronous speed.

λ = Twice the pole pitch (or wave length).

$\Delta = \cosh \beta g + (\alpha \mu_0 / \beta \mu) \sinh \beta g.$

g = Air gap length.

$\alpha^2 = \beta^2 + j\, s\, \omega \mu_0 \sigma.$

Re = Real part of.

L = Width of the primary.

ω = Input frequency.

$\beta = 2\pi / \lambda = \pi / \tau.$

τ = pole pitch.

It was pointed out that sinusoidal space distribution of the windings, resulting in a sinusoidally varying air gap field, is ideal and desirable. However, in actuality, especially in linear machines, such a sinusoidal distribution of the windings cannot be achieved. As a consequence, the produced magnetomotive force (mmf) of the windings has harmonics. Generally, the only fundamental of this distribution is considered as the source of the air gap field shown in Figure 2.1.2. The amplitude of the current sheet, J_m, can be found from the relationship :

J_m=(Maximum total current along machine periphery)/

(Length of machine x Total winding factor)

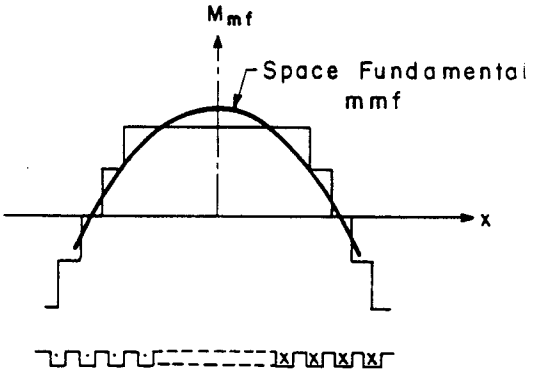

Figure 2.1.2 The fundamental of the mmf.

The winding factor comes into consideration due to the deviation from a sinusoidal distribution harmonics and slots. Therefore, the expression can be written as follows:

$$J_m = \frac{m\,(2\,T_{ph}\sqrt{2}\,I)}{2\,p\,\tau}\,K_w = \frac{\sqrt{2}\,m\,T_{ph}\,I\,K_w}{p\,\tau} \quad A/m$$

where:

m = Number of phases.

2 p τ= Length of the machine.

p= Number of pole pairs.

τ= pole pitch.

T_{ph} = Number of turns per phase.

$\sqrt{2}$ I= Maximum phase current.

k_w= Total winding factor.

2.2 Selected Design Considerations

A linear BDFM has certain topological and operational differences from its rotary counterpart which are due to the presence of the large air gap, end-effects, and normal forces. Each of the mentioned phenomena has its own particular influence on the behavior of the machine which can be described separately.

Influence of Large Air Gap:

In most linear machines, the mechanical air gap or clearance, g_m, ranges from 2 to 15 mm. Large air gaps lead to a relatively large air gap leakage reactance. In such a case, the field equations require a correction factor k_1 obtained from [1] & [4], such that :

$$K_1 = \frac{\sinh\left(\pi \frac{g_o}{\tau}\right)}{\pi \frac{g_o}{\tau}}$$

where:

$g_o = g_m + d.$

d = secondary plate thickness ~ 2 to 6 mm.

τ = Pole pitch.

Hence, the effective air gap, g_e, becomes :

$$g_e = k_1 g_o$$

End Effect

There are static and dynamic end effects. Static end effects are due to the open air gap of the magnetic circuit in linear machines. As a result, the self and mutual inductances of the primary phases are not symmetrical. However, the difference may be negligible especially when the number of poles is large. The dynamic end effects are caused by the relative motion of the short primary with respect to the secondary or vice versa . It has been shown in reference [4] that the air gap field for linear induction motor, has the form of :

$$H_x = C_1 \ e^{\gamma_1(x-2p\tau)} + C_2 \ e^{\gamma_2 x} + C_3 \ e^{-j(\pi x/\tau)} \qquad (2.2)$$

The air gap flux density given by equation (2.2) has 3 components or three traveling waves. The first one is the conventional unattenuated traveling forward wave with the pole pitch τ and speed $n_s = 2\pi f$. The other two attenuated traveling waves represent the end-effects and move back and forward, having the pole pitch $\tau_e = \pi/\gamma_i$ and speed $n_e=2\tau_e f_1$. The backward end-effect wave attenuates more quickly than the forward end-effect wave. Thus, only the forward end-effect wave

generally need be considered. If end-effects are negligible, modified versions of the formulas developed to the rotary version of the BDFM can be used to obtain the equivalent circuit of the linear BDFM and its parameters.

2.3 Primary Requirements of the LBDFM

The primary of the LBDFM is made of a laminated core with open slots. The variation in stator core design, however, does indeed affect the performance of the LBDFM. For example, for a constant volume of copper in the slot, a machine with narrower teeth generates more thrust and has better efficiency and higher power factor than does a machine with wider teeth. This is due to the fact that a machine with narrower teeth has lower primary and secondary leakage inductances, resulting in a smaller secondary time constant. The smaller secondary time constant, the smaller magnitude of the end-effect traveling wave will be [1]. This leads to larger output power and higher efficiency.

As was pointed out in a previous chapter, the LBDFM is basically an extension of the linear induction motor and its design and development are of those for the LIM. However, the complication of

this device is due to the presence of two sets of three phase systems with different number of poles in the primary. The more specific details about the design of the primary, winding layout, and execution of the two sets of 3-phase windings will be addressed in the ensuing chapter.

To summarize the effects of the primary of the LBDFM on the overall performance of the machine, another design criterion known as the "Goodness Factor" [4] can be defined in order to have a better tool for the primary design.

It has been found in most papers that the goodness factor is a convenient measure for assessing the quality of a linear machine. The goodness factor is related to the real part of the air gap field, B_y , and denotes the active component or the force-producing component. Using the mathematical proof for explaining this factor in Ref. [1], the fundamental definition of the goodness factor for the secondary in terms of magnetizing reactance is defined as:

$$G = X_m / R_2$$

where X_m is the magnetizing reactance and R_2 is the secondary resistance. The goodness factor is a useful tool in the preliminary

design of linear induction motor. The importance of this factor comes into consideration when the design of the machine is underway. The design of the machine should meet the required performance standards at minimum cost. For the laboratory prototype expense is not a criterion of design since this model is merely experimental. The goodness factor relates the ability of a machine to convert power from one form to another: it specifically relates the power conversion from the electric circuit to the magnetic circuit. Both X_m and R_2 are machine parameters that can be calculated, permitting G to be evaluated before any performance calculations are carried out. Thus, the criteria of large goodness factor and small input power per unit of output thrust may be used to asses the design. Other parameters such as starting force and starting current, running force and running current, efficiency, power factor, tooth flux density, primary and secondary leakage reactances, exit-end power loss, and eventually the ratio of magnetizing current to the load component of primary current must meet given requirements as well.

Therefore, to optimize the design of the machine, certain parameters could be varied to achieve a good design. Enhancing the goodness factor in low-speed applications is a satisfactory criterion to

obtain a high efficiency. Conversely, in high-speed applications due to end-effects, efficiency will be lower if the G increases. In such a case, the optimum goodness factor, G_0, can be defined in which the total thrust is zero at zero slip, meaning that if the thrust, F_x, in the presence of exit-end effect wave is zero at slip=0, the G_0 is optimum. This situation requires that at G_0, F_x=0 @ s=0. The plot depicted in Figure 2.3.1, indicates variation of G_0 vs number of poles in the primary for design purpose. A reasonable range to select G_0 for the

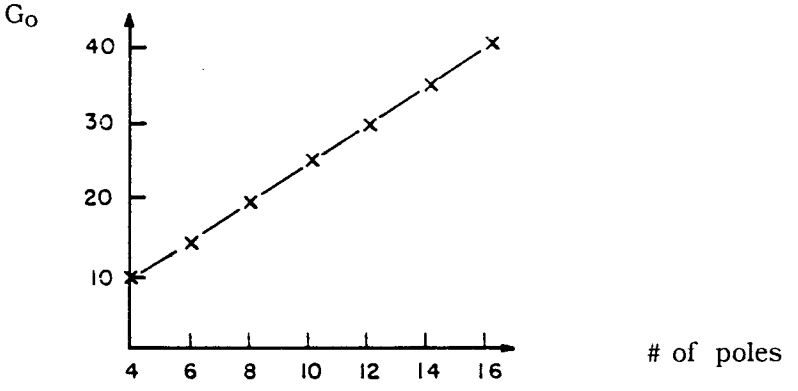

Figure 2.3.1 G_0 vs number of poles

initial design is: $1.6 < S_r G_0 < 2.0$ where S_r = rated slip [1]. Therefore, it can be concluded that the effect of the primary parameter variations are as follows:

a) Increasing the air gap results in a larger magnetizing current and

larger exit-end loss. Conversely, decreasing the air gap leads to an increase in the goodness factor, output force, and efficiency.

b) Increasing the number of poles yields smaller end-effects, and decreasing the number of poles causes larger secondary leakage reactance.

c) An increase in pole pitch (τ) results in a smaller goodness factor, while a decrease in τ leads to a larger number of poles.

d) Increasing the tooth width of the primary core (w) and thus decreasing gap between teeth, results in a larger primary leakage reactance and decrease in w leads to a large output force and large efficiency.

2.4. Secondary Requirements

In general, the secondary of a linear induction motor may be constructed of an aluminum or copper sheet with or without a solid back iron plate. In the LBDFM , however, the fluxes produced by each of the 3-phase windings of the flat stator, with different number of poles, increase the complexity of the secondary design compared to the conventional ladder or solid sheet. In the doubly-fed mode of operation, from a consideration of the flux interaction of the two

primary windings with different number of poles, a secondary design requires an special configuration to be implemented. The primary of the LBDFM contains a power winding with 2p poles and is fed from a power grid of f_6 (60 HZ) frequency. The control winding with 2q pole number is fed from a power electronic converter with adjustable frequency f_2 . Since the windings in the primary are designed with different number of poles, there is no direct coupling between these two systems. As a consequence of the primary configuration, an observer sitting on the side of the primary, would see two traveling fields with the speeds of n_p and n_q meter per second in opposite directions. Each of these two traveling fields induce currents in the secondary. The corresponding secondary fields that result can then interact with the other primary system. For these conditions to be satisfied, secondary circuits must form both 2p and 2q fields of the primary [5-6-7]. Likewise, the secondary must be capable of handling currents of shifted phases. If it is assumed that the current of merely one frequency, f_s, exists in the secondary (the so-called "synchronism condition"), the following equations can be derived [8]:

$$f_r/p = f_6/p - n_r$$

and:

$$f_r/q = f_2/q - n_r$$

hence;

$$n_r = (f_6 - f_2) / (p + q)$$

A design to satisfy the stated criteria was first developed for the rotary BDFM by Broadway [6]. He proposed the rotor to be constructed in four identical nests shown in Figure 2.4.1, to assure the synchronous

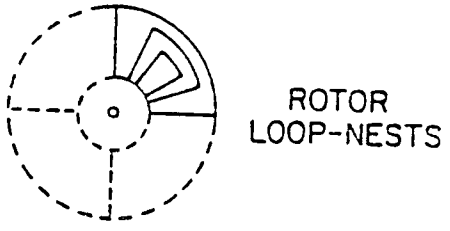

Fig. 2.4.1 Rotor configuration of the rotary BDFM

performance of the machine. Further investigations on the rotor configuration of the rotary BDFM has been conducted by Wallace [9] to optimize the configuration of the rotor. The simulation program used for that study investigates the current and torque distribution in each loop and bar of the nested rotor for the best possible efficiency and economical rotor design of the rotary BDFM.

In order to react with a combined field produced by the primaries of the machine and to minimize harmonic effects, the secondary of the

LBDFM shall be constructed such that nested loops of conductors exist between the shorted edge bars. This pattern can be repeated along the secondary in applications where the primary of the LBDFM is the moving part and secondary is the stationary track. Figure 2.4.2 illustrates such a design for the secondary of the LBDFM. This results

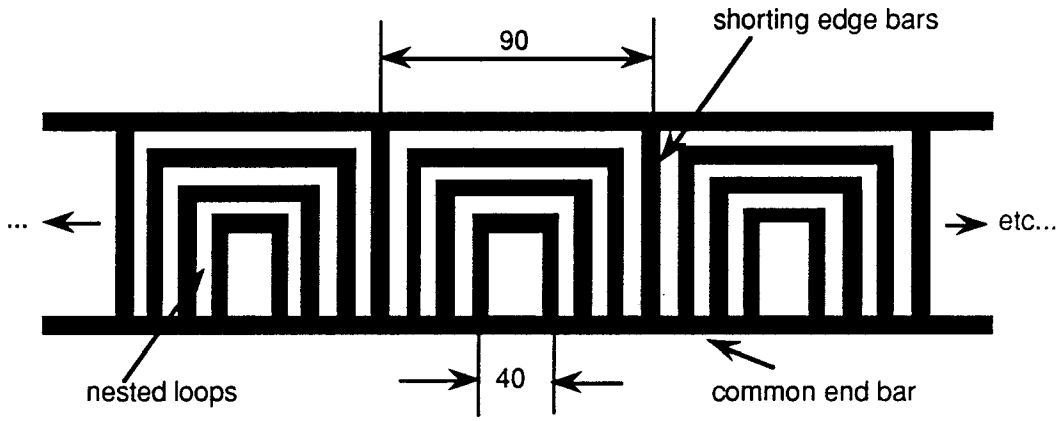

Fig. 2.4.2 Secondary configuration of the LBDFM

in a configuration for the secondary with a number of repeatable poles or sections equal to the mean of the pitch of the primary poles produced by the two system connections. The figure shows that for each section, there are two shorted bars which are 90° apart for a primary system of p=3 and q=1. This distance corresponds to one segment of the physical length of the primary. It can be realized that for a whole length of the primary, 4 corresponding sections with

shorted nests shown in Fig. 2.4.2, exist in the secondary, and this pattern of the construction is repeated along the path of the track, assuming that the primary is the moving segment and the secondary as a reaction rail, is fastened to the ground.

This special design for the secondary of the LBDFM restricts the paths of the AC currents induced in the secondary conductors. The induced currents set up an multi-pole field which is in motion relative to the secondary. The large magnitude of cumbersome harmonics also affects the performance of the machine. It is shown in [6-8] that an increase in the secondary bars decreases referred leakage reactance significantly. In this arrangement of secondary construction, it can be found that the secondary-current distribution approaches the ideal composite sinusoidal waveforms of 2p and 2q poles with increasing load in the doubly-fed mode of operation.

In general, the form of secondary described in this section is clearly best suited to close-ratio pole combinations of the primary [6]. For pole numbers which are widely apart, the chording factors of the short circuited bars in each nest would be small with respect to at least one of the pole numbers and would adversely affect the overall performance of the machine.

For propulsion system applications it is economically more appropriate to design the system with primaries in the vehicle fleet and secondary along the track [11]. The cost of such system is considerably lower than installation of the primaries along the track and one or two segments of secondary in the vehicle. Wallace [11], has proposed and investigated a number of electromagnetic configurations for the secondary of the linear induction motor in transit systems. Based on the order of complexity and cost, these configurations are listed as follows:

a) Solid-sheet steel,

b) 12 mm sheet steel with extruded aluminum top cap,

c) 24 mm sheet steel with extruded aluminum top cap,

d) Laminated steel with extruded aluminum top cap,

e) Laminated steel with aluminum cage,

f) laminated steel with copper cage.

Although case (a) may be applicable for certain limited applications, it has been found that it is not considered in detail for intermediate capacity transit system due to the flexibility required of the propulsion system. Combination of stand still and full dynamic test indicated that improvement in thrust production were achieved for a given primary current for configuration (c) as zero percent, (d) 30%, (e) 22%, and finally (f) 35%.

For secondary design of the LBDFM for transit propulsion applications, depending on the requirements for the different vehicle operating conditions and different guide way alignment scenarios, the use of different back irons, different top-cap resistances, and different clearances are all applicable solutions in the development of the economically optimized reaction rail systems.

3. DESIGN, ESTIMATION & CONSTRUCTION OF THE PROTOTYPE

This chapter covers the design efforts for the laboratory prototype machine. It is the intention to test the prototype linear BDFM in both singly-fed (induction) and doubly-fed (synchronous) modes whereas, only the synchronous mode would constitute "normal" operation. The design of the machine must take this into account. The machine operating in a singly-fed mode is only operating in the induction mode similar to a regular linear induction motor. The objective of this design is such that two primary windings with the pole numbers of 6 and 2 , are separately placed in the primary core to meet the above interests. As far as the synchronous mode of operation is concerned, however, the doubly-fed excitation with the same frequency in each source facilitates the machine to be at stand-still in the synchronous mode. In this mode, the velocity of the secondary is locked to the waveform frequencies of the currents which are fed into the two sets of primary windings. Both windings of the primary are designed based on 230 volt line to line voltage. The machine can also be operated in either *wye* or *delta* connection as desired.

3.1 Windings layout

The primary core of the LBDFM consists of a rectangular block of slotted structures, shown in Figure 4.1.1, built from a stack of steel laminations. Within the slots of the primary block two 3-phase windings are laid to produce the linearly traveling magnetic fields. Many winding configurations were examined during the course of the design for LBDFM along with the advantages and disadvantages of those winding topologies. The considerations are related to manufacturing costs, capacity for producing air gap field distribution approaching a purely forward traveling wave, and availability of the materials in our facilities for the test machine prototype. The following topologies were considered :

1. Independent single-layer windings for each of the 2-pole and 6-pole systems.
2. Independent double layer windings for each system.
3. Integrated winding for both 2-pole and 6-pole systems.

The design for all above topologies are completely valid for construction of the LBDFM with 2-pole and 6-pole. For option 2, the disadvantages are physical complexity and possibly a heavier core for the same power ratings, and need for greater number of empty slots. The main advantage for this option, however, is reduction of spacial

harmonics by a significant percentage compared with the single layer winding option. Option 3 was rejected due to a greater number of required slots (in this case 45 slots), in the primary of the lab prototype machine to implement the 2-pole and 6-pole integrated winding. The number of available slots on the primary of the available laminations is 40. The need for the larger number of slots makes the iron core heavier and increases end-effect phenomenon. The advantages of implementation of the single windings for 2-pole and 6-pole are the ability to utilize the volume of each slot better, increase in the conductor area laid in each slot of the primary winding, hence reduction in copper losses and higher efficiency, and decrease in leakage reactances which results in higher thrust production. It is worthwhile to point out that a single integrated winding may produce more phase harmonics than two separated windings [16]. Moreover, nature of the connection produces circulating currents which cause the distortion of the mmf and heating of the windings [10].

In consideration of all the above mentioned advantages and disadvantages of proposed topologies, option 1 was approved for construction of the LBDFM laboratory prototype machine. Figures 3.2.1 and 3.2.2 show the independent winding layouts designed for the

3-phase 2-pole and 6-pole, respectively. The primary of the LBDFM is wound with all twelve terminals of the two three phase systems brought out so that they may be energized independently for testing purposes and may be connected either in *delta* or *wye* .

The laminations obtained for this study have 40 slots of which 36 slots were used for the designed winding configurations of 6-pole and 2-pole. The 2-pole winding is located in the bottom of the slot and the 6-pole winding is placed on the top of the 2-pole winding. As is seen from Figures 3.1.1 and 3.1.2, both 2-pole and 6-pole windings occupy 36 slots. Thus half of the slot space is allocated to each of the 3-phase systems. It can be observed from the figures that each of the 3-phase systems of 2-pole and 6-pole winding contains 18 coil groups with equal pitch to establish the 2-pole and 6-pole connections with separated windings. The arrows on the figures indicate the windings orientation in the primary slots. In the figures the resulting pole structure of all phases are indicated. The pole pitch for the 2-pole system is 18 slots which has the advantage of drawing less magnetizing current than 6-pole due to the larger phase impedance. The estimation and calculation presented in the ensuing chapters of this thesis, have led to design each coil of the required 18 coils of

6-pole with 50 turns and 2-pole with 20 turns. The number of winding turns ought to be selected by calculations based on the geometry of the machine to assure an adequate level of flux in the air gap. The greater number of turns causes a reduction of the air gap flux under voltage limited conditions. A sufficient level of air gap flux is needed to produce the adequate starting thrust since the magnetizing current of the machine, in general, is proportional to $V_S/(f_S \cdot T_{ph}^2)$ with V_S the supply voltage, f_S the supply frequency, and T_{ph} the number of turns.

The produced mmf waveforms for each phase of both the 6-pole and 2-pole 3-phase system obtained using a computer program, are presented in Figures 3.1.3 through 3.1.8. The resultant 3-phase mmf of doubly-fed connection where both 2-pole and 6-pole are directly fed is illustrated in Figure 3.1.9. The combination of the 3-phases has the effect of smoothing the steps in the mmf wave forms as shown. The mmf wave forms on the figure also clearly confirm the 6-pole and 2-pole structure of the two 3-phase set of windings. Finally, the overall mmf of the LBDFM in the doubly-fed mode of operation was obtained by superimposing the mmf's of the 2-pole and 6-pole which is shown in Figure 3.1.10.

Layout specifications of the 2-pole System:

S = 36 " Total number of utilized slots in the primary "

2p = 2 " Number of poles "

y = S/2p ==> y = 36/2 = 18 " Width of each pole in terms of slot pitch "

m = 3 " Number of phases "

q = y/m ==> q = 18/3 = 6 " Number of slots per pole per phase "

α_{ez} = 360 p/S = 360/36 = 10° " Electrical degree of each slot "

Beginning of each phase in terms of slot number :

Phase A --------> 1

Phase B --------> 1 + 120/α_{ez} =13

Phase C --------> 1 + 240/α_{ez} = 25

Convention :

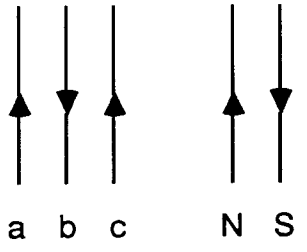

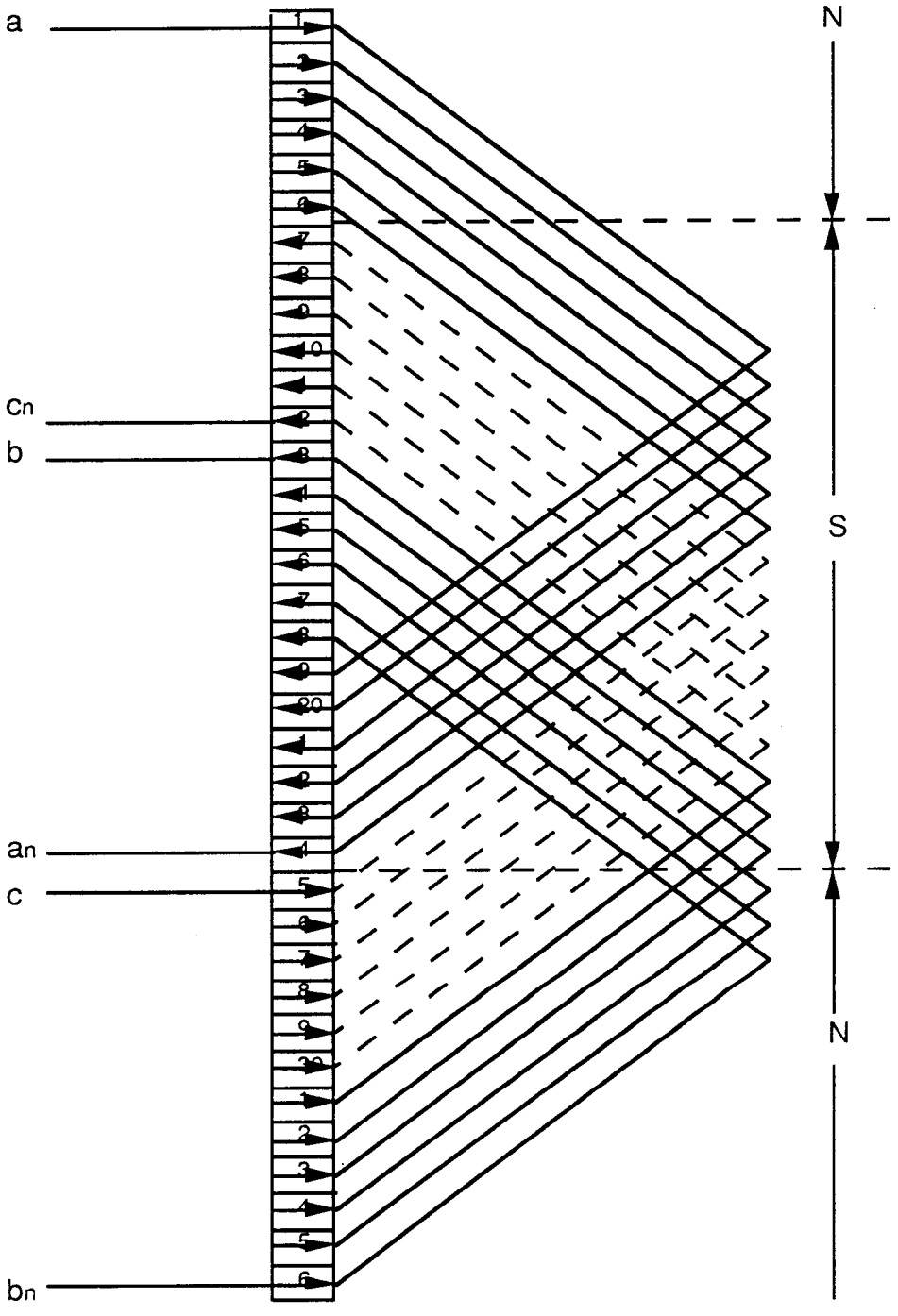

Fig. 3.1.1 Winding layout of the 2-pole system

Layout Specifications of the 6-pole system:

S = 36 " Number of utilized slots in the primary "

2p = 6 " Number of phases "

y = S/2p ==> y = 36/6 = 6 " Pole pitch, coil span"

m = 3 " Number of phases "

q = y/m ==> q = 6/3 = 2 " Number of slots per pole per phase "

α_{ez} = 360p/S ==> α_{ez} = (360)(3)/36 = 30° " Electrical degree of each slot "

Beginning of each phase in terms of slot number :

A -------> 1

B -------> 1 + 120/α_{ez} = 5

C -------> 1 + 240/α_{ez} = 9

Convention :

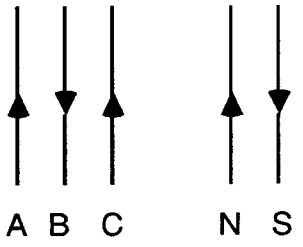

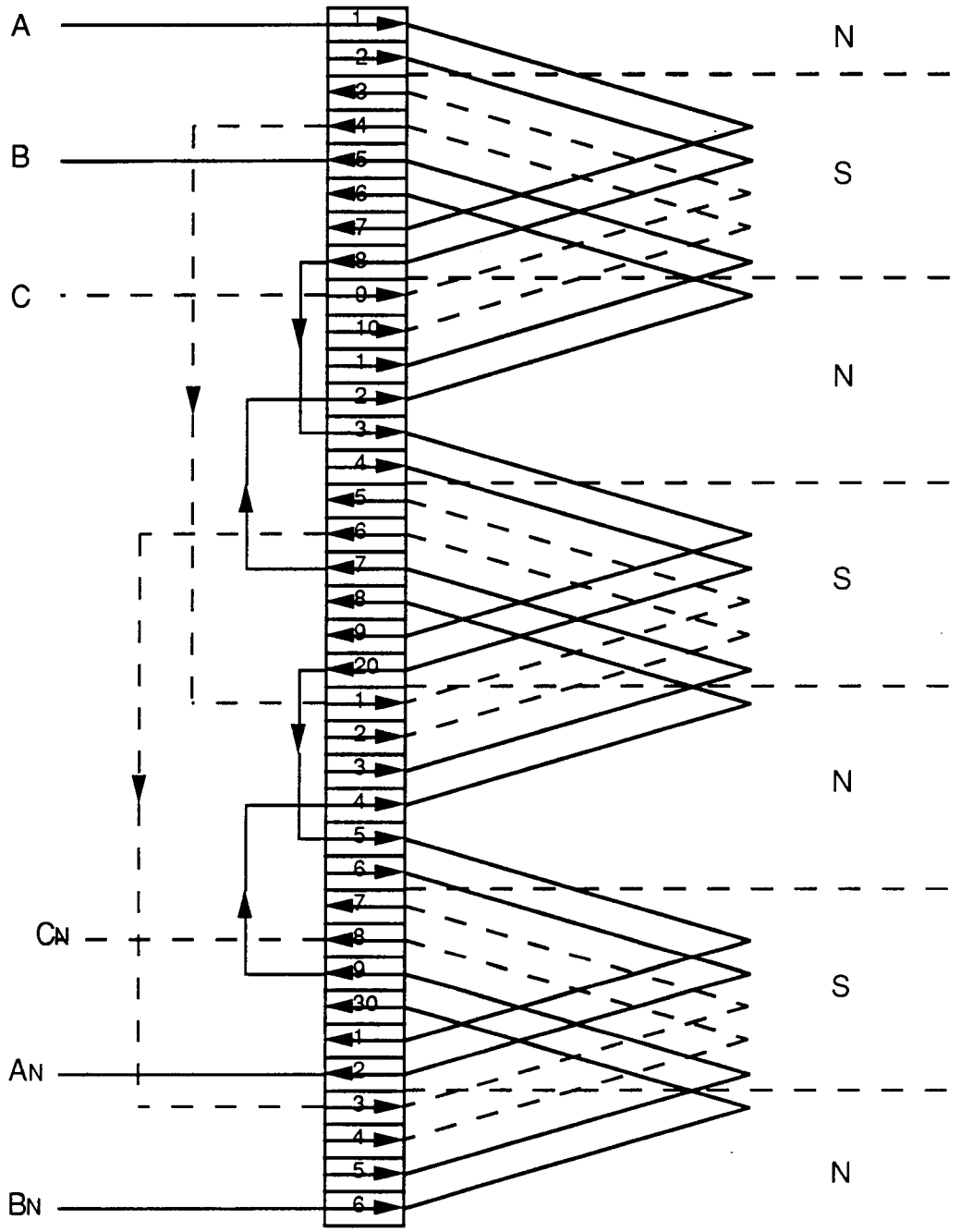

Fig. 3.1.2 Winding layout of the 6-pole system

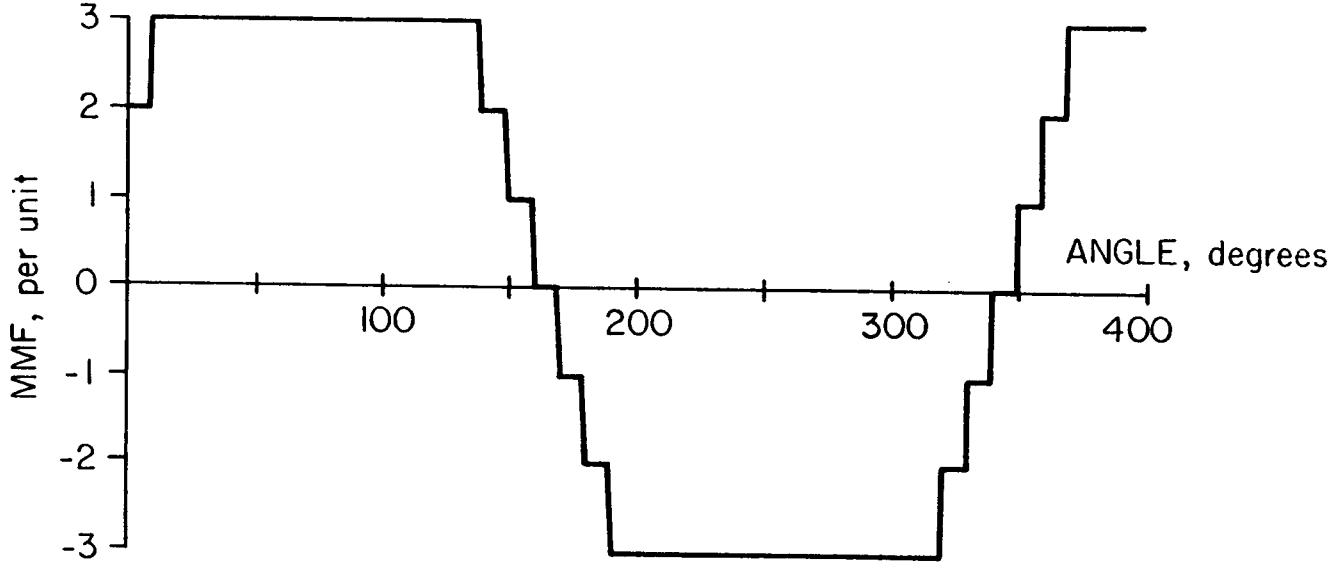

Fig. 3.1.3 Phase "a" mmf of the 2-pole

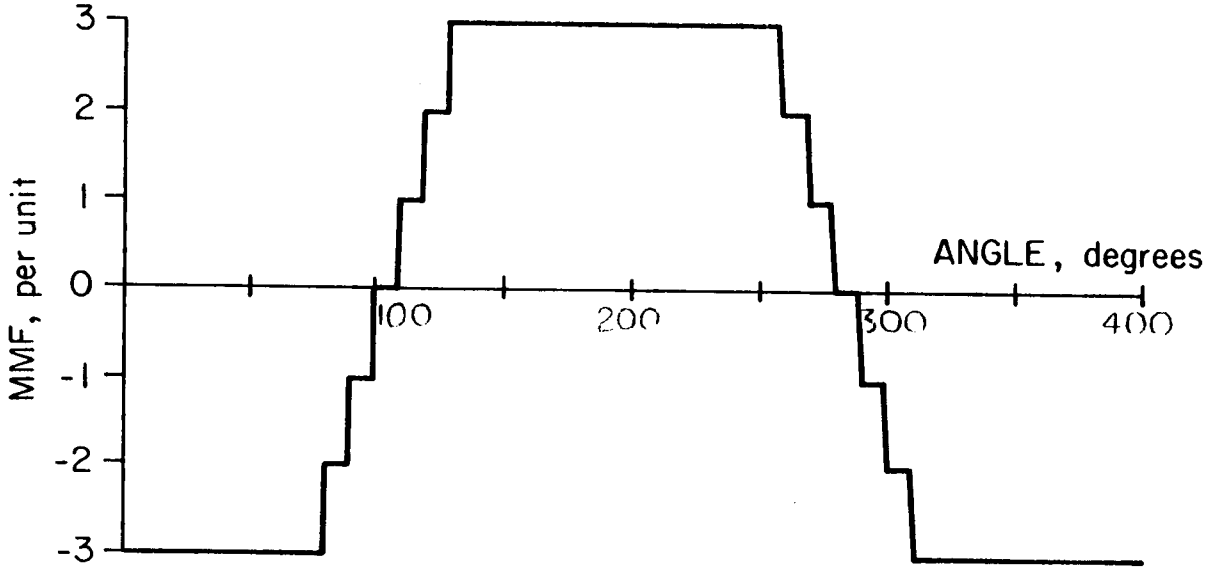

Fig. 3.1.4 Phase "b" mmf of the 2-pole

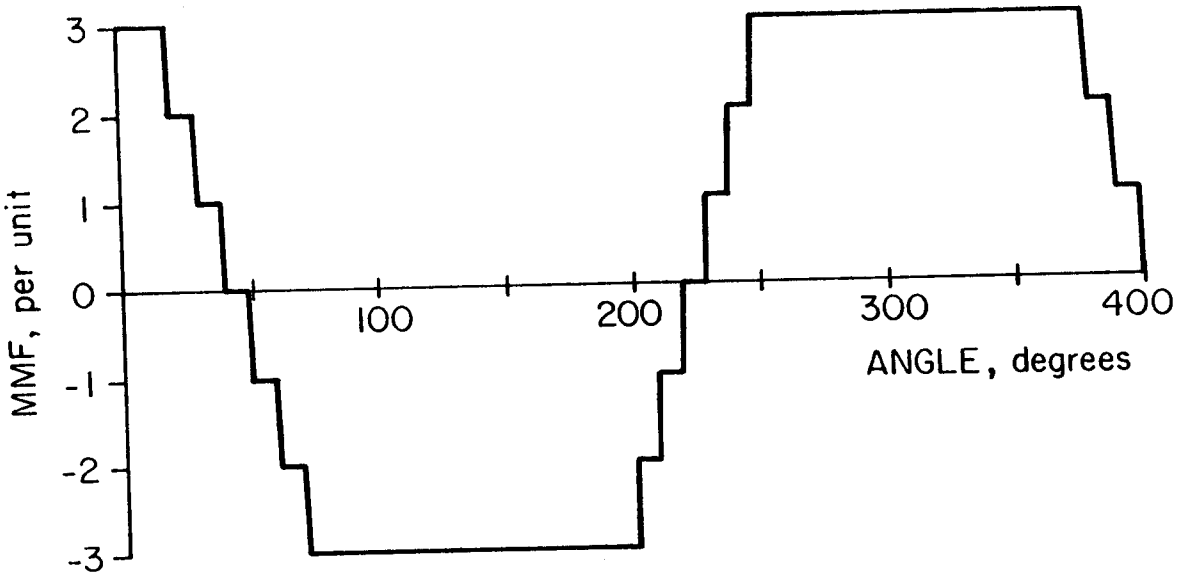

Fig. 3.1.5 Phase "c" mmf of the 2-pole

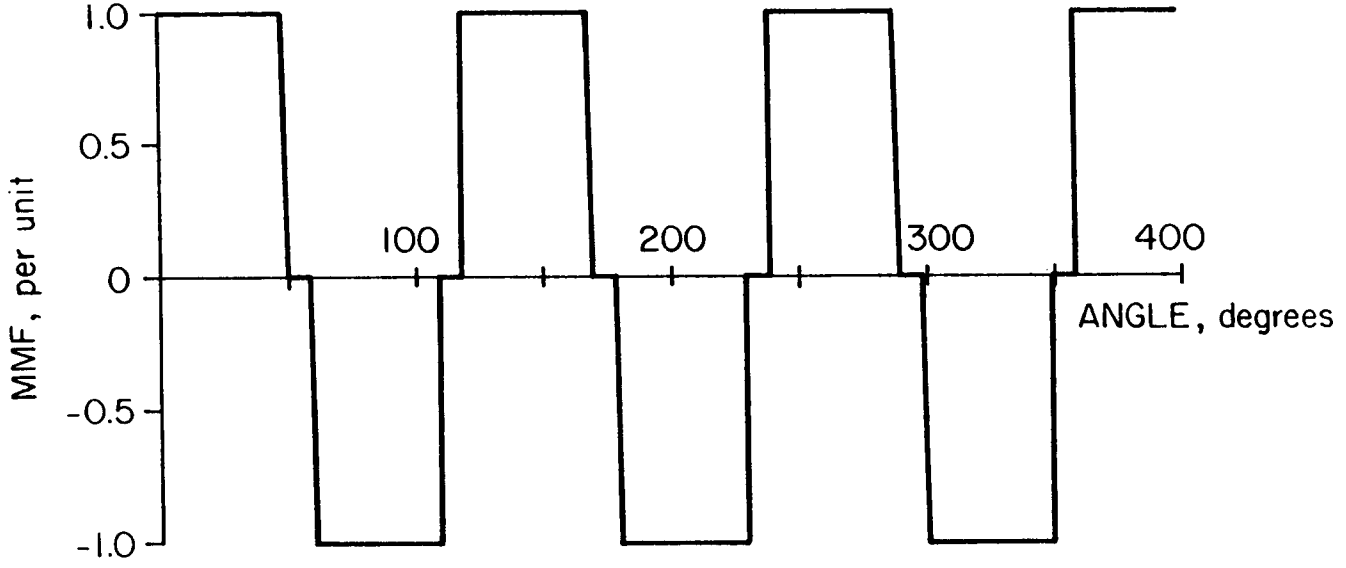

Fig. 3.1.6 Phase "A" mmf of the 6-pole

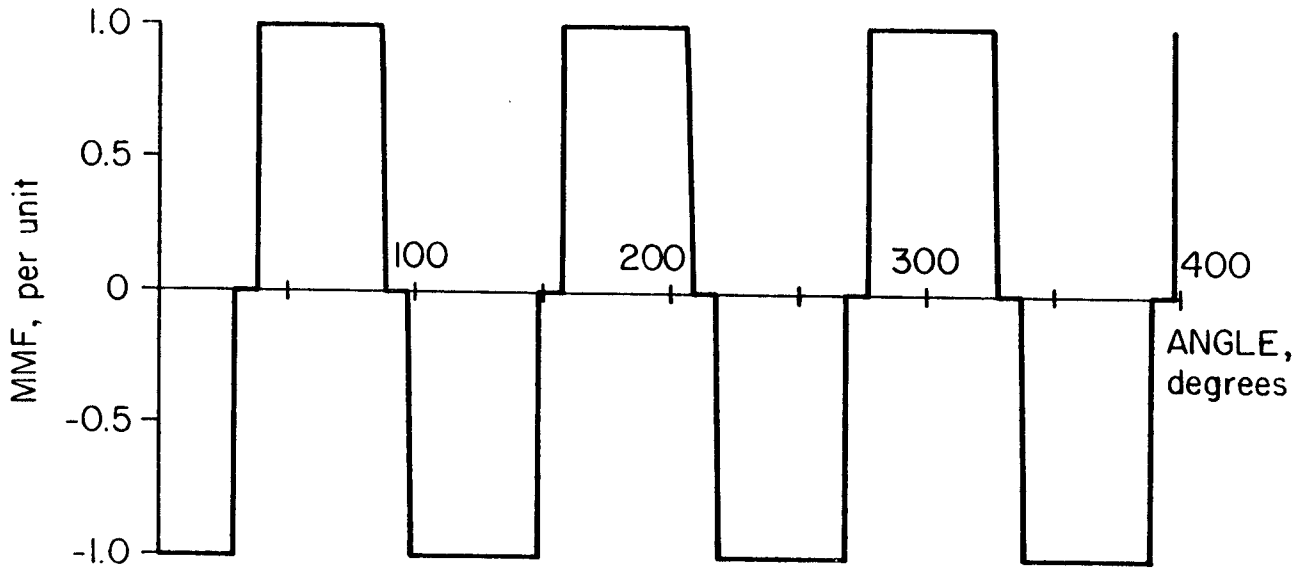

Fig. 3.1.7 Phase "B" mmf of the 6-pole

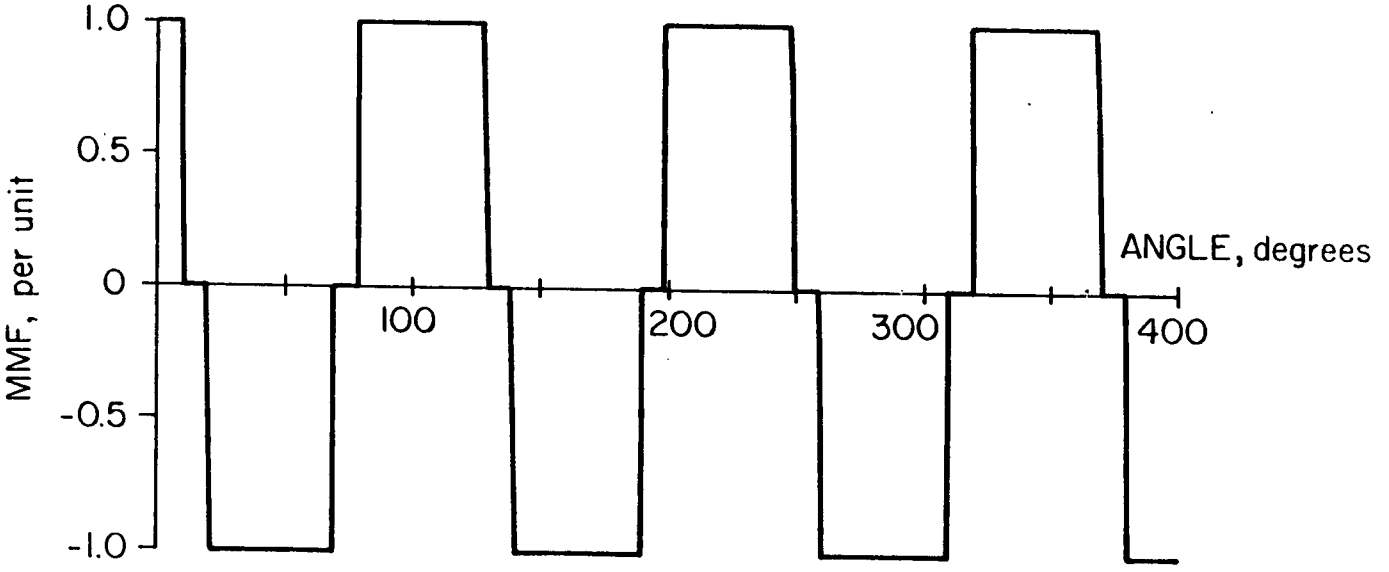

Fig. 3.1.8 Phase "C" mmf of the 6-pole

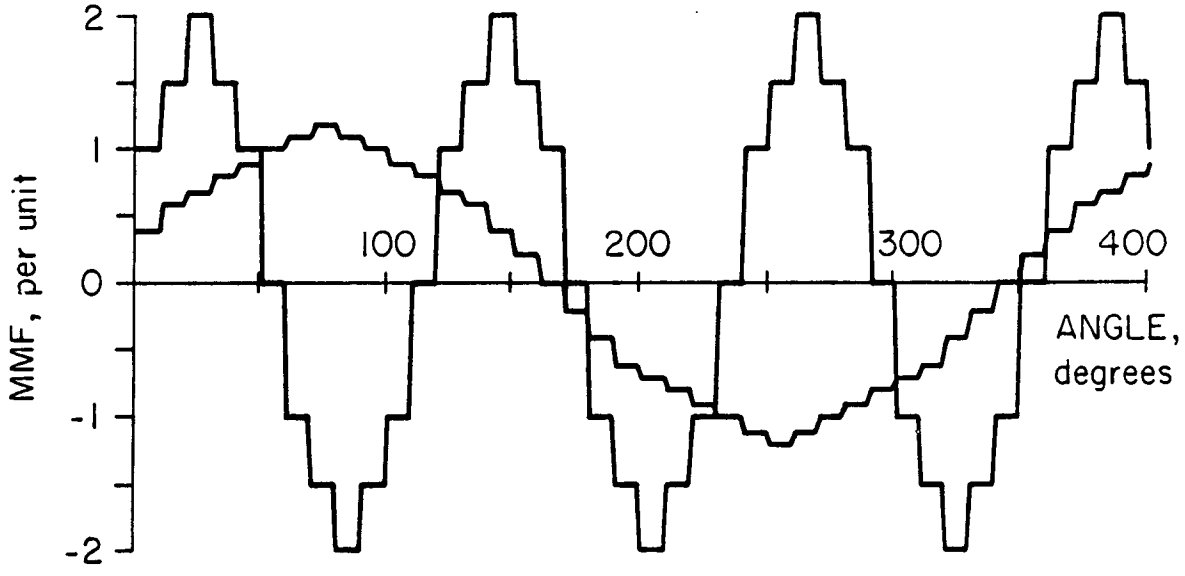

Fig. 3.1.9 Three-phase 2-pole & 6-pole mmf's

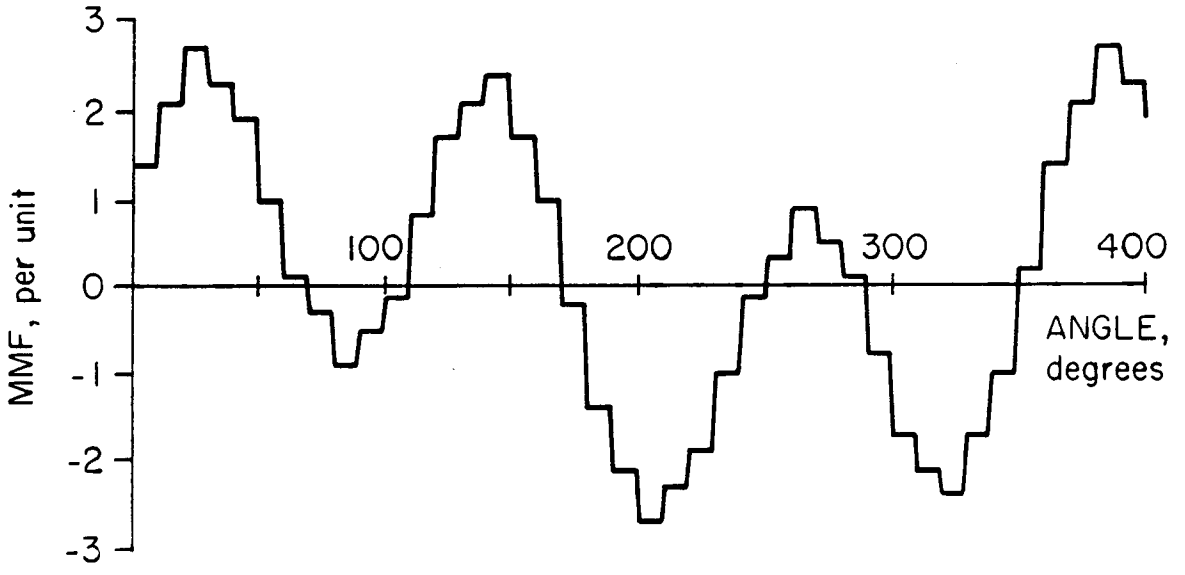

Fig. 3.1.10 Overall mmf of the LBDFM

3.2 Construction of the LBDFM Secondary

In order to practically obtain the characteristics and performance of the LBDFM, an adequate secondary must be constructed. The LBDFM is considered as having a primary with 2 sets of 3-phase windings with 2p and 2q poles. As a result of the primary design and nature, there would be two traveling magnetic fields in the air gap with diverse velocities. This nature of the primary requires a secondary with some complexity in its design and construction. In other words, the secondary must appear to form both 2p and 2q pole patterns and be capable of supporting currents of displaced phases. It is required that in the synchronous mode of LBDFM operation, a current of only one frequency (f_s) exists in the secondary which can be found from:

$$f_s=(f_p- f_q)/(p+q)$$

This expression comes from the fact that combined current distribution in the secondary is shaped by p/2 and q/2 current distribution with merely one frequency. However, the shape of the overall current distribution in the secondary has more harmonic distortion which is unavoidable with finite numbers of conductors.

A recent investigation for rotor modeling and development of the rotary BDFM [9], has suggested several alternatives for rotor configurations. A simulation model has been used to identify the optimal design which would meet the highest torque production and efficiency for the rotary BDFM. The computed analysis for different alternatives indicates that the most effective bars are located close to 60° of each segment of the secondary. Bars at 40° or less contribute so little and common bars located at 90° don't have significant contribution for thrust production. Using this principle, the secondary of the LBDFM was designed and built during the course of the investigation as illustrated in Figure 3.2.1. The figure shows two long aluminum bars, which are the equivalent of rotor end rings, are located at each side of a back-iron (magnetic circuit) along the track. Each section of the secondary which corresponds to 90 degree of the fundamental 2-pole geometry has 2 shorted bars which are connected to both end bars. The 90 degree division of the secondary construction is equivalent to the actual physical length of each ideal quarter of the primary of the machine. In other words, there are four 90 degree divisions in each segment of the secondary to cover the whole segment of the primary. Between the shorted bars, there are three nested loops all of which are connected to one side of the track bar or

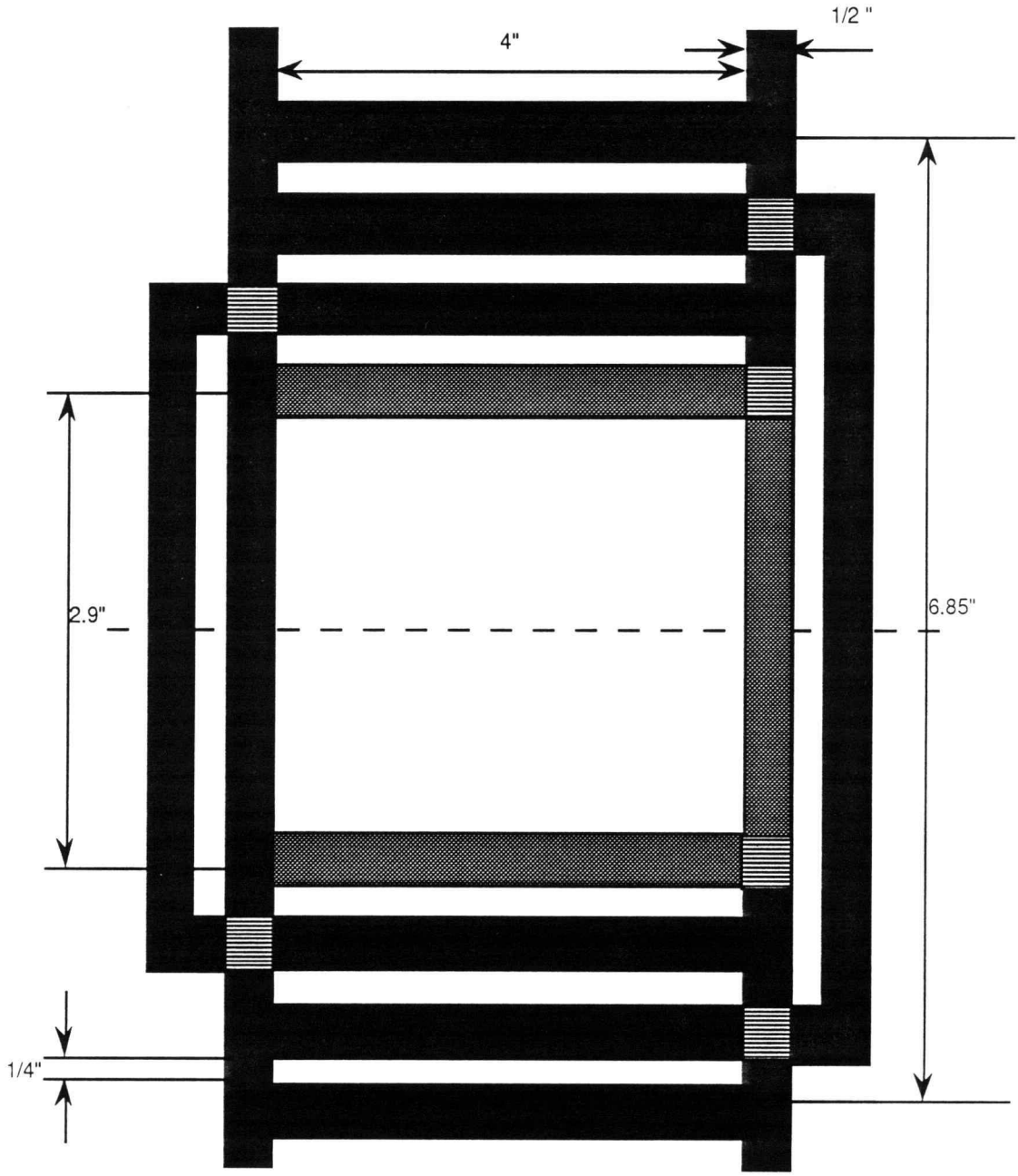

Fig. 3.2.1 Secondary of the prototype machine

end bar. As it is indicated in the figure, two arms of the smallest nest are 40° apart which is equivalent to 2.90 inch of the actual physical length of the secondary.

The width of the track is such that the primary of the machine can cover the effective arms of the nested loops. Therefore, the flux produced in the air gap would easily cross the arms of the nested loops and induce current in the secondary. For the testing purposes the overall length of the secondary is made twice as great as the primary length. Therefore, a total of eight sections or divisions similar to what is shown in Figure 3.2.1 is constructed along the track of the secondary.

To conclude the secondary design and construction of the Linear BDFM, following considerations need to be taken into account.

a. Unlike a conventional linear induction motor, the bars in the secondary of the LBDFM shall not be placed homogeneously along the track.

b. Nested loops located in each division of the secondary and are apart less than 30° don't contribute to the thrust production and can be eliminated.

c. Secondary loops that are closest in span to 60° are the most and effective efficient in terms of force production and overall efficiency.

d. Shorted outer bars of each division of the secondary which are 90° apart are insignificant at low 2-pole frequency, but increase substantially with frequency rise.

The total length of the secondary track for the laboratory prototype LBDFM is 60 inch. This contains eight repeatable sections of nested loops and shorted bars made of aluminum on top of an inverted steel channel. This secondary configuration was built according to these design considerations. Figures 3.2.2 and 3.2.3 show the photographs of the wound primary and secondary, respectively.

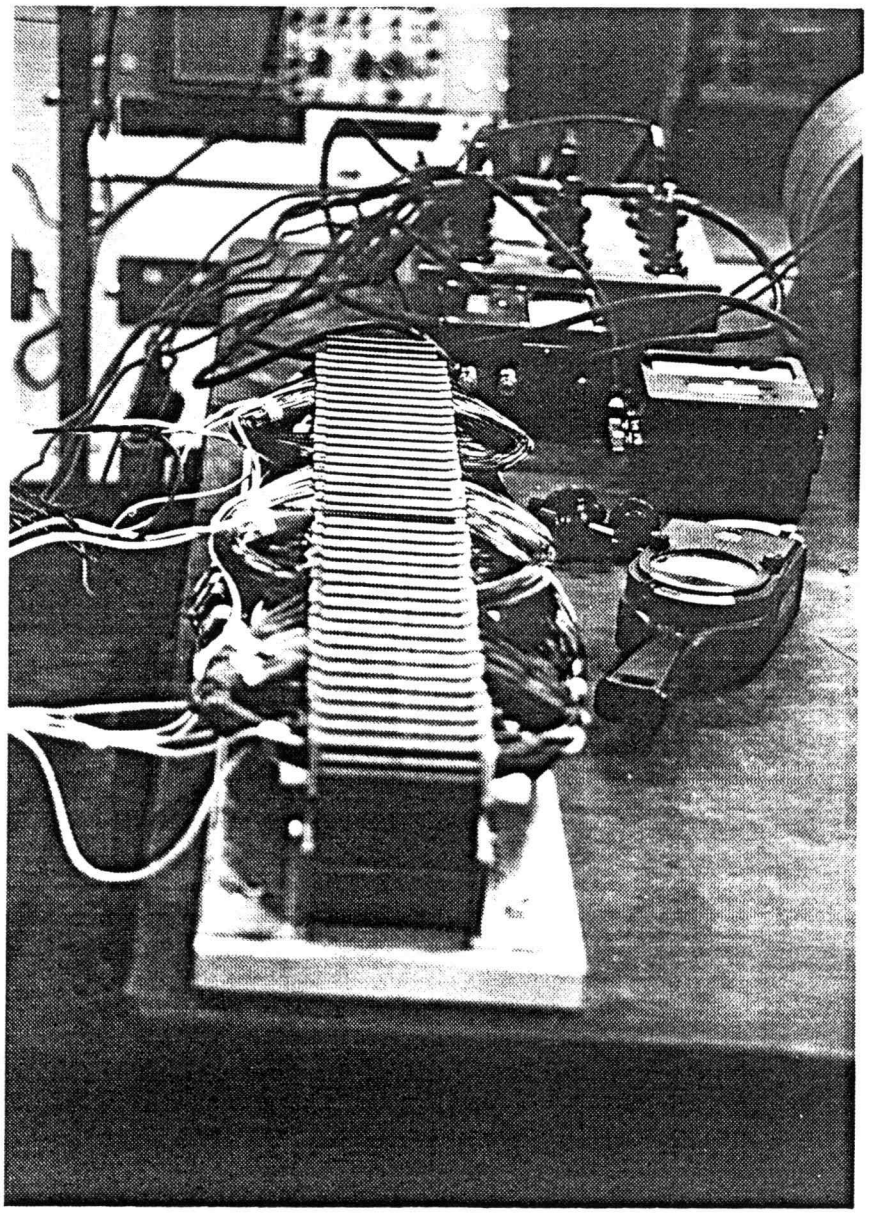

Fig. 3.2.2 Photograph of the prototype's primary

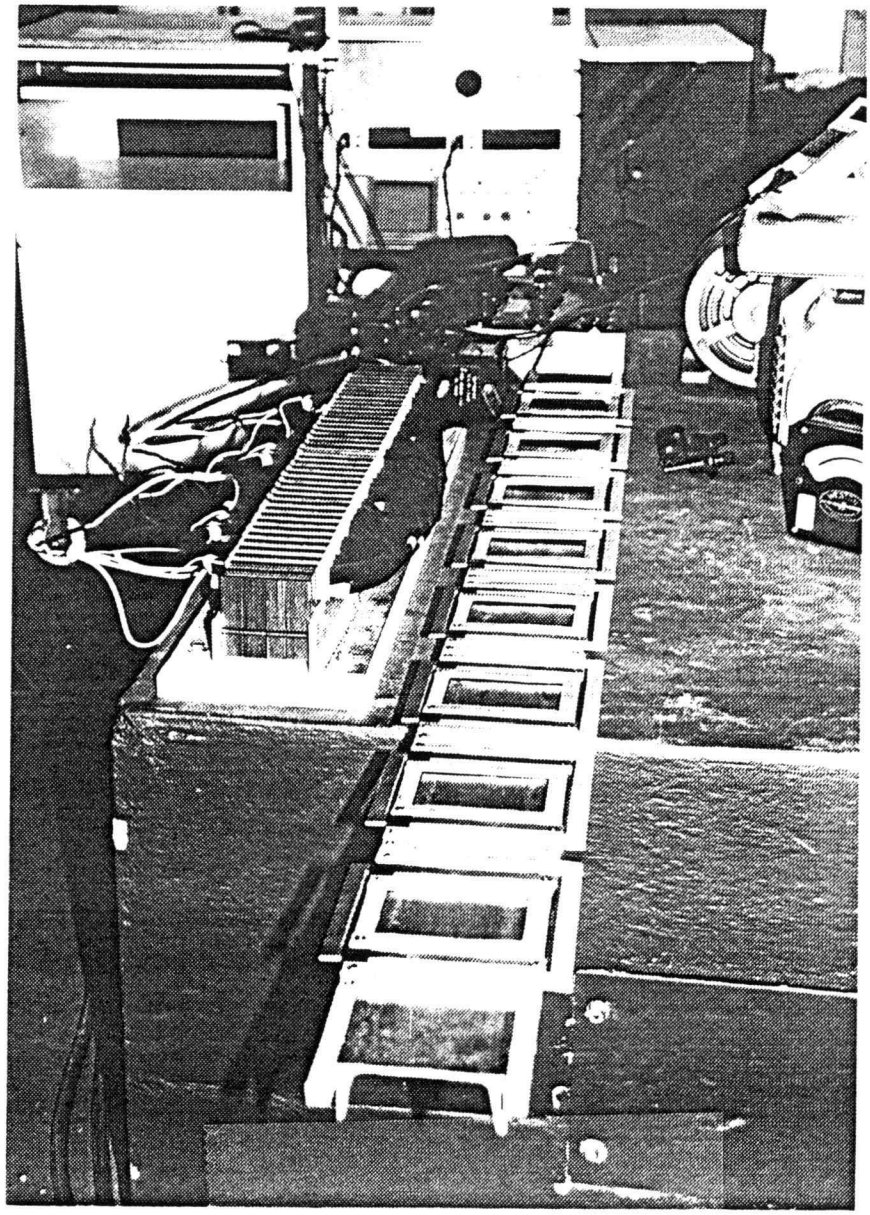

Fig. 3.2.3 Photograph of the prototype's secondary

4. PRELIMINARY DESIGN ESTIMATION

After the design of the windings layout for the LBDFM lab prototype, parameter estimations are required to evaluate number of effective turns for each coil of the primary windings belonging to each set of 3-phase systems and the size of the wires used for each set. Therefore, before going through the calculation to do the parameter estimation, it is essential to introduce the geometry of the lab prototype as following:

Width of the primary, L=8.057 [cm]

Length of the primary core, D=69.691 [cm]

Selected air gap between the primary & secondary, g=6 [mm]

Depth of the back iron of the primary, h_r=4.15 [cm]

Slot depth, h_t=3.5 [cm]

Tooth width, b_z=0.9 [cm]

Number of primary slots, Z=36

Slot width, b_s=1 [cm]

Figure 4.1.1 displays the schematic of the primary core with above dimensions identified. All the numbers on the figure are in [Cm].

The process of design estimation is to obtain the electrical particulars of a machine to satisfy the given specifications covering

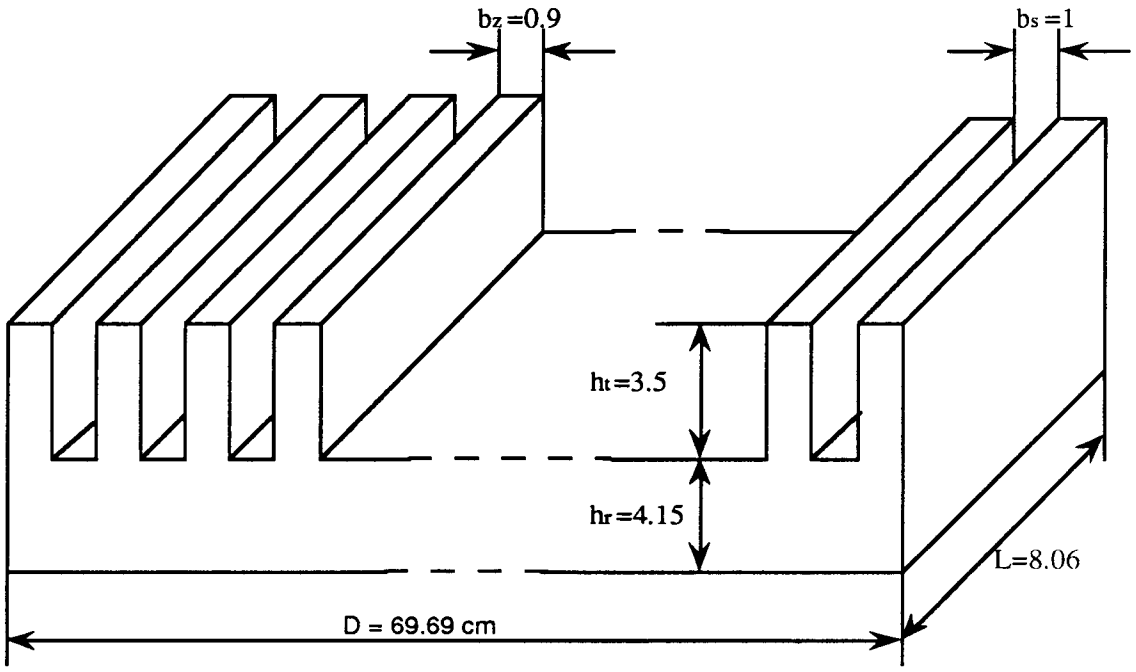

Figure 4.1.1 Primary core structure of the LBDFM

horse-power, speed, and condition of utilization.

4.1 Calculation of Number of Turns

For the prototype machine, two set of primary windings have been designed to provide the synchronous speeds of the traveling

fields in the air gap of n_{sp}=14 meter/sec. and n_{sq}=42 meter/sec. for the 6-pole and 2-pole respectively with 60 Hz excitation. Apparent power, S, is the electrical rating of the machine in [VA] which can be found in terms of its phase emf and current. $S=3\ E_{ph}\ I_{ph}$, where $E_{ph}=4.44\ K_w f\ T_{ph}\ \Phi_m$ [Volt]. In this expression, T_{ph} is the number of turns per phase, K_w is the overall winding factor, f is the supply frequency, and Φ_m is maximum flux produced in each phase. Considering only the fundamental frequency component, for each set:

$$S=13.32\ K_w\ f\ T_{ph}\ I_{ph}\ \Phi_m\ [VA]$$

where, $\Phi_m = B_m$. A, where A is the area covered by each pole and is defined as: $A= \tau_p$. L. where τ_p is pole pitch length or width of each pole.

4.1.1 Estimation of the 6-pole Winding

Based on geometry of the prototype machine, area occupied by each pole can be calculated as follows:

$$\tau_p = D/2p = 69.691/6=11.615 \quad [cm]$$

$A = \tau_p \cdot L = (11.615)(8.057) = 93.582$ [cm^2] or 9.3588×10^{-3} [m]

Using the Fourier series expansion, the average flux density for the fundamental is: $B = (2/p)\, B_{max}$ [17], therefore, $\Phi = (2/p)\, B_{max} \cdot A$. The flux density, B, directly influences the core loss and magnetizing current, thus, it has a significant effect on power factor. Flux determines the pull-out thrust. If the machine is required to provide a thrust very much greater than its full load, the requirement could be satisfied by the use of wide teeth and small narrow slots, giving a large working flux, relatively small leakage and a short circuit current many times full-load current. The use of deeper, wider slots would increase the rating at the expense of pull-out thrust. The number of primary turns per phase, therefore, would have to be increased, which would result in a higher thermal rating properties.

For design convenience, the loading specifications shall be defined as follows [18]:

* *Specific magnetic loading* ; Which is the average flux density over the whole surface of the air gap, B is limited by saturation and losses in the teeth.

$$B = \frac{2p\,\phi_m}{D.L} \qquad [\frac{weber}{m^2}]$$

* *Specific electric loading (ac)* ; The number of r.m.s current per unit length of gap-surface, or the r.m.s current density;

$$ac = 3.\frac{2\,T_{ph}\,I_{ph}}{D} \qquad [\frac{\text{amp-conductor}}{\text{meter}}]$$

Parameter ac affects I^2R losses and secondary reaction. The losses must be dissipated by cooling so that the choice of specific loadings are affected by the size, construction, speed, type of winding, and insulation of the machine be restricted to several loading specifications. With given specific loadings and with f=p.n,

$$S = 4.44\,K_w\,p\,n\,[\frac{D\,L\,B}{2p}]\,0.5\,D\,ac$$

$$S = 1.11\,K_w\,B\,D^2\,L\,n\,ac \qquad \text{[volt-ampere]}$$

This expression states that the rating is proportional to the average gap density B, the surface current density ac, dimension of the core D^2 L, and speed n. Parameter S is referring here to the electrical input [KVA]. In terms of the mechanical output, P_m, in [KW] or [Horse-power].

$$S = \frac{P_m}{\eta.\cos\varphi} = \frac{(HP)\ 0.746}{\eta.\cos\varphi} \qquad \text{[KVA]}$$

where η, efficiency and $\cos\phi$, power factor, are estimated at full load

values. B lies between 0.3 and 0.6 wb/m^2 for normal 50 to 60 Hz machines, rising to 0.65 wb/m^2 for crane, rolling-mill, and other similar applications. In most smaller scale applications flux density, B, for the design purpose can be chosen 0.43 wb/m^2 [18]. Therefore, number of turns for each phase of the 6-pole system can be estimated as:

$$T_{ph} = \frac{E_{ph}}{4.44\, f \frac{2}{p} B_{max}\, A\, K_w}$$

$$T_{ph} = \frac{230}{\frac{2}{p} 4.44 \times 60 \times 0.43 \times 9.358 \times 10^{-3} \times 0.955} \Rightarrow T_{ph} \cong 353 \text{ turns/phase}$$

Since each phase of the 6-pole set in the primary contains 6 coils, therefore, the number of turns for each coil of the 6-pole system is :

$$T_{coil} = T_{ph} / 6, \text{ hence, } T_{coil} = 59 \text{ turns.}$$

However, due to the unavailability of enough space in the slot, T_{coil} was restricted to 50 turns for the prototype.

4.1.2 Estimation of the 2-Pole Winding:

Using the same procedure described in section 4.1, the parameter estimation for the 2-pole system can be evaluated as

follows:

$$\tau_p = \frac{D}{2p} \Rightarrow \tau_p = \frac{69.692}{2} = 34.846 \text{ [cm] or } 0.348 \text{ [m]}$$

Hence ;

$$A = \tau_p.L = 34.846 \times 8.057 = 280.754 \text{ [cm}^2\text{] or } 0.028 \text{ [m}^2\text{]}$$

Then ;

$$T_{ph} = \frac{E_{ph}}{\frac{2}{p} 4.44 \, f \, B_{max} \, A \, K_w}$$

$$T_{ph} = \frac{230}{\frac{2}{p} \times 4.44 \times 60 \times 0.43 \times 0.028 \times 0.955} \Rightarrow T_{ph} \cong 118 \text{ Turns.}$$

Hence ; T_{coil} = 19.7 ~ 20 turns.

4.2 Size Determination of the Windings

To do this task, two more factors need to be defined, as follows :

* *Output Coefficient* ; This factor is defined as:

$$G = \frac{S}{D^2 L n} = 1.11 \, B \, ac \times 10^{-3} \quad S \text{ is in [KVA]}$$

where n is the speed of the traveling field and depends on the number of poles. By specifying adequate values to B and ac , The D^2L product for a given rating S in [KVA] at speed n can be obtained using table in

reference [18]. S is referring here to the electrical input. The electric loading, ac, varies between 5000 and 45000 and the current density, J, may lie within 3 to 8 amp/mm^2 .

* *Dimension Consideration* ; The D^2L product appearing in the previous equations has two components, D and L . For normal speed, a roughly square pole of pole-pitch $\tau = D/2P$ equal to the core length L, gives good electrical design especially in terms of leakage reactance. The design tendency is to use a restricted core depth and greater core-length to decrease the proportion of inactive copper in the slots of the machine and obtain a more economical machine.

The air gap length is determined by the magnetizing current to avoid having too low power factor. Generally, the air gap ought to be made as small as is mechanically possible. In propulsion systems for transit applications a reasonable range of 6 to 13 mm for mechanical clearance is found to be practical .

At this point, other parameters of the machine such as primary phase resistances of both 6-pole and 2-pole sets need to be evaluated in order to estimate the conductor size and copper losses of each system under rated loading.

A. For 6-pole system :

In order to calculate the 6-pole equivalent phase resistance of the primary, it is necessary first to find the length per phase of the conductor for 6-pole system winding. This number can simply be estimated by measuring a coil circumference of the 6-pole winding which for the lab machine is 54 cm. Therefore, Conductor Length Per Phase of the 6-pole is:

$$6x50x54^{cm} = 162 \ [m].$$

Then, the rated current of the machine for each phase of the 6-pole winding needs to be calculated. To estimate the rated current of the 6-pole set, the defined factor, ac, which is the number of r.m.s ampere-conductors per length of gap surface can be taken out of the table in reference [18] based on the frame size of the machine. Frame size, moreover, is the function of number of poles or speed of the machine. By a good approximation ac can be chosen 22500. Hence, by using this value, the phase current of the 6-pole system can be estimated as following:

$$I_{ph} = \frac{ac\,D}{3\times2\times T_{ph}} \quad \text{i.e.}$$

$$I_{ph} = \frac{22500\times0.69691}{6\times300} \Rightarrow I_{ph} = 8.71 \ [\text{ampere}]$$

Taking the current density of J = 4 [amp/mm2] , the cross sectional area of the conductor for 6-pole system can be estimated as below:

Conductor cross sectional area = 8.71/4 = 2.17 [mm^2].

Then, the diameter of the conductor for 6-pole winding is:

d = 1.6 [mm]

To determine the American standard wire gauge for this size of conductor, since a mil is 1/1000 of an inch, therefore ;

d = 63 [mils]

Hence, by using table 4.3.1, the wire gauge number selected for this particular conductor is :

wire gauge = 14

Now, the equivalent resistance of each phase of the 6-pole winding for the LBDFM can be obtained as follow:

6-pole conductor length per phase was found to be 162 meter or 531.52 [ft]. Then, from Table 4.3.1, resistance of standard copper at 65° centigrade is:

$R_{1\text{-}6\ pole}$ = 1.6 [Ω] per phase

B. For 2-pole system:

To do the 2-pole calculation, the same procedure described in part (A) of section 4.3 is used. The only difference in two pole estimation arises due to the variable supply frequency and/or voltage. Therefore, fixed voltage and/or frequency can not be assumed to find phase current, however, by using an acceptable approximation which is 11000 for the parameter ac, the phase resistance of the 2-pole system can be estimated. Then:

$$I_{ph\ 2\text{-}p} = \frac{ac\,D}{3\times 2\times T_{ph}}$$

$$I_{ph\ 2\text{-}p} = \frac{11000\times 0.69691}{3\times 2\times 118} \Rightarrow I_{ph\ 2\text{-}p} = 10.82 \text{ [amps]}$$

Using current density of J=4 [amp/mm^2], conductor cross-sectional area = 10.82/4.0 = 2.705 [mm^2]. Hence, diameter of the conductor, d=1.8 [mm] or d=71.53 [mils]. Again, by using table 4.3.1, the American standard wire gauge for the 2-pole set of the LBDFM is:

$$\text{wire gauge}_{\ 2\text{-}p} = 13$$

To determine the 2-pole phase resistance;

2-pole /phase conductor length = (6)(102)(20) = 122.4 [m] or 401.59 [ft], therefore, the phase resistance of the 2-pole at 65 ^{o}

centigrade using standard copper from Table 4.3.1 is:

$$R_{2\text{-}p\ @\ 65^{\circ}\,c} = 0.947 \quad [\Omega]$$

4.3 Copper Losses of the Primary

Copper losses for all phases of the 6-pole and 2-pole can simply be calculated using the equation; losses = $3\ I^2\ R$, for each system separately as below:

6-pole copper loss=$(3)(1.6)(7.35)^2$ =259.308 [watt]

2-pole copper loss=$(3)(0.947)(10.34)^2$ =303.747 [watt]

In the doubly-fed mode of operation however, copper losses of the 2-pole system, depending on the thrust contribution of the 2-pole, may be smaller than the above value.

Gauge number	Diameter, mils	Ohms per 1000 meters		Ohms per 1000 ft	
		25°C	65°C	25°C	65°C
0000	460	0.164	0.190	0.050	0.058
000	410	0.207	0.240	0.063	0.073
00	365	0.262	0.302	0.080	0.092
0	325	0.328	0.381	0.100	0.116
1	289	0.413	0.479	0.126	0.146
2	258	0.522	0.604	0.159	0.184
3	229	0.659	0.761	0.201	0.232
4	204	0.830	0.958	0.253	0.292
5	182	1.05	1.21	0.319	0.369
6	162	1.32	1.53	0.403	0.465
7	144	1.67	1.92	0.508	0.586
8	128	2.10	2.42	0.641	0.739
9	114	2.65	3.06	0.808	0.932
10	102	3.35	3.87	1.02	1.18
11	91	4.20	4.86	1.28	1.48
12	81	5.31	6.14	1.62	1.87
13	72	6.69	7.74	2.04	2.36
14	64	8.46	9.74	2.58	2.97
15	57	10.66	12.30	3.25	3.75
16	51	13.42	15.52	4.09	4.73
17	45	16.93	19.55	5.16	5.96
18	40	21.36	24.64	6.51	7.51
19	36	26.94	31.10	8.21	9.48
20	32	34.12	39.04	10.4	11.9
21	28.5	42.98	49.54	13.1	15.1
22	25.3	54.13	62.34	16.5	19.0
23	22.6	68.24	78.74	20.8	24.0
24	20.1	85.96	99.08	26.2	30.2
25	17.9	108.3	125.0	33.0	38.1
26	15.9	136.5	157.5	41.6	48.0
27	14.2	172.2	198.8	52.5	60.6
28	12.6	217.2	250.7	66.2	76.4
29	11.3	273.6	315.9	83.4	96.3
30	10.0	344.5	397.0	105	121
31	8.9	436.4	502.0	133	153
32	8.0	547.9	633.2	167	193
33	7.1	692.3	797.2	211	243
34	6.3	872.7	1007	266	307
35	5.6	1099	1270	335	387
36	5.0	1388	1601	423	488
37	4.5	1749	2018	533	615
38	4.0	2208	2546	673	776
39	3.5	2782	3212	848	979
40	3.1	3510	4035	1070	1230

Table 4.3.1 Resistance of standard copper wire

5. DETAILED CALCULATION OF THE LBDFM

The tasks in this chapter are to derive and calculate the LBDFM impedances. In this analysis, the representation of the primary coil connections have a significant role as well as the secondary configuration. As it was shown in Figures 3.1.1 and 3.1.2, the primary of the LBDFM has two electrically isolated 3-phase windings with 2 and 6 poles. Each winding configuration contains 9 coils which are distributed in the primary slots. Therefore, to calculate the phase impedances of the primary, individual values of all inductances and their mutuals must be estimated as described in this chapter in full detail.

For all these calculations, a bit of time and effort was devoted to develop several programs to compute all the parameters of the LBDFM using principles and modified equations from reference [14].

5.1 Primary Inductances

Due to the nature and construction of the LBDFM, the primary inductance of the machine in a general form can be written as:

$$L_{ss} = \begin{bmatrix} L_{66} & L_{62} \\ L_{26} & L_{22} \end{bmatrix}$$

In which, L_{66} represents 6-pole system inductances, L_{22} stands for 2-pole system inductances, L_{62} includes the mutual inductances of 6-pole and 2-pole system, and L_{26} is a transpose of L_{62}. It is clear that each of the elements of L_{ss} matrix are representing a sub matrix with the dimension of 18 by 18 for the developed prototype.

5.1.1 Computation of Coil Self-Inductances

The whole existing inductance of each coil is considered as due to the *main* or *useful* flux which contributes to the energy production, and the *leakage* flux which contributes only to reversible energy storage. Thus, the actual flux is considered as the combination of working and leakage fluxes.

[18] introduces two main physical subdivisions of the leakage flux as: (i) the *overhang leakage*, which is a true, separate flux caused by end-windings. Its value depends on the arrangement of the end-windings. (ii) *circumferential gap leakage* which is caused by the "solenoid" action of the two opposing sets of ampere-turns in combination on the gap. Further subdivisions of (ii) are *(a) slot* and *(b)*

zig-zag components. To briefly point these out, slot leakage crosses the conductors from one tooth to the next and it is in phase with the current for all conductors in a particular phase group. Its value depends only on the magnitude of the current. Zig-zag leakage depends on the gap length and relative position of two sets of teeth and tends to "zig-zag" across the gap. Figure 5.1.1; (a), (b), (c), (d), and (e) show the described fluxes.

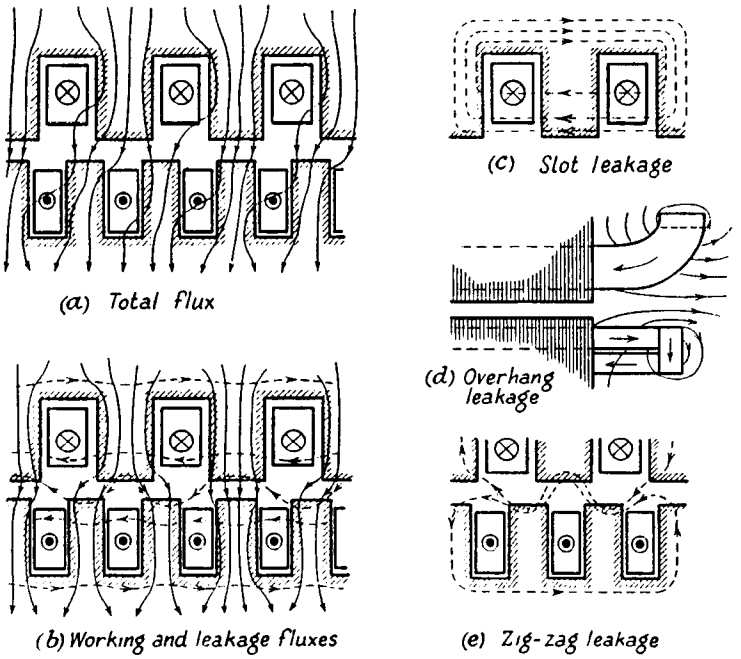

Fig. 5.1.1 Flux leakage

Both 6-pole and 2-pole primary windings, each have a total of 18 coils for all the three phases. Due to the design criteria, 6-pole coils, span 6 slots of the whole 40 slots of the primary core, while the 2-pole coils span 18 slots of the total 40. The primary coil air gap inductance can be derived as follows for calculation of the self inductance of each coil.

$$Ls_a = \frac{\mu_0 N^2 L D(S-C) C}{g s^2}$$

Where in this formula;

Ls_a= Coil self inductance in [Henry].

μ_o = Permeability of free space and is equal to $4\pi \times 10^{-7}$.

N = Number of turns for each coil.

D = Width of the primary core in [meter].

L = Length of the primary core in [meter].

S = Number of primary slots.

C = Coil span in number of slot pitches.

g = Air gap length in [meter].

5.1.2 Computation of Primary Mutual Inductances

A. *Mutual between 6-pole coils:* By looking at Figure 3.1.2, it

can be observed that coil number (1) of 18 existing coils of the 6-pole system produces air gap flux which spans from slot # 1 to $1+C_6$ (C_6 is a coil span of the 6-pole system). This flux has a relative magnitude over two parts of the primary core which can be considered as positive flux in the region 1 to C_6 and negative flux in the region C_6+1 to 1. Now to calculate the mutual inductance of any of the 6-pole coils with respect to this coil, we must find out the number of positive flux and negative flux slots that that particular coil links due to the flux of our chosen coil i.e. coil # 1. Figure 5.1.2.1, shows such a relationship in

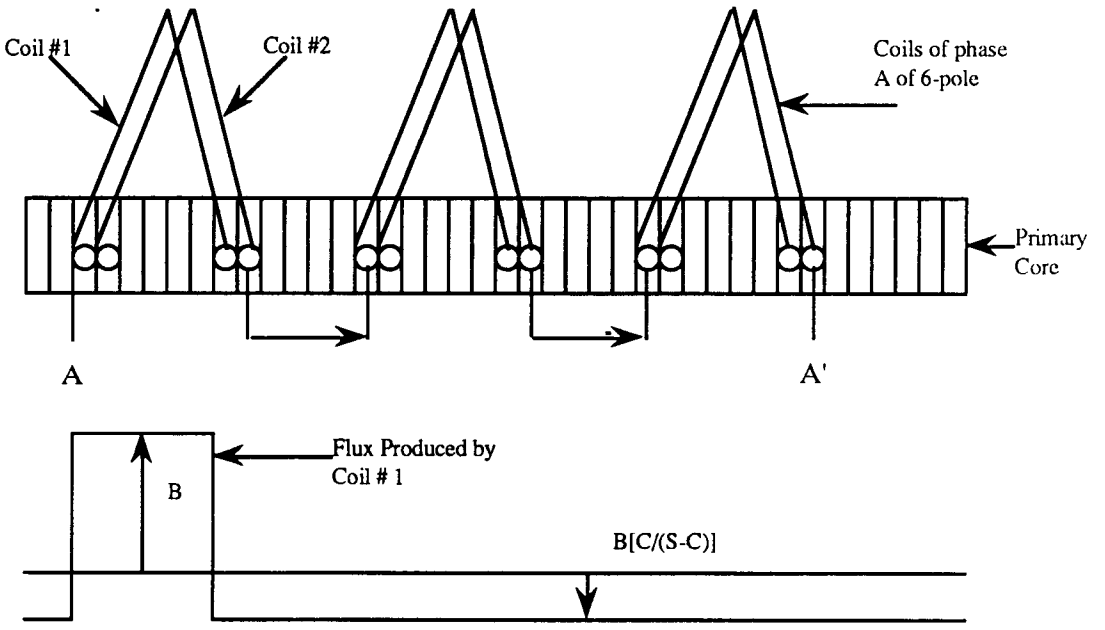

Fig. 5.1.2.1 Demonstration of phase A coils in the primary

terms of flux linkages between any pair of coils. As an example, coil #2

links 6 slots positive flux and 1 slot negative flux with coil #1. Hence, based upon this analysis, the general formula to calculate the mutual inductances between coils can be derived as following:

$$M_{i,j}=\frac{\mu_o N^2 LD}{g s^2}\left\{(S-C_6)(C_6+1-FC)-C_6(FC-1)\right\}$$

Where in this equation:

$M_{i,j}$ = Mutual inductance between coil # i and coil # j [Henry].

C_6 = Coil span of 6-pole set in terms of # of slots.

FC = Variable factor to determine the +ve linkage between any pair of coils in terms of number of slots.

Other parameters in the above equation have been defined previously. The computed results of the 6-pole coils self and mutual inductances which are the elements of the L_{66} matrix are:

$$[\ L_{66}\ ] =$$

4.481,	3.602,	2.723,	1.845,	.966,	.088,	-.791,	-.791,	-.791,	-.791,	-.791,	-.791,	-.791,	-.791,	-.791,	-.791,	-.791,	-.791,
3.602,	4.481,	3.602,	2.723,	1.845,	.966,	-.791,	-.791,	-.791,	-.791,	-.791,	-.791,	-.791,	-.791,	-.791,	-.791,	-.791,	-.791,
2.723,	3.602,	4.481,	3.602,	2.723,	1.845,	-.791,	-.791,	-.791,	-.791,	-.791,	-.791,	-.791,	-.791,	-.791,	-.791,	-.791,	-.791,
1.845,	2.723,	3.602,	4.481,	3.602,	2.723,	-.791,	-.791,	-.791,	-.791,	-.791,	-.791,	-.791,	-.791,	-.791,	-.791,	-.791,	-.791,
.966,	1.845,	2.723,	3.602,	4.481,	3.602,	-.791,	-.791,	-.791,	-.791,	-.791,	-.791,	-.791,	-.791,	-.791,	-.791,	-.791,	-.791,
.088,	.966,	1.845,	2.723,	3.602,	4.481,	-.791,	-.791,	-.791,	-.791,	-.791,	-.791,	-.791,	-.791,	-.791,	-.791,	-.791,	-.791,
-.791,	-.791,	-.791,	-.791,	-.791,	-.791,	4.481,	3.602,	2.723,	1.845,	.966,	.088,	-.791,	-.791,	-.791,	-.791,	-.791,	-.791,
-.791,	-.791,	-.791,	-.791,	-.791,	-.791,	3.602,	4.481,	3.602,	2.723,	1.845,	.966,	-.791,	-.791,	-.791,	-.791,	-.791,	-.791,
-.791,	-.791,	-.791,	-.791,	-.791,	-.791,	2.723,	3.602,	4.481,	3.602,	2.723,	1.845,	-.791,	-.791,	-.791,	-.791,	-.791,	-.791,
-.791,	-.791,	-.791,	-.791,	-.791,	-.791,	1.845,	2.723,	3.602,	4.481,	3.602,	2.723,	-.791,	-.791,	-.791,	-.791,	-.791,	-.791,
-.791,	-.791,	-.791,	-.791,	-.791,	-.791,	.966,	1.845,	2.723,	3.602,	4.481,	3.602,	-.791,	-.791,	-.791,	-.791,	-.791,	-.791,
-.791,	-.791,	-.791,	-.791,	-.791,	-.791,	.088,	.966,	1.845,	2.723,	3.602,	4.481,	-.791,	-.791,	-.791,	-.791,	-.791,	-.791,
-.791,	-.791,	-.791,	-.791,	-.791,	-.791,	-.791,	-.791,	-.791,	-.791,	-.791,	-.791,	4.481,	3.602,	2.723,	1.845,	.966,	.088,
-.791,	-.791,	-.791,	-.791,	-.791,	-.791,	-.791,	-.791,	-.791,	-.791,	-.791,	-.791,	3.602,	4.481,	3.602,	2.723,	1.845,	.966,
-.791,	-.791,	-.791,	-.791,	-.791,	-.791,	-.791,	-.791,	-.791,	-.791,	-.791,	-.791,	2.723,	3.602,	4.481,	3.602,	2.723,	1.845,
-.791,	-.791,	-.791,	-.791,	-.791,	-.791,	-.791,	-.791,	-.791,	-.791,	-.791,	-.791,	1.845,	2.723,	3.602,	4.481,	3.602,	2.723,
-.791,	-.791,	-.791,	-.791,	-.791,	-.791,	-.791,	-.791,	-.791,	-.791,	-.791,	-.791,	.966,	1.845,	2.723,	3.602,	4.481,	3.602,
-.791,	-.791,	-.791,	-.791,	-.791,	-.791,	-.791,	-.791,	-.791,	-.791,	-.791,	-.791,	.088,	.966,	1.845,	2.723,	3.602,	4.481,

B. *Mutual between 2-pole coils:* The same logic and procedure were used for mutual inductance computation of the 2-pole system. The only difference in this case is that, 2-pole coils span 18 slots and are distributed uniquely in the primary as phase a, c, and b to provide the linear motion as described before. The computed self and mutual inductances are the elements of L_{22} matrix as below:

$$[\, L_{22} \,] =$$

1.392,	1.251,	1.110,	.970,	.829,	.689,	.548,	.408,	.267,	.127,	-.014,	-.155,	-.295,	-.436,	-.576,	-.717,	-.857,	-.998,
1.251,	1.392,	1.251,	1.110,	.970,	.829,	.689,	.548,	.408,	.267,	.127,	-.014,	-.155,	-.295,	-.436,	-.576,	-.717,	-.857,
1.110,	1.251,	1.392,	1.251,	1.110,	.970,	.829,	.689,	.548,	.408,	.267,	.127,	-.014,	-.155,	-.295,	-.436,	-.576,	-.717,
.970,	1.110,	1.251,	1.392,	1.251,	1.110,	.970,	.829,	.689,	.548,	.408,	.267,	.127,	-.014,	-.155,	-.295,	-.436,	-.576,
.829,	.970,	1.110,	1.251,	1.392,	1.251,	1.110,	.970,	.829,	.689,	.548,	.408,	.267,	.127,	-.014,	-.155,	-.295,	-.436,
.689,	.829,	.970,	1.110,	1.251,	1.392,	1.251,	1.110,	.970,	.829,	.689,	.548,	.408,	.267,	.127,	-.014,	-.155,	-.295,
.548,	.689,	.829,	.970,	1.110,	1.251,	1.392,	1.251,	1.110,	.970,	.829,	.689,	.548,	.408,	.267,	.127,	-.014,	-.155,
.408,	.548,	.689,	.829,	.970,	1.110,	1.251,	1.392,	1.251,	1.110,	.970,	.829,	.689,	.548,	.408,	.267,	.127,	-.014,
.267,	.408,	.548,	.689,	.829,	.970,	1.110,	1.251,	1.392,	1.251,	1.110,	.970,	.829,	.689,	.548,	.408,	.267,	.127,
.127,	.267,	.408,	.548,	.689,	.829,	.970,	1.110,	1.251,	1.392,	1.251,	1.110,	.970,	.829,	.689,	.548,	.408,	.267,
-.014,	.127,	.267,	.408,	.548,	.689,	.829,	.970,	1.110,	1.251,	1.392,	1.251,	1.110,	.970,	.829,	.689,	.548,	.408,
-.155,	-.014,	.127,	.267,	.408,	.548,	.689,	.829,	.970,	1.110,	1.251,	1.392,	1.251,	1.110,	.970,	.829,	.689,	.548,
-.295,	-.155,	-.014,	.127,	.267,	.408,	.548,	.689,	.829,	.970,	1.110,	1.251,	1.392,	1.251,	1.110,	.970,	.829,	.689,
-.436,	-.295,	-.155,	-.014,	.127,	.267,	.408,	.548,	.689,	.829,	.970,	1.110,	1.251,	1.392,	1.251,	1.110,	.970,	.829,
-.576,	-.436,	-.295,	-.155,	-.014,	.127,	.267,	.408,	.548,	.689,	.829,	.970,	1.110,	1.251,	1.392,	1.251,	1.110,	.970,
-.717,	-.576,	-.436,	-.295,	-.155,	-.014,	.127,	.267,	.408,	.548,	.689,	.829,	.970,	1.110,	1.251,	1.392,	1.251,	1.110,
-.857,	-.717,	-.576,	-.436,	-.295,	-.155,	-.014,	.127,	.267,	.408,	.548,	.689,	.829,	.970,	1.110,	1.251,	1.392,	1.251,
-.998,	-.857,	-.717,	-.576,	-.436,	-.295,	-.155,	-.014,	.127,	.267,	.408,	.548,	.689,	.829,	.970,	1.110,	1.251,	1.392,

C. *Mutuals between 2-pole & 6-pole coils:* To compute these inductances, the same principle was used to derive an equation for 2-pole to 6-pole mutuals as below:

$$M_{i,j} = \frac{\mu_o N_2 N_6 L D}{g S^2} \left\{ FC^{+}(S - C_2) - FC^{-} C_2 \right\}$$

Where:

N_2 = Number of turns of the 2-pole coils.

N_6 = Number of turns of the 6-pole coils.

C_2 = Coil span of the 2-pole coils.

FC^+ = Number of positive flux linkage in terms of slot.

FC^- = Number of negative flux linkage in terms of slot.

The computed results which are the elements of L_{26} matrix are :

$$[\ L_{26}\ ] =$$

1.160,	1.160,	1.160,	1.160,	1.160,	1.160,	1.160,	.808,	.457,	.105,	-.246,	-.597,	-.949,	-.949,	-.949,	-.949,	-.949,	-.949,
.808,	1.160,	1.160,	1.160,	1.160,	1.160,	1.160,	1.160,	.808,	.457,	.105,	-.246,	-.949,	-.949,	-.949,	-.949,	-.949,	-.949,
.457,	.808,	1.160,	1.160,	1.160,	1.160,	1.160,	1.160,	1.160,	.808,	.457,	.105,	-.949,	-.949,	-.949,	-.949,	-.949,	-.949,
.105,	.457,	.808,	1.160,	1.160,	1.160,	1.160,	1.160,	1.160,	1.160,	.808,	.457,	-.949,	-.949,	-.949,	-.949,	-.949,	-.949,
-.246,	.105,	.457,	.808,	1.160,	1.160,	1.160,	1.160,	1.160,	1.160,	1.160,	.808,	-.949,	-.949,	-.949,	-.949,	-.949,	-.949,
-.597,	-.246,	.105,	.457,	.808,	1.160,	1.160,	1.160,	1.160,	1.160,	1.160,	1.160,	-.949,	-.949,	-.949,	-.949,	-.949,	-.949,
-.949,	-.597,	-.246,	.105,	.457,	.808,	1.160,	1.160,	1.160,	1.160,	1.160,	1.160,	-.949,	-.949,	-.949,	-.949,	-.949,	-.949,
-.949,	-.949,	-.597,	-.246,	.105,	.457,	1.160,	1.160,	1.160,	1.160,	1.160,	1.160,	-.597,	-.949,	-.949,	-.949,	-.949,	-.949,
-.949,	-.949,	-.949,	-.597,	-.246,	.105,	1.160,	1.160,	1.160,	1.160,	1.160,	1.160,	-.246,	-.597,	-.949,	-.949,	-.949,	-.949,
-.949,	-.949,	-.949,	-.949,	-.597,	-.246,	1.160,	1.160,	1.160,	1.160,	1.160,	1.160,	.105,	-.246,	-.597,	-.949,	-.949,	-.949,
-.949,	-.949,	-.949,	-.949,	-.949,	-.597,	1.160,	1.160,	1.160,	1.160,	1.160,	1.160,	.457,	.105,	-.246,	-.597,	-.949,	-.949,
-.949,	-.949,	-.949,	-.949,	-.949,	-.949,	1.160,	1.160,	1.160,	1.160,	1.160,	1.160,	.808,	.457,	.105,	-.246,	-.597,	-.949,
-.949,	-.949,	-.949,	-.949,	-.949,	-.949,	1.160,	1.160,	1.160,	1.160,	1.160,	1.160,	1.160,	.808,	.457,	.105,	-.246,	-.597,
-.949,	-.949,	-.949,	-.949,	-.949,	-.949,	.808,	1.160,	1.160,	1.160,	1.160,	1.160,	1.160,	1.160,	.808,	.457,	.105,	-.246,
-.949,	-.949,	-.949,	-.949,	-.949,	-.949,	.457,	.808,	1.160,	1.160,	1.160,	1.160,	1.160,	1.160,	1.160,	.808,	.457,	.105,
-.949,	-.949,	-.949,	-.949,	-.949,	-.949,	.105,	.457,	.808,	1.160,	1.160,	1.160,	1.160,	1.160,	1.160,	1.160,	.808,	.457,
-.949,	-.949,	-.949,	-.949,	-.949,	-.949,	-.246,	.105,	.457,	.808,	1.160,	1.160,	1.160,	1.160,	1.160,	1.160,	1.160,	.808,
-.949,	-.949,	-.949,	-.949,	-.949,	-.949,	-.597,	-.246,	.105,	.457,	.808,	1.160,	1.160,	1.160,	1.160,	1.160,	1.160,	1.160,

Finally to find the last sub matrix of the L_{ss} which is the 6-pole to 2-pole mutuals, we can simply find the transpose of the L_{26} which is already known. Thus, $[\ L_{62}\ ] = [\ L_{26}\ ]^T$.

5.2 Determination of the Phase Inductances

Now that all elements of the L_{ss} matrix are determined, it is necessary to compute the phase parameters of the machine for both 2 and 6 pole systems. This task can be accomplished by using following expression:

$$[L_{phase}] = [C] [L_{ss}] [C]^T$$

Where;

$[L_{phase}]$ = Phase inductance of the primary which is a 6x6 matrix.

[C] = Connection matrix of all 36 coils which is a 6 by 36 matrix.

$[C]^T$ = Transpose of [C] and is a 36 by 6 matrix.

[Lss] = Coil inductances of both 6 and 2-pole systems which is a 36 by 36 matrix.

It is worthwhile to notice that LBDFM windings have been designed so that for each set of the 3-phase windings production of a traveling field in the primary be provided to produce linear motion. To satisfy the above criteria, be able to fit all phases of both systems in 36 slots, and avoid leaving extra slots in the primary, phase C of both the 6-pole and the 2-pole windings were constructed in reverse direction compared to phases A and B. Therefore, in the connection matrix, this

criterion must be met. The following presents the $[C]^T$ matrix. The negative signs in phase C of both systems are due to the above specification.

$$[C]^T =$$

1.,	0.,	0.,	0.,	0.,	0.,
1.,	0.,	0.,	0.,	0.,	0.,
0.,	0.,	-1.,	0.,	0.,	0.,
0.,	0.,	-1.,	0.,	0.,	0.,
0.,	1.,	0.,	0.,	0.,	0.,
0.,	1.,	0.,	0.,	0.,	0.,
1.,	0.,	0.,	0.,	0.,	0.,
1.,	0.,	0.,	0.,	0.,	0.,
0.,	0.,	-1.,	0.,	0.,	0.,
0.,	0.,	-1.,	0.,	0.,	0.,
0.,	1.,	0.,	0.,	0.,	0.,
0.,	1.,	0.,	0.,	0.,	0.,
1.,	0.,	0.,	0.,	0.,	0.,
1.,	0.,	0.,	0.,	0.,	0.,
0.,	0.,	-1.,	0.,	0.,	0.,
0.,	0.,	-1.,	0.,	0.,	0.,
0.,	1.,	0.,	0.,	0.,	0.,
0.,	1.,	0.,	0.,	0.,	0.,
0.,	0.,	0.,	1.,	0.,	0.,
0.,	0.,	0.,	1.,	0.,	0.,
0.,	0.,	0.,	1.,	0.,	0.,
0.,	0.,	0.,	1.,	0.,	0.,
0.,	0.,	0.,	1.,	0.,	0.,
0.,	0.,	0.,	1.,	0.,	0.,
0.,	0.,	0.,	0.,	0.,	-1.,
0.,	0.,	0.,	0.,	0.,	-1.,
0.,	0.,	0.,	0.,	0.,	-1.,
0.,	0.,	0.,	0.,	0.,	-1.,
0.,	0.,	0.,	0.,	0.,	-1.,
0.,	0.,	0.,	0.,	0.,	-1.,
0.,	0.,	0.,	0.,	1.,	0.,
0.,	0.,	0.,	0.,	1.,	0.,
0.,	0.,	0.,	0.,	1.,	0.,
0.,	0.,	0.,	0.,	1.,	0.,
0.,	0.,	0.,	0.,	1.,	0.,
0.,	0.,	0.,	0.,	1.,	0.,

Results of the computation for the primary phase inductances of both 2-pole and 6-pole systems are as follows:

$$[L_{phase}] = \begin{bmatrix} 29.5140 & -7.3890 & -13.6950 & 7.3110 & 7.3110 & -.2830 \\ -7.3890 & 29.5140 & -13.6950 & 7.3110 & 7.3110 & -.2830 \\ -13.6950 & -13.6950 & 29.5140 & -10.1220 & -10.1220 & -2.5280 \\ 7.3110 & 7.3110 & -10.1220 & 40.2560 & -10.6250 & -19.7360 \\ 7.3110 & 7.3110 & -10.1220 & -10.6250 & 40.2560 & -19.7360 \\ -.2830 & -.2830 & -2.5280 & -19.7360 & -19.7360 & 40.2560 \end{bmatrix}$$

All the inductances presented in the above matrix are in milli-Henry.

5.3 Secondary Impedance Z_{rr}

As it was described in chapter 3, secondary of the LBDFM consists of 8 identical flat sections in which, each section contains 4 nested loops made of aluminum. Unlike the rotary machine, these nested loops are not located in slots. However, for calculation of the self and mutual inductance of the nested loops, the assumption of a slotted secondary instead of considering the actual geometry of the loops, will not significantly affect the final answer for inductance calculations. By looking at the expressions derived for calculation of

the self and mutual inductances, there is a relative flux linkages between any pair of coils which determines the amount of mutual couplings that exist between those two coils. This factor can be expressed either in physical distance (meter) or other divisions like slot number. Therefore, relative to the primary core, we can assume that all these aluminum loops and edge bars are placed in slots which correspond to the whole segment of the primary. Hence, by measuring the width of the aluminum arms and counting them, for a whole corresponding segment of secondary which contains four nested sections each with four loops on the flat end bars, 44 slots for the secondary can be assumed in which 28 slots are considered to be filled with aluminum arms. Although all these loops and edge bars are not so well evenly spaced, the error for calculation of inductances would not be significant.

5.3.1 Secondary Loop Resistances

By having each loop geometry, resistivity of material, and cross-sectional area, the dc resistance of any loop of the secondary can be obtained using:

$$R = \frac{l}{\gamma A}$$

Where;

R = DC resistance of a conductor in [Ω] @ 20° C.

γ = Conductivity of the material which for aluminum at 20° centigrade is 36 [meter/(Ω mm^2)].

l = Length of the conductor in [meter].

A = Cross-sectional area of conductor in [mm^2].

Resistance (R) of conductor at any particular temperature β in degrees centigrade can be found from:

$$R = R_{20} [1 + \alpha (\beta - 20^{o} C)]$$

where;

R_{20} = Resistance of a conductor @ 20° C in [Ω].

α = Temperature coefficient which for aluminum at 20 degree centigrade is 0.0039 [1/° C].

β = Any particular temperature.

To approximate the 60 Hz ac value of the resistances, we can simply multiply the calculated values (i.e. dc) by 115% .

The followings are the results of calculations for secondary loop resistances at 65° C and 60 Hz.

Rw = 3.2840E-4 [OHM]
Rx = 4.6890E-4 [OHM]
Ry = 4.2603E-4 [OHM]
Rz = 3.2890E-4 [OHM]

5.3.2 Secondary Loop Self-Inductances

Using the assumption in section 5.3, total number of slots for the secondary would be 44. Therefore, in each nest of the secondary four loops are located. The loop spans are : W=5, X=7, Y=9, and finally Z=11. The order of W, X, Y, and Z are from inside toward the edge shown in Figure 5.3.2.1.

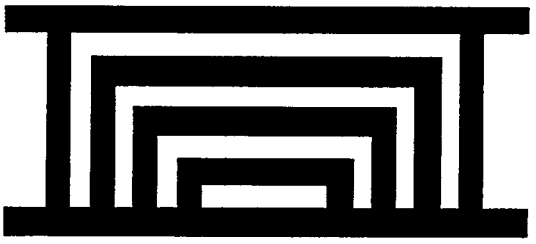

Fig. 5.3.2.1 Loop spans of the secondary

This configuration is similar to a 4 coil group winding in which, each

coil has only one turn. Therefore, to find the self inductance of each loop of the secondary, an equation similar to that used in section 5.1.1, can be written as:

$$L_r = \frac{\mu_0 L D (R - C) C}{g R^2}$$

Where in this equation:

L_r = Secondary loop self inductance in [H].

R = Total number of secondary slots.

C = Span of the secondary loops. This factor for each time of calculation is replaced by W, X, Y, and Z.

Other parameters have been defined before.

5.3.3 Secondary Mutuals Within the Same Nest

To find the mutual between any pair of loops within a particular nest, due to the consideration of positive and negative fluxes produced by induced unit current, the equation used in section 5.1.2 can be modified to:

$$M_{w,x} = \frac{\mu_0 L D}{g R^2} (W.R - W.X)$$

Where:

$M_{w,x}$ = Mutual inductance between loops W and X in [H].

Parameters W and X can be substituted by other loop spans such as Y and Z to find the mutual between other loops as appropriate.

5.3.4 Secondary Mutuals Between Different Nests

Based on flux distribution pattern described in section 5.2.1, it is clear that there is always negative linkage between loops located in different nests. Therefore, the mutual inductance between loops e.g. W of one of the nests and X' of any other nests, is always negative. Hence, mutual inductance in this case is a result of following expression.

$$M_{w,x'} = -\frac{\mu_0 L D W X}{g R^2}$$

Where:

$M_{w,x'}$ = Mutual inductance between loop "W" of one nest to loop "X" of adjacent nest in [H].

By applying appropriate substitution for W and X, mutual inductances between any other loops of the secondary can be obtained.

The followings are the results of the secondary loops self and mutual inductance computations for each nest and any two adjacent nests.

```
SECONDARY SELF INDUCTANCES IN ORDER OF W-X-Y-Z
   1      .16554E-05
   2      .20911E-05
   3      .24686E-05
   4      .27881E-05
SECONDARY MUTUALS WITHIN THE SAME NEST IN ORDER W-X-Y-Z
   1        2      .15683E-05
   1        3      .14812E-05
   1        4      .13940E-05
   2        3      .19749E-05
   2        4      .18587E-05
   3        4      .23234E-05
SECONDARY MUTUALS BETWEEN DIFFERENT NESTS IN ORDER W-X-Y-Z
   1        1     -.26138E-06
   1        2     -.34851E-06
   1        3     -.43564E-06
   1        4     -.52276E-06
   2        2     -.46468E-06
   2        3     -.58085E-06
   2        4     -.69702E-06
   3        3     -.72606E-06
   3        4     -.87127E-06
   4        4     -.10455E-05
```

5.4 Primary to Secondary Mutual Computation

The mutual inductance between any loop of the secondary and any coil of the primary depends upon the relative displacement

between primary and secondary. Therefore, mutual inductances vary depending on where the loops are located at any instant of time. Figure 5.4.1 (a) explicitly shows relative location of coil #1 of the primary and one nest of the secondary at the time zero as an example. In this figure, it is assumed that axis of coil #1 and axis of the secondary nest have zero displacement at first. Figure (b) shows some time after when coil #1 is displaced from that nest by "Angle" degree.

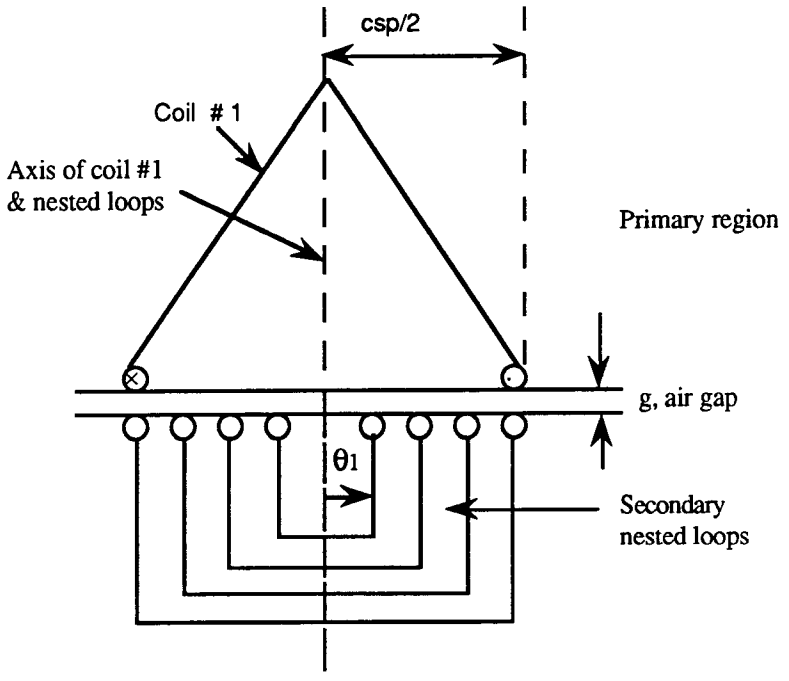

(a)

Fig. 5.4.1 Relative displacement of primary coil & secondary nest

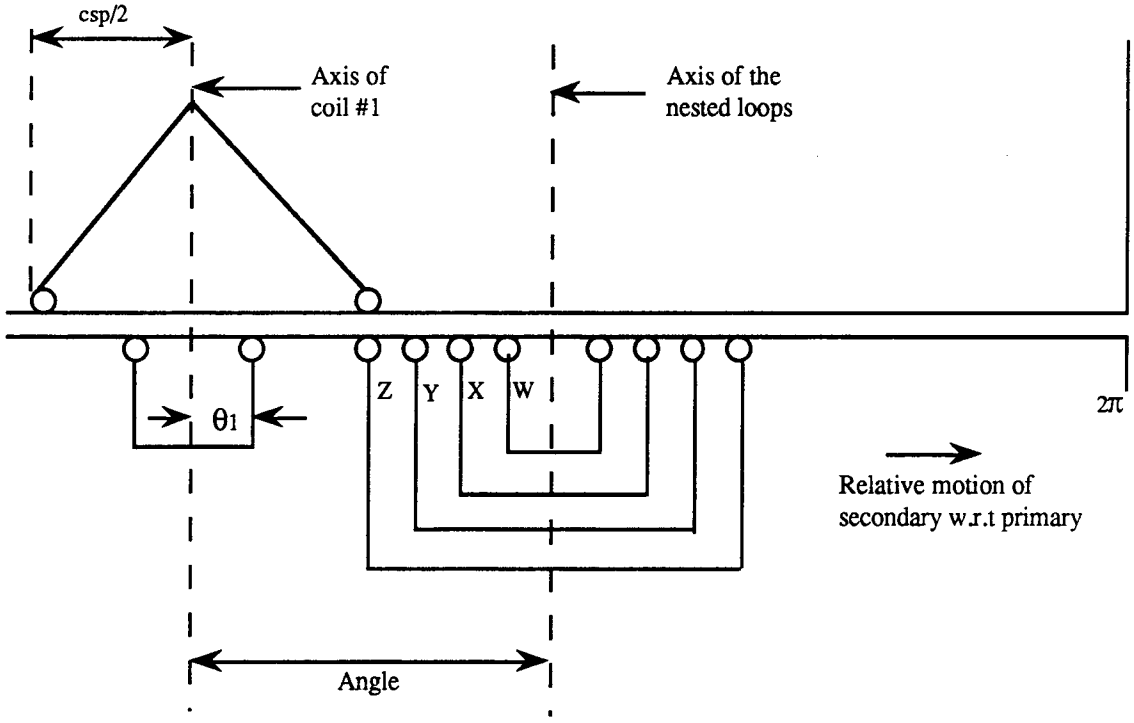

(b)

Fig. 5.4.1 continued

By examination of Figure 5.4.1, it can be shown that if;

$0 < \text{Angle} < \text{csp}/2 - \theta_i$, then $M_{ps} = M^+$, where M^+ stands for a constant and positive mutual inductance, M_{ps} presents mutual inductance between primary coil and secondary loop, "csp" denotes to coil span of the primary, and θ_i is the representation of the nested loops displacement to their axis. The next scenario is when the

mutual starts to decrease with a slope at:

$$csp/2 - \theta_1 < Angle < csp/2 + \theta_1$$

At this time mutual inductance can be written:

$$M_{ps} = M^+ - slope[\ Angle - (csp/2 - \theta_1)]$$

where:

$$M^+ = \frac{\mu_o N L D(S - csp)W}{g S R}$$

The slope between these points is:

$$slope = \frac{dM}{d\theta} = \frac{\mu_o N L D(2csp - S)}{2\pi g S}$$

The next region is when:

$$csp/2 + \theta_1 < Angle < 360 - csp/2 - \theta_1$$

At this time the mutual would be constant and negative:

$$M_{ps} = M^-$$

where the magnitude of the negative constant inductance can be written as:

$$M^- = \frac{\mu_o N L D\ csp\ W}{g S R}$$

At the time that:

$$360 - csp/2 - \theta_1 < Angle < 360 - csp/2$$

the mutual starts to increase from its negative value with a slope. Therefore:

$$M_{ps} = M^{-} + \text{slope}[\text{ Angle} - (360 - csp/2 - \theta_1)]$$

The last region for a whole period of movement of loop "W" with respect to the primary coil is when:

$$360 - csp/2 < \text{Angle} < 360$$

At this region, the mutual has its positive and constant value as M^{+}.

The mutual magnitudes (both M^{+} & M^{-}) and mutual inductance over the whole period of relative movement (360^{o}) of any primary coil with other loops of each nest can be obtained by replacing W to X, Y, or Z as appropriate. By applying the above principle into a program, the mutual inductance between all the loops of the secondary nests and any particular coil of the primary for each degree of relative movement over 360^{o} were obtained. Figures 5.4.2 through 5.4.7 show the mutual inductance between coils of phase "A" of the 6-pole system and loops W, X, Y, and Z of a secondary nest. As it can be observed from the figures, since all the six coils of phase A of the 6-pole system are distributed in slots (1,2 and 7,8), (13,14 and 19,20), and finally (25,26 and 31,32), the magnitude of mutual inductances remain the same but shifted with respect to correspondent coils over a whole

period of motion. Figures 5.4.8 through 5.4.13 show the variation of mutual inductances of all six coils of phase "a" of the 2-pole system and all the loops of a secondary nest respectively. Winding distribution of the 2-pole system is such that all the coils belonged to each phase are close and placed one after another. Therefore, the magnitude of mutual inductances are slightly shifted.

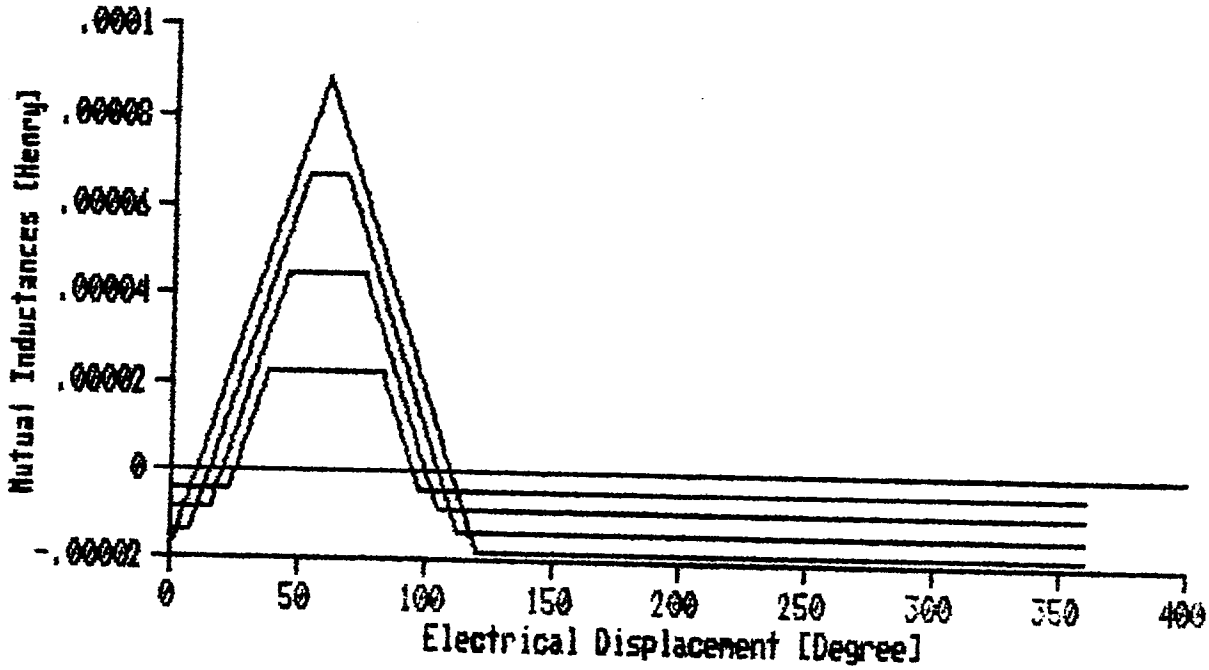

Fig. 5.4.2 Primary coil #1 of phase A of 6-pole & secondary loops mutuals

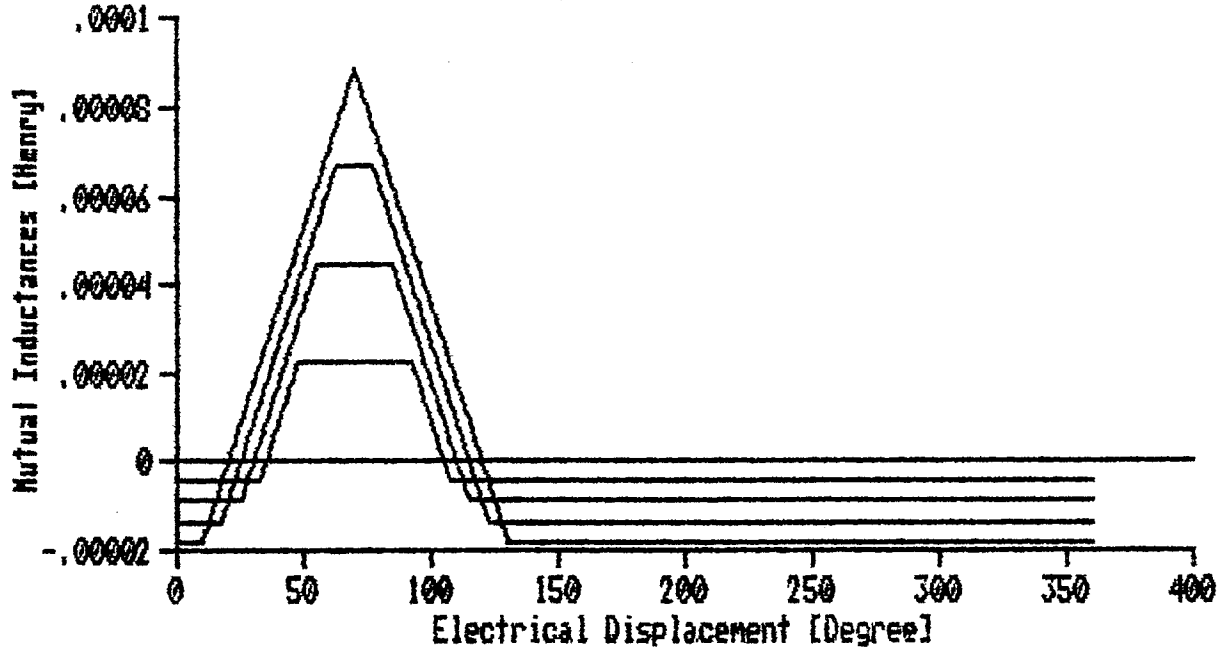

Fig. 5.4.3 Primary coil #2 of phase A of 6-pole & secondary loops mutuals

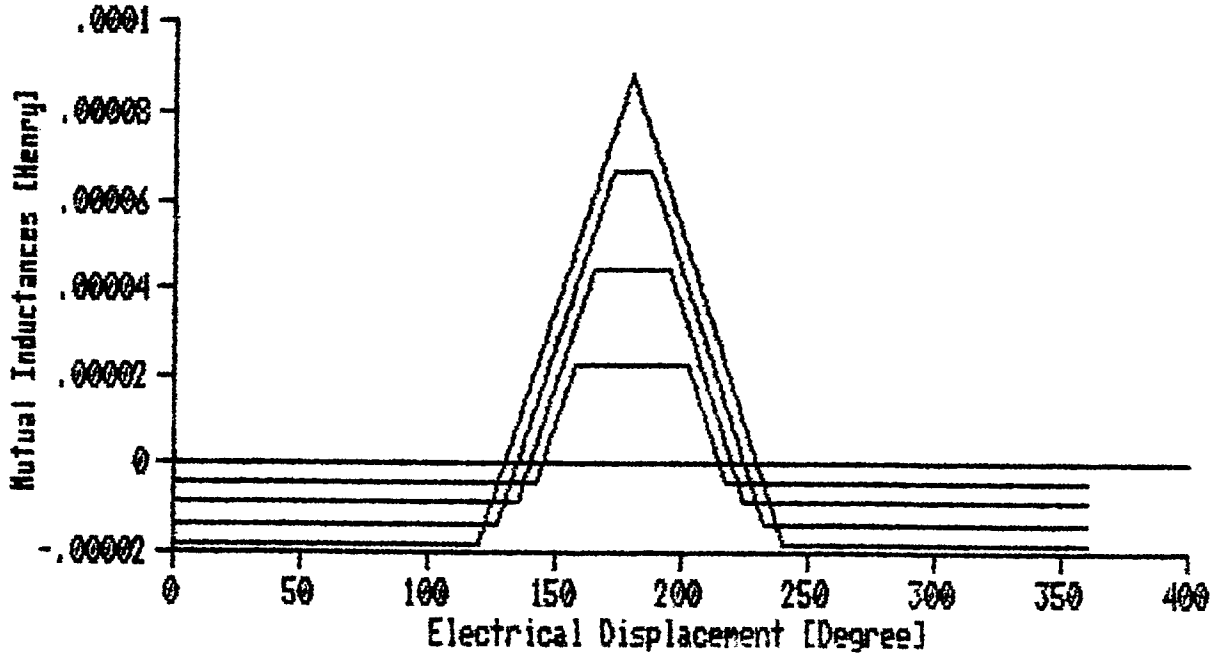

Fig. 5.4.4 Primary coil #3 of phase A of 6-pole & secondary loops mutuals

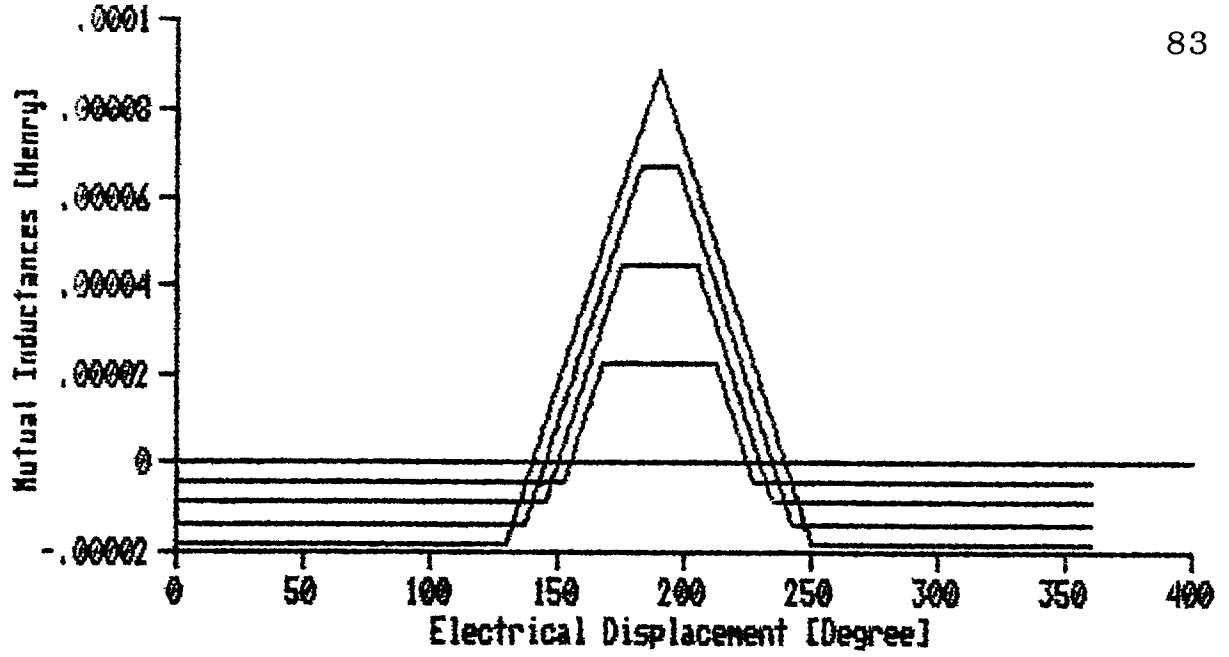

Fig. 5.4.5 Primary coil #4 of phase A of 6-pole & secondary loops mutuals

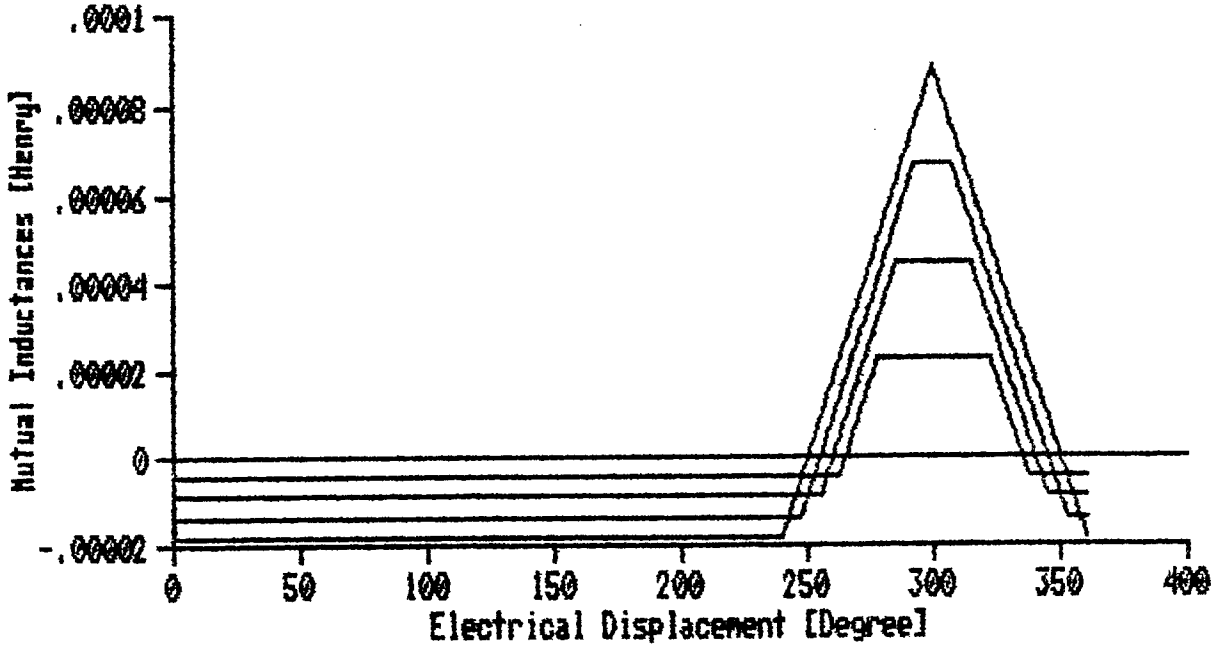

Fig. 5.4.6 Primary coil #5 of phase A of 6-pole & secondary loops mutuals

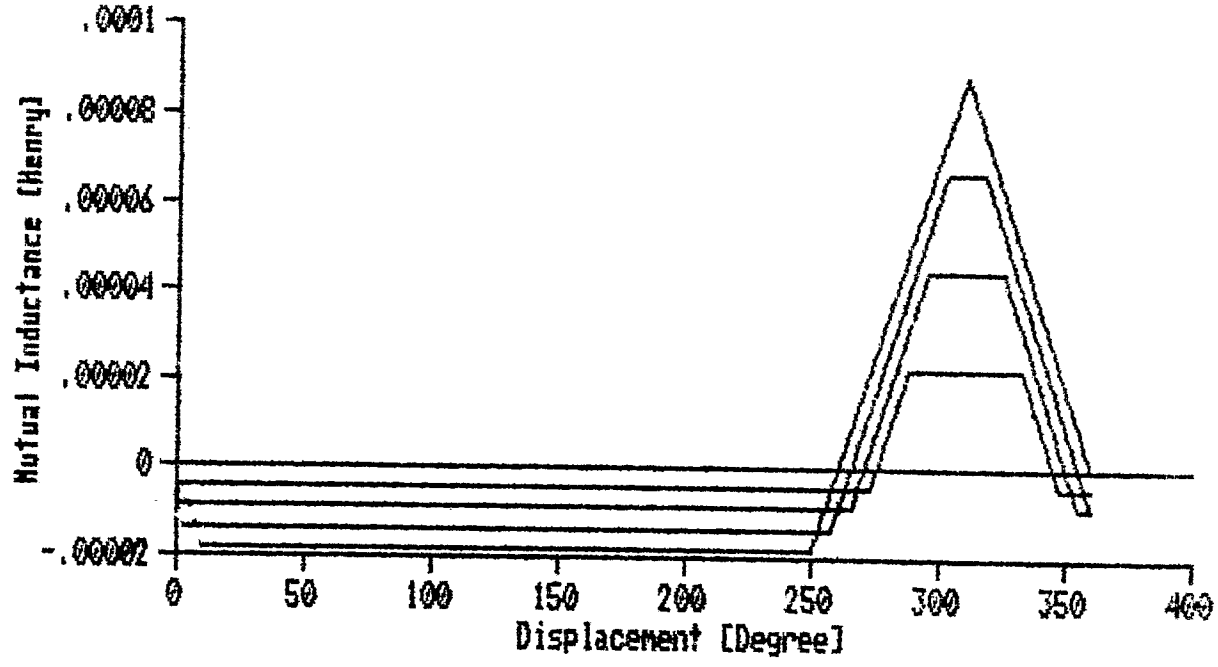

Fig. 5.4.7 Primary coil #6 of phase A of 6-pole & secondary loops mutuals

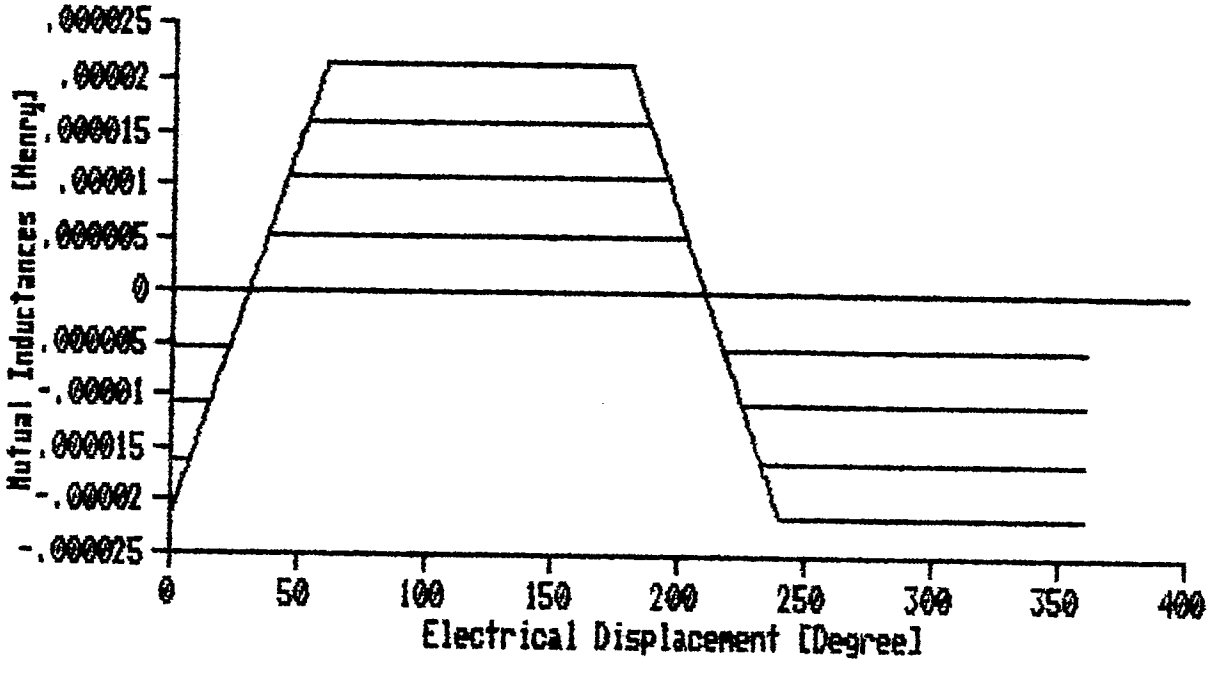

Fig. 5.4.8 Primary coil #1 of phase "a" of 2-pole & secondary loops mutuals

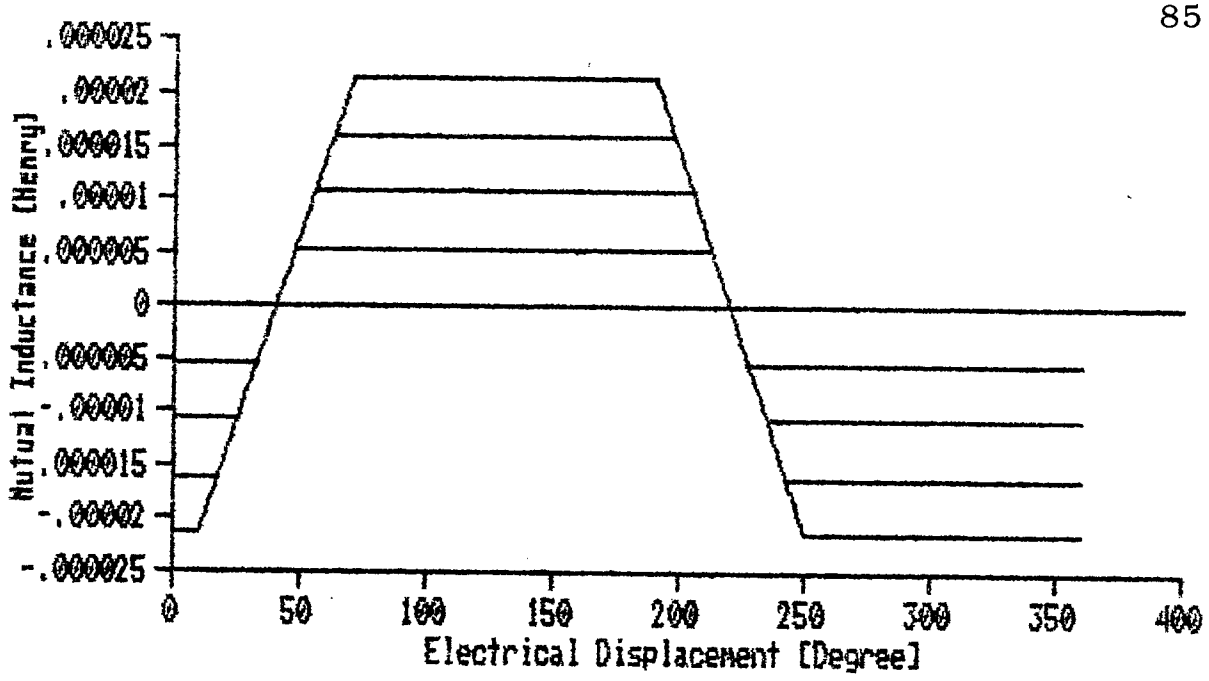

Fig. 5.4.9 Primary coil #2 of phase "a" of 2-pole & secondary loops mutuals

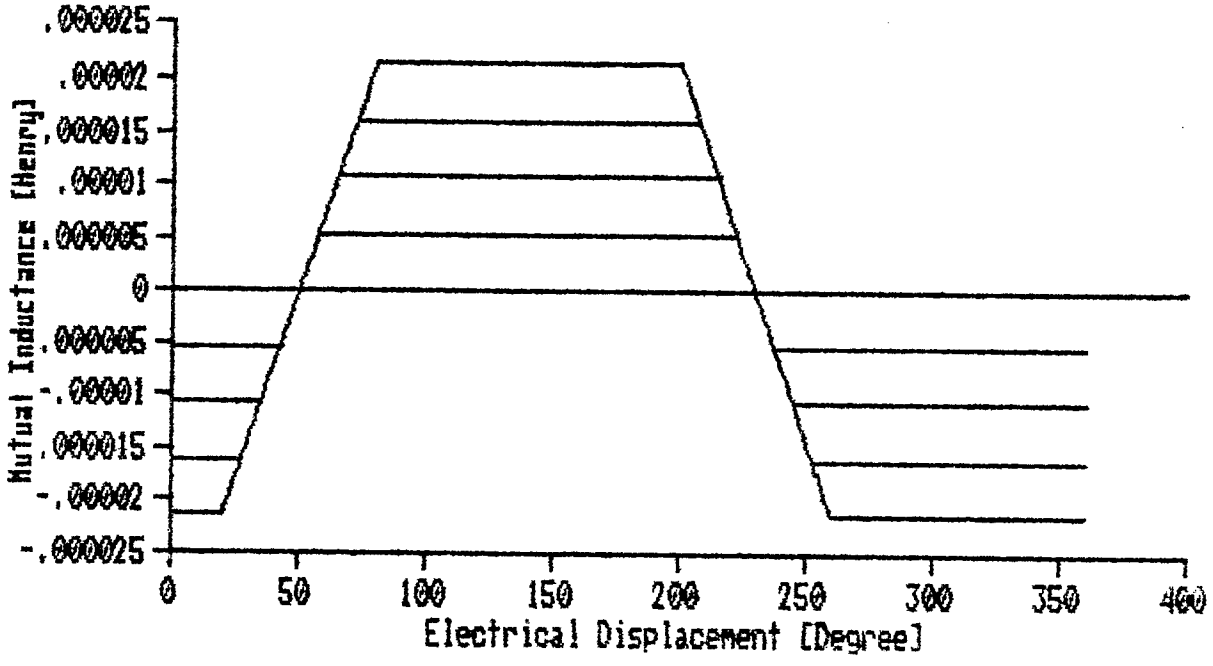

Fig. 5.4.10 Primary coil #3 of phase "a" of 2-pole & secondary loops mutuals

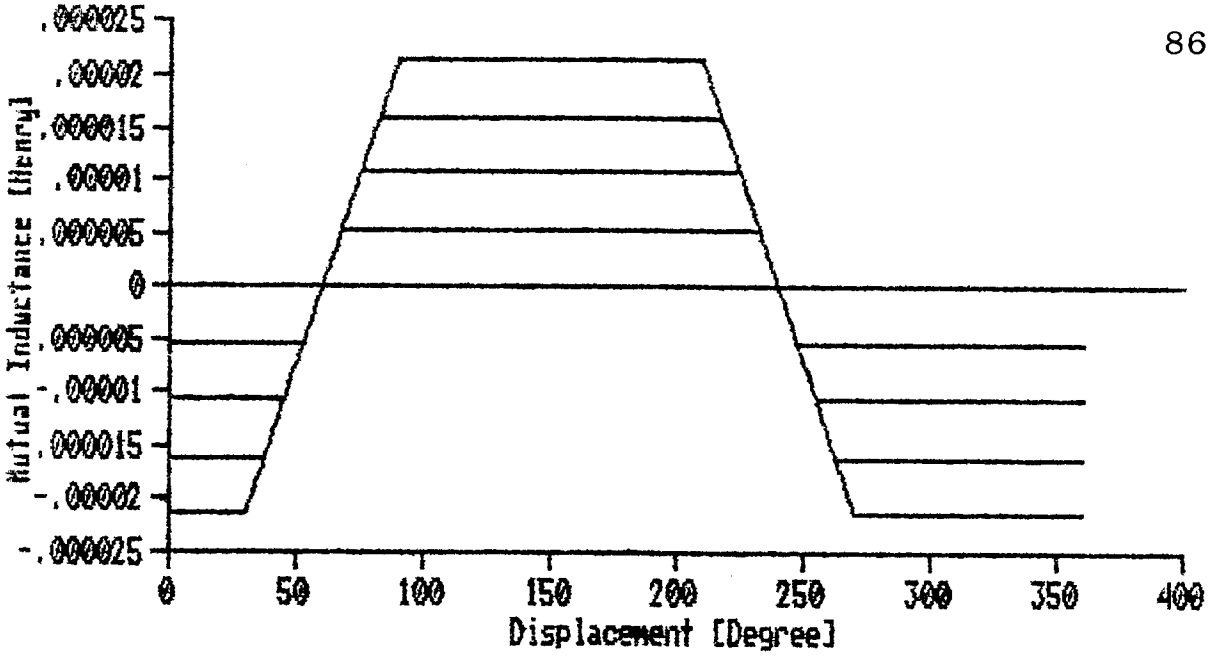

Fig. 5.4.11 Primary coil #4 of phase "a" of 2-pole & secondary loops mutuals

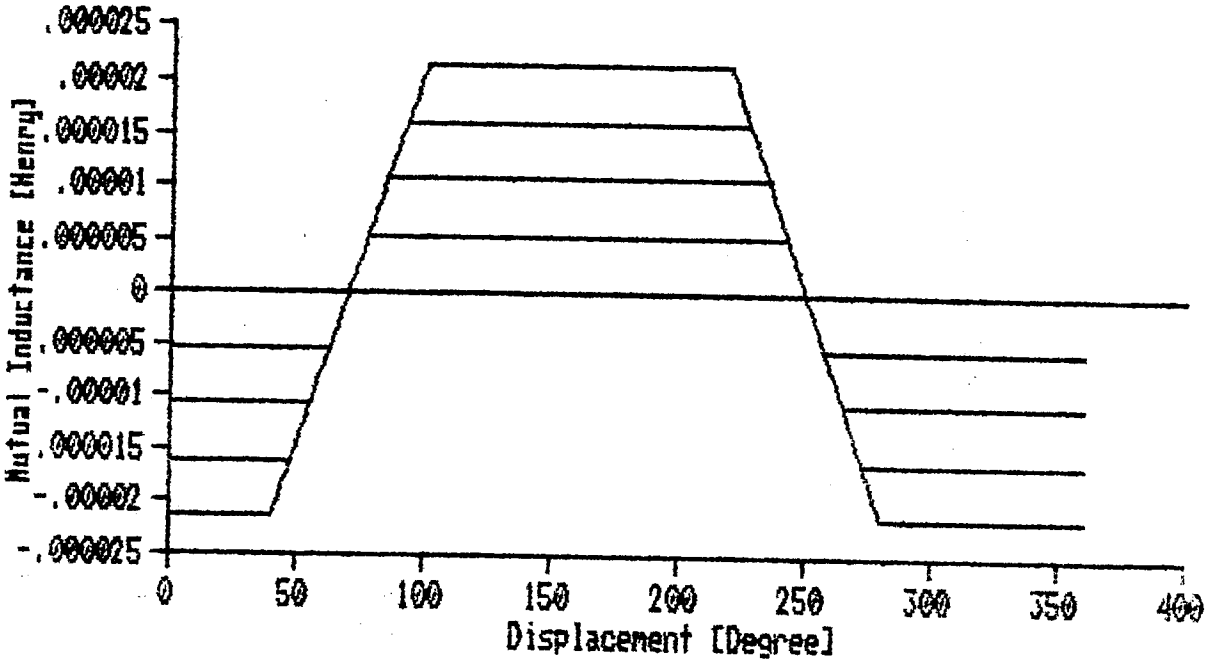

Fig. 5.4.12 Primary coil #5 of phase "a" of 2-pole & secondary loops mutuals

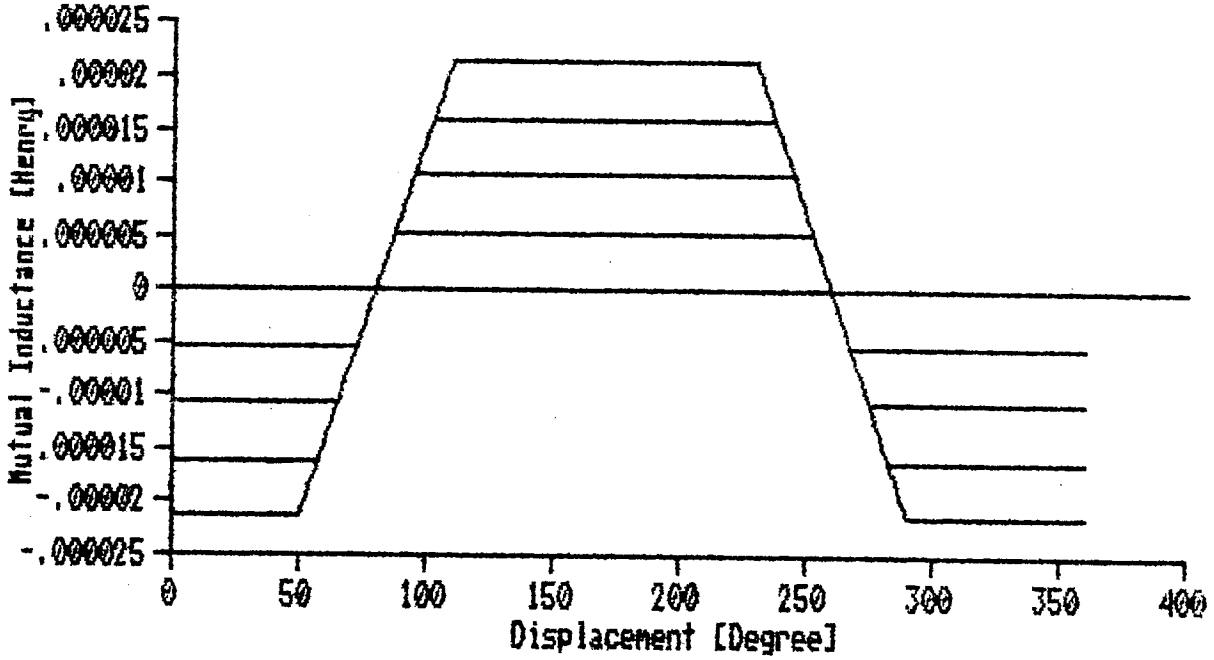

Fig. 5.4.13 Primary coil #6 of phase "a" of 2-pole & secondary loops mutuals

The mutual inductances of the remaining coils (coils of the other phases) of both 6 & 2-pole systems can be simply obtained by running the program and plotting the data for those particular coils of the primary. These mutuals are exactly identical to those shown in the figures but shifted due to the mechanical degree separation of each slot of the primary by 10^o ($\alpha_{me} = 360^o/S = 10^o$).

5.5. Discussion on Equivalent Circuit

Now that all the machine parameters based upon the geometry

and specifications of the prototype have been identified, the attempt to possibly develop an equivalent circuit for this device can now be investigated. The equivalent circuit for the rotary BDFM can be derived from the two-axis model and development [12-13]. In a rotary machine in which the windings share a common magnetic circuit, mutual independence between the stator windings can be achieved only by designing the 3-phase windings for different number of poles [5-6]. In other words, if a single winding is to act as doubly fed system, it should be one pole number for one set terminals and of a second pole number for second terminals. This avoids flow of current from either of the supplies to the other. Windings developed for this purpose have been described in references [5] and [10] for the rotary BDFM. The winding layout for the LBDFM in the case where both 3-phase systems have common winding, was pointed out in the previous chapter of this thesis, and advantages and disadvantages of this type of winding configuration for the linear counterpart of the BDFM was addressed.

Incidentally, there are two sets of 3-phase systems on the flat primary having different number of poles (in this case for our laboratory prototype, 6-pole and 2-pole) and a secondary system which

behaves and interacts with both fields forced by the primary. Therefore, for a system with three electrically isolated properties, voltage equations can be expressed as follows:

$$\begin{bmatrix} V_{s6} \\ V_{s2} \\ V_r \end{bmatrix} = \begin{bmatrix} Z_{s6} & Z_{s6,s2} & Z_{s6,r} \\ Z_{s2,s6} & Z_{s2} & Z_{s2,r} \\ Z_{r,s6} & Z_{r,s2} & Z_r \end{bmatrix} \cdot \begin{bmatrix} i_{s6} \\ i_{s2} \\ i_r \end{bmatrix}$$

In this matrix equation, indexes s6, s2, and r indicate parameters and properties of the 6-pole, 2-pole, and secondary systems respectively. The sub matrices Z_{s6} and Z_{s2} represent the primary 6-pole and 2-pole impedance matrices. $Z_{s6,s2}$ express the mutual impedance matrix between 6-pole and 2-pole systems of the primary. Sub matrices $Z_{s6,r}$ and $Z_{s2,r}$ each represents the mutual inductance matrices between 6 and 2-pole systems and secondary nested loops respectively and are 3 by 16 primary-secondary displacement dependent matrices since the corresponding secondary segment consists of totally 16 loops. Finally Z_r represents impedance matrix of the secondary system and is a 16 by 16 matrix. It is significant to point out that elements of matrices Z_{s6}, Z_{s2}, and Z_r are all independent from the relative displacement and motion between the primary and secondary. The only

displacement dependent terms in the Z matrix are $Z_{s6,r}$ and $Z_{s2,r}$ ($Z_{r,s6}$ and $Z_{r,s2}$ are transpose of $Z_{s6,r}$ and $Z_{s2,r}$ respectively). This phenomenon was experimentally observed in the research lab while the parameters measurement task was underway. It is also mathematically proven in references [20] and [21] that rotor displacement angle does not affect the self and mutual inductances of the stator in non-salient induction machines. The assumption of neglecting direct coupling between the 6-pole and the 2-pole systems [5-6-12], drives the elements of sub matrix $Z_{s6,s2}$ and its transpose to zero. Therefore, the matrix form equation expressed earlier in this section can be simplified by substituting zero terms for $Z_{s6,s2}$ and its transpose.

By transforming three balanced phase to two balanced d_s and q_s phases in space quadrature, and finally two phase to two axis stationary reference frame transformation, the d-q model of the rotary BDFM has been obtained [12-13]. Figure 5.5.1. illustrates the equivalent circuit for the rotary BDFM for the steady-state synchronous operation. In this model, parameters are defined as follows:

r_{s6} = 6-pole winding phase resistance

L_{ls6} = 6-pole winding phase leakage inductance

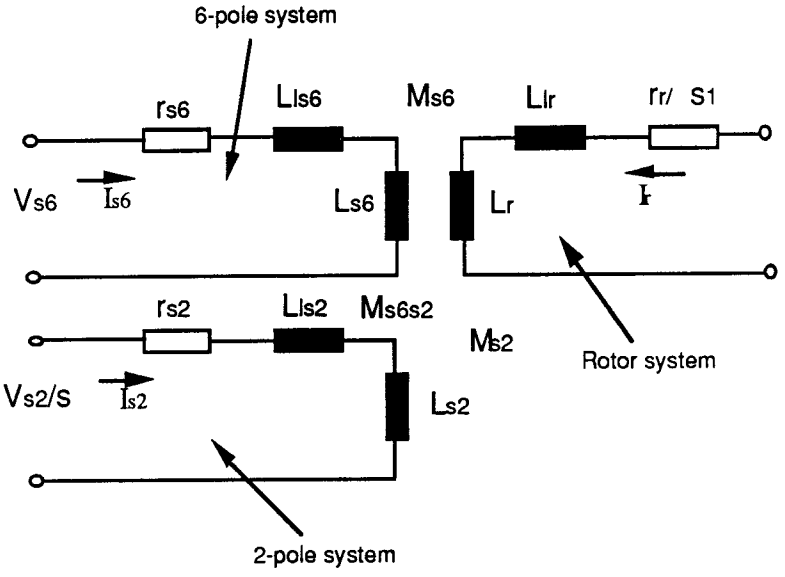

Fig. 5.5.1 Per-phase equivalent circuit of the rotary BDFM

L_{s6} = 6-pole winding phase magnetizing inductance.

M_{s6} = 6-pole to rotor mutual inductance.

r_{s2} = 2-pole winding phase resistance.

L_{ls2} = 2-pole winding phase leakage inductance.

L_{s2} = 2-pole winding phase magnetizing inductance.

M_{s2} = 2-pole to rotor mutual inductance.

M_{s6s2} = 6-pole to 2-pole mutual inductance.

r_r = rotor resistance.

L_{lr}= rotor leakage inductance.

L_r = rotor magnetizing inductance.

s_6= 6-pole slip.

s_2= 2-pole slip.

s= overall slip and is equal to f_2/f_6 .

5.6 Parameter Calculation of the Equivalent Circuit

From [12-20-21] due to the perfect symmetry of the magnetic path in the stator of the rotary BDFM and Induction motors, the self and mutual inductance matrices for both 6-pole and 2-pole systems of the stator have the forms:

$$L_{s6}=\begin{bmatrix} L_A & -\frac{1}{2}L_A & -\frac{1}{2}L_A \\ -\frac{1}{2}L_A & L_A & -\frac{1}{2}L_A \\ -\frac{1}{2}L_A & -\frac{1}{2}L_A & L_A \end{bmatrix} \text{ and } L_{s2}=\begin{bmatrix} L_a & -\frac{1}{2}L_a & -\frac{1}{2}L_a \\ -\frac{1}{2}L_a & L_a & -\frac{1}{2}L_a \\ -\frac{1}{2}L_a & -\frac{1}{2}L_a & L_a \end{bmatrix}$$

Where $-1/2(L_A)$= -M and $-1/2(L_a)$= -m. (Stator's 6 and 2-pole leakage inductances are included in L_A and L_a respectively). This property makes the d-q-0 transformed matrices balanced and symmetrical with

off diagonal terms zero as shown here:

$$Z_{dq0\text{-}6} = \begin{bmatrix} Z_{d6} & 0 & 0 \\ 0 & Z_{q6} & 0 \\ 0 & 0 & Z_{06} \end{bmatrix} = \begin{bmatrix} r_6+(L_A-M)p & 0 & 0 \\ 0 & r_6+(L_A-M)p & 0 \\ 0 & 0 & r_6+L_{16}p \end{bmatrix}$$

and for the 2-pole of the stator:

$$Z_{dq0\text{-}2} = \begin{bmatrix} Z_{d2} & 0 & 0 \\ 0 & Z_{q2} & 0 \\ 0 & 0 & Z_{02} \end{bmatrix} = \begin{bmatrix} r_2+(L_a-m)p & 0 & 0 \\ 0 & r_2+(L_a-m)p & 0 \\ 0 & 0 & r_2+L_{12}p \end{bmatrix}$$

As it is seen from these equations, parameters in the first and second row associated with "d" and "q" pseudo stationary systems are identical and represent per-phase quantities of the equivalent circuit under steady state condition. In the Linear BDFM, however, due to the openness of the magnetic path, nature of the windings which are not physically balanced, and end-effect phenomenon, the 6-pole and the 2-pole inductance matrices are not in the form similar to the rotary machine. These sub-matrices (L_{s6} and L_{s2}) for the Linear BDFM, were obtained from the detailed computation of the machine parameters presented in sections 5.1.2(a) and 5.1.2(b) for the 6-pole and 2-pole

systems respectively. By approximating the ratio of the self to mutual inductances of each system, the inductance matrices for both systems of the primary can be written as follows:

$$L_{s6}=\begin{bmatrix} L_A & -\frac{1}{4}L_A & -\frac{1}{2}L_A \\ -\frac{1}{4}L_A & L_A & -\frac{1}{2}L_A \\ -\frac{1}{2}L_A & -\frac{1}{2}L_A & L_A \end{bmatrix} \text{ and } L_{s2}=\begin{bmatrix} L_a & -\frac{1}{4}L_a & -\frac{1}{2}L_a \\ -\frac{1}{4}L_a & L_a & -\frac{1}{2}L_a \\ -\frac{1}{2}L_a & -\frac{1}{2}L_a & L_a \end{bmatrix}$$

As it is seen from the above equations, the mutual inductances between phases of both systems of the primary are not identical. In other words, these matrices are not balanced. By applying the three-phase to two-axis transformation to the above three-phase sub matrices of 6-pole and 2-pole, following models were obtained for the d-q-o equivalent inductance matrices of the primary. The transformation matrix is changed so that $(K_s)^T = (K_s)^{-1}$. The transformation matrix used for this analysis is in the primary reference frame as follows:

$$K=\sqrt{\frac{2}{3}}\begin{bmatrix} \cos\theta & \cos(\theta-\frac{2\pi}{3}) & \cos(\theta+\frac{2\pi}{3}) \\ \sin\theta & \sin(\theta-\frac{2\pi}{3}) & \sin(\theta+\frac{2\pi}{3}) \\ \frac{1}{\sqrt{2}} & \frac{1}{\sqrt{2}} & \frac{1}{\sqrt{2}} \end{bmatrix}$$

Therefore;

$$Z_{dqo\text{-}6} = K^{-1} Z_{s6} K = \frac{2}{3} L_A \begin{bmatrix} 2\frac{1}{4} & \frac{\sqrt{3}}{8} & \frac{\sqrt{2}}{16} \\ \frac{\sqrt{3}}{8} & \frac{3\sqrt{3}+3}{8} & \frac{\sqrt{6}}{16} \\ \frac{\sqrt{2}}{16} & \frac{\sqrt{6}}{16} & \frac{1}{4} \end{bmatrix}$$

and for the 2-pole:

$$Z_{dqo\text{-}2} = K^{-1} Z_{s2} K = \frac{2}{3} L_a \begin{bmatrix} 2\frac{1}{4} & \frac{\sqrt{3}}{8} & \frac{\sqrt{2}}{16} \\ \frac{\sqrt{3}}{8} & \frac{3\sqrt{3}+3}{8} & \frac{\sqrt{6}}{16} \\ \frac{\sqrt{2}}{16} & \frac{\sqrt{6}}{16} & \frac{1}{4} \end{bmatrix}$$

In these equations, unlike d-q-o model of the rotary BDFM, off-diagonal terms are non-zero terms. From this mathematical expression, it may be interpreted that there is a mutual coupling between the d, q, and zero components of the two-axis model of the primary system which makes the analysis of the LBDFM more difficult and prevents the derivation of a simple equivalent circuit similar to its rotary counterpart.

By proving the above fact, it is unnecessary to continue work on derivation of the d-q-o model for the secondary system of the LBDFM. As it can be predicted from the above analysis, since the LBDFM has a flat secondary circuit with open magnetic path, the result of the transformation for the d-q-o model of the secondary would be fruitless. The purpose of deriving a two-axis model for this device is to simplify the analysis and performance evaluation. The obtained models for the primary systems of the machine not only provide a simpler path for performance study, but introduce more analytical problems to be solved.

Therefore, further studies and trying other tools and techniques need to be investigated to possibly derive an equivalent circuit for the LBDFM. For the sake of discussion, it is possible to make a balanced system out of an unbalanced machine by implementing the compensation windings to the primary to make those 6-pole and 2-pole 3-phase matrices balanced. This criterion indeed would make the design process of the machine much more complicated especially for the secondary system.

6. PARAMETER MEASUREMENT OF THE LBDFM

Up to this point, all the parameters of the machine have been calculated based on the theoretical analysis and classical procedures. It is now necessary to evaluate parameters of the machine based on measurement. Also by using appropriate techniques to compare the results of the theoretical investigation and measured quantities to ensure that there is a correlation between a mathematical model and the actual device.

6.1 Machine Impedances

Incidentally, the prototype has two distinct 3-phase windings of 6-pole and 2-pole in the primary. Figure 6.1.1 shows the representation of both windings in the primary. Terminals A, B, and

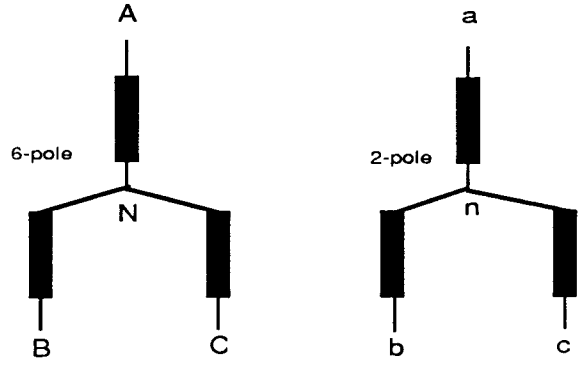

Fig. 6.1.1 Representation of the primary coils.

C denote the leads of phases of 6-pole set. For the ease of measurements both systems were connected in *"wye"*, therefore, terminals A', B', and C' which are the ends of the phase coil groups of 6-pole, are connected together and make one node indicated by letter N. Terminals a, b, and c denote leads of the 2-pole set and n is the center of the*"wye"*.

For parameter measurements of the machine, we are limited to measure merely primary circuits since secondary circuits are not accessible to apply any measurement technique. Consequently, we can not have a measured value for the self inductances of nested loops, mutual inductances within a nest and any two adjacent nests, and mutual inductances between the primary coils and secondary loops.

6.2 Primary Impedances

6.2.1 Phase Resistances

For phase resistance measurements since the neutral point and the ends of all phases are brought out, we can directly measure dc value of phase resistances and with an accepted approximation

multiply them by 1.15 to correct for skin effects and hence obtain the 60 Hz ac values. For this measurement, a very accurate bridge from the instrumentation lab was used to get very precise values. The measured dc values of phase resistances at room temperature corrected by 15% are as follows:

6-pole	2-pole
R_A = 1.798 [Ω]	R_a = 0.844 [Ω]
R_B = 1.812 [Ω]	R_b = 0.842 [Ω]
R_C = 1.819 [Ω]	R_c = 0.860 [Ω]

Referring to the calculated values presented in chapter 4, it is evident that the measured and calculated values correlate reasonably well. The small percentage of error between these two sets of quantities are probably due to the unbalance of the windings and errors in the estimation of the coil length.

6.2.2 Primary Self & Mutual Inductances

To do this task, a system of two coils was considered for each

phase of measurement. Figure 6.2.1, shows such a test strategy circuit for this purpose. The procedure for inductance measurement

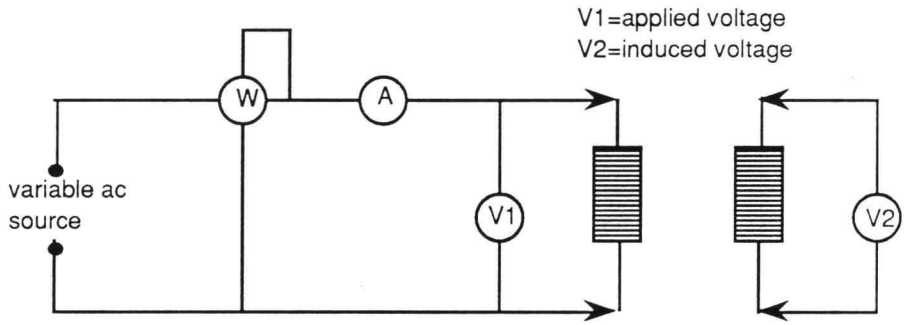

Fig. 6.2.1 Test circuit for inductance measurement

can be implemented by measuring voltages, currents, and power of the above circuit. The first step is to excite one phase at a time with an ac source and measure the current passing through that coil, applied voltage, power and, finally the induced voltages across all the other coils. It is important to provide a magnetic path for the fluxes produced each time by the excited coils. Thus, for this purpose a stack of steel laminations was placed on the top of the primary core. These steel laminations virtually covered the whole surface of the primary core. A constant air gap of 5 [mm] was maintained during the entire procedure. This experiment first was done by using regular cold rolled steel (in the form of the steel channel) as the

magnetic path. The results of measurement were significantly improved when laminated iron was used as a magnetic path. This improvement could be due to the decrease in eddy currents and better magnetic material with better B-H characteristic than regular steel. Applying this technique, phase values of the self and mutual inductances for both systems can be determined. These values can be shown in a matrix form as below:

$$L_{ss} = \begin{bmatrix} L_{66} & L_{62} \\ L_{26} & L_{22} \end{bmatrix}$$

Where each element of the above matrix is defined as:

$$L_{66} = \begin{bmatrix} L_{AA} & L_{AB} & L_{AC} \\ L_{BA} & L_{BB} & L_{BC} \\ L_{CA} & L_{CB} & L_{CC} \end{bmatrix}$$

2-pole self and mutuals:

$$L_{22} = \begin{bmatrix} L_{aa} & L_{ab} & L_{ac} \\ L_{ba} & L_{bb} & L_{bc} \\ L_{ca} & L_{cb} & L_{cc} \end{bmatrix}$$

6-pole to 2-pole mutuals:

$$L_{62} = \begin{bmatrix} L_{Aa} & L_{Ab} & L_{Ac} \\ L_{Ba} & L_{Bb} & L_{Bc} \\ L_{Ca} & L_{Cb} & L_{Cc} \end{bmatrix}$$

and finally 2-pole to 6-pole mutuals, L_{26}, which a transpose of L_{62}, i.e.

$$[\, L_{26} \,] = [\, L_{62} \,]^T$$

Based on described test procedure, each phase coil of both 3-phase systems was individually excited and the following measurements, shown in table 6.2.1, were obtained.

Excited Coils	I[amp]	P[w]	VAN	VBN	VCN	Van	Vbn	Vcn
A N	3.60	21.10	50.25	6.15	22.90	12.81	17.12	3.88
B N	3.67	22.00	6.28	50.20	23.00	16.41	12.31	2.91
C N	3.75	21.00	22.80	22.47	50.02	18.14	18.45	0.7
a n	3.19	13.00	11.27	14.02	15.96	50.43	2.40	28.25
b n	3.26	13.10	15.34	10.90	16.64	2.46	50.45	28.40
c n	2.97	10.60	3.10	2.28	0.55	25.62	25.09	50.75

Table 6.2.1 Measured values of the test machine

In the above table all the voltages are in volts, currents in amperes, and powers in watts. By processing these measured quantities, self and mutual inductances of both 6 and 2 pole systems and 6-pole to 2-pole mutuals can be found as shown here:

$$[\ L_{phase}\ ] = \begin{bmatrix} 32.259 & 8.216 & 16.875 & 9.439 & 12.615 & 2.859 \\ 8.154 & 31.479 & 16.625 & 11.862 & 8.898 & 2.103 \\ 16.133 & 15.899 & 30.566 & 12.835 & 13.055 & .495 \\ 9.375 & 11.662 & 13.276 & 39.710 & 10.315 & 23.500 \\ 12.486 & 8.872 & 13.544 & 10.142 & 38.829 & 23.116 \\ 2.637 & 1.939 & .468 & 21.790 & 21.339 & 43.162 \end{bmatrix}$$

By comparing the computed [L_{phase}], presented in section 5.2 and measured primary inductances,[L_{phase}], the validity of the design and parameters measurement can be observed. It is worthwhile to notice that in the actual machine due to the manufacturing tolerances, the windings of all the phases of both 6 and 2-pole systems can not be precisely identical. Therefore, unbalance in the machine can not be avoided. It is also understood that during the parameter measurements task, not all the circumstances can be identical. For instance, sudden increases in excitation current, voltage, and power readings occurred which introduce to some practical, experimental errors. To slightly overcome and improve these error factors, the parameters measurement procedure was

repeated several times. The above measured primary inductances are the result of the fastest measurement with possibly the most stabilized voltage sources.

The other lack of informations that measured parameters don't provide are indication of positive and negative inductances. By looking at L_{66}, L_{62}, and L_{22} phase sub matrices of computed [L_{phase}], it is found that the mutual inductances between phases "A", "B", and "C" of the 6-pole and "a", "b", and "c" of the 2-pole are negative. This fundamental appears in the calculated parameters due to the direction of the flux linkages over the whole segment of the airgap which was indicated in the equations used for computation. This feature may not be recognized by ordinary equipment when dealing with alternating currents. Therefore, in the measured inductances this lack of information is seen.

Due to the technical and theoretical limitations, other parameters of the machine e.g. R and L of the secondary loops and nests and mutual inductance between the primary coils and secondary loops could not be identified based on measurement. However, calculated values of all those parameters are presented in the previous chapters.

7. STATIC THRUST TEST AND RESULTS

The initial effort was devoted to analysis, design, construction, and parameter evaluation of the machine. When the configurations and dimensions are finalized, a test capability is needed to evaluate the performance of the prototype to prove the concept of the investigation.

Various tests are possible to obtain directly the characteristics of the LBDFM. Similar to its rotary counterpart, no-load and on-load tests for the Linear BDFM can be applicable. However, especially load tests on linear machines are considerably different. Generally, experiments on linear machines belong to three basic categories as; belt test, wheel test, and track test. It is however, relatively difficult task to implement and perform tests in motion for linear machines. Therefore, as an alternative, this machine can be tested by simulation of dynamic test.

7.1 Standstill Test

Due to our limited facilities and resources in the research lab, a track test which is the most appropriate experiment for ground

transportation application can not be conducted. A track test relates the motion of the primary with respect to the secondary. This test is also very expensive due to the construction of a long track or secondary, transmission lines and collectors, etc. Hence, as an adequate alternative, a standstill test can be conducted. Figure 7.1.1 portrays the test arrangement for this purpose.

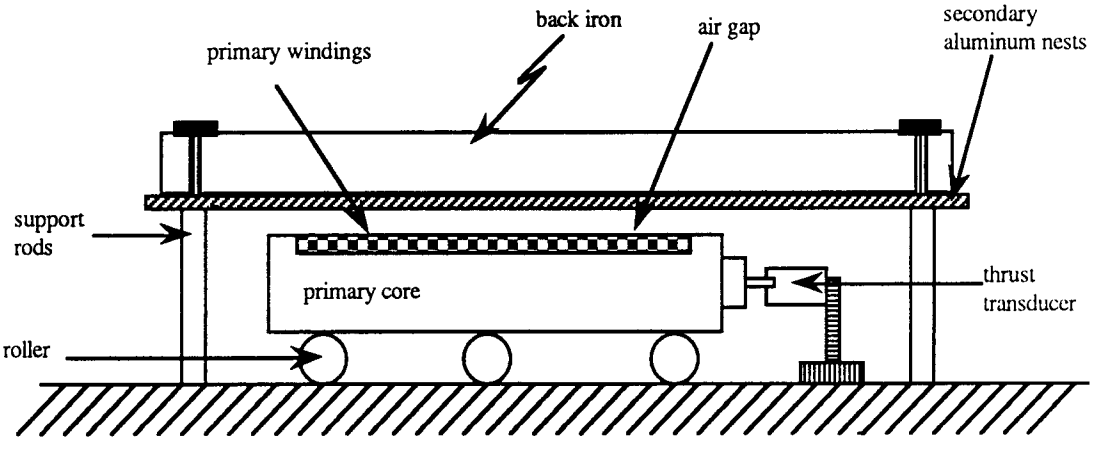

Fig. 7.1.1 Test arrangement

As the figure indicates, there is a thrust transducer holding the primary of the machine for thrust measurements. It is also possible to identify the levitation or normal force characteristics of the machine by using three more transducers placed in the bottom of the primary rollers to measure the levitation force. The secondary of

the test machine, with nested aluminum loops, is installed on the back iron and is held by two support rods on each side. This faces the primary core as shown in Figure 7.1.1. Figure 7.1.2 shows a photograph of the test arrangement which was conducted in the research lab.

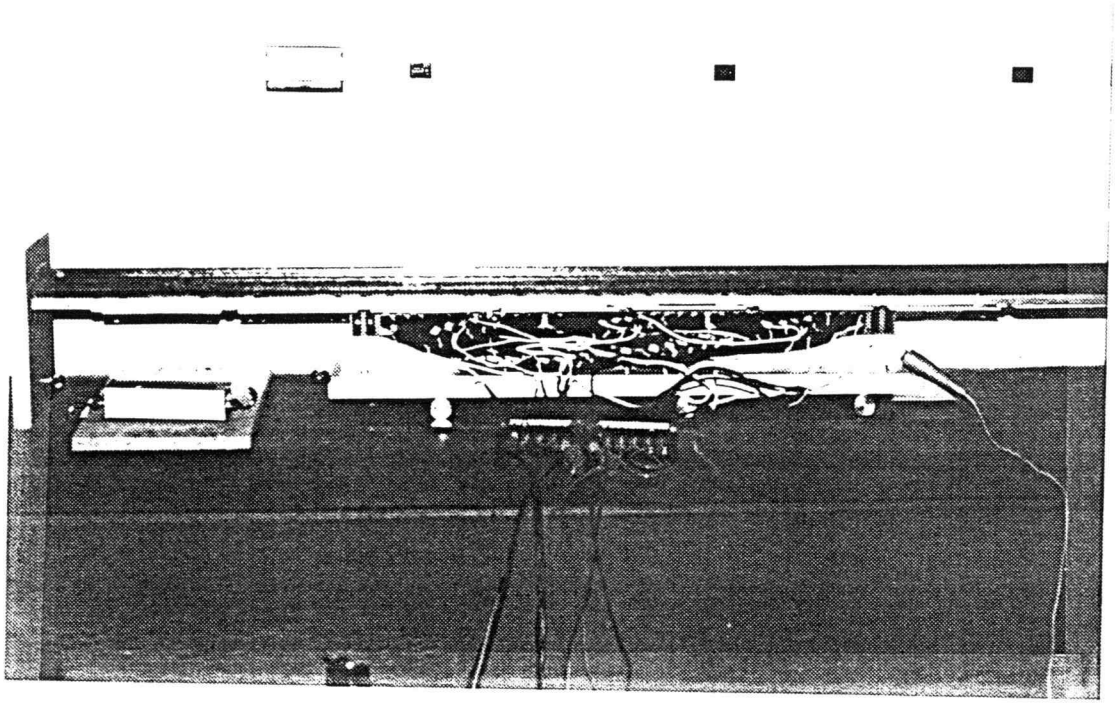

Fig. 7.1.2 Photograph of the test arrangement.

7.2 Testing Procedure and Results

With an excitation or input of adjustable frequency and voltage, some characteristics of the LBDFM can be obtained.

7.2.1 Singly-Fed Mode of Operation

It has been the intention of this investigation to test the prototype under two basic mode of operations i.e. singly-fed and doubly-fed. In the singly-fed mode, each 3-phase system is tested separately to first assure the validity of the design, and second to have better information about the behavior of the machine in doubly-fed excitation mode. To do this task, by using a variable 3-phase voltage source, each of the 6-pole and 2-pole systems is excited separately by increasing the voltage from zero to the rated values and measure the thrust production at any applied voltage. Figure 7.2.1 shows the voltage-thrust characteristic of the 6-pole for two different senarios. As it is seen in this figure, the amount of thrust increases as the 2-pole terminals are short-circuited. Similar characteristics for the 2-pole system are shown in Figure 7.2.2 for open and short circuited 6-pole terminals. The next performance evaluation is Thrust-Frequency characteristic as shown in Fig. 7.2.3

for the 6-pole system. This characteristic shows a square-law increase in thrust while the frequency increases. Figure 7.2.4 shows T-F curve for the 2-pole system as 6-pole terminals are open and short circuited. Power factor versus input current can be obtained from:

$$\cos\varphi = \frac{P_{in}}{\sqrt{3}\, V_{in}\, I_{in}} = \frac{W_1 \pm W_2}{\sqrt{3}\, V_{in}\, I_{in}}$$

where V_{in}, I_{in}, and P_{in} are input voltage, current, and power respectively. W_1 and W_2 are measured power of 2-wattmeter readings. Figures 7.2.5 and 7.2.6 show such characteristics for 6-pole and 2-pole systems respectively.

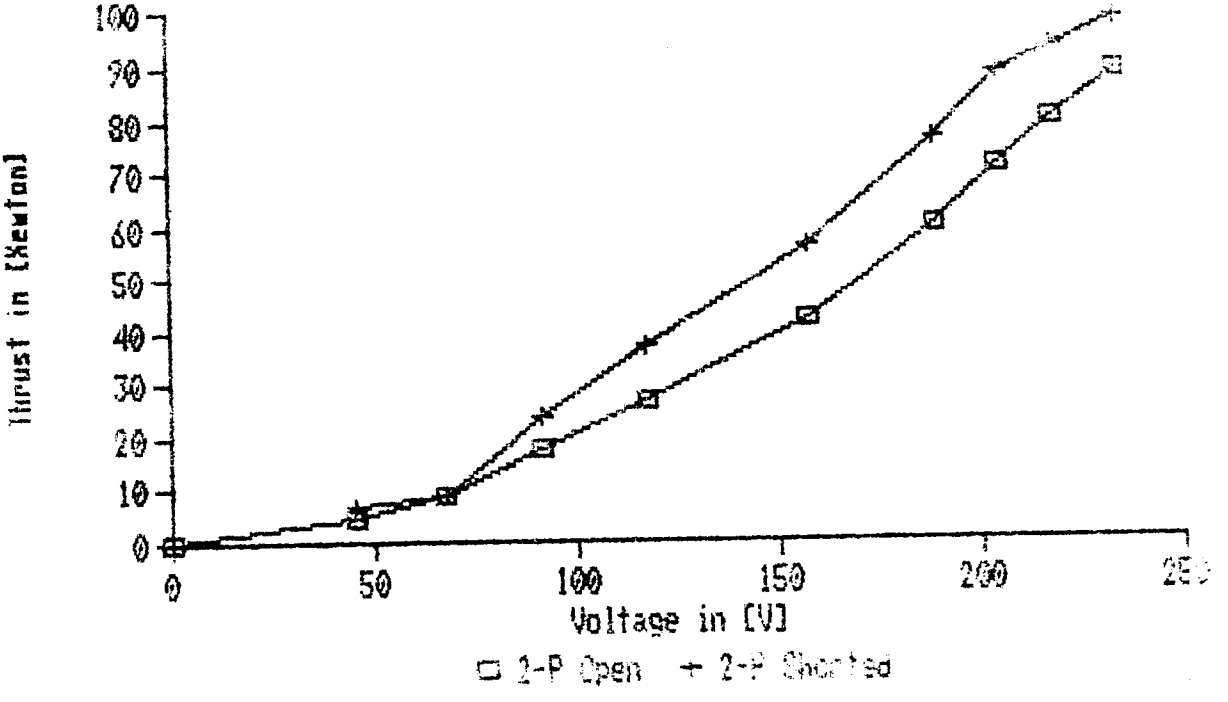

Fig. 7.2.1 Thrust versus voltage of the 6-pole at 60 Hz.

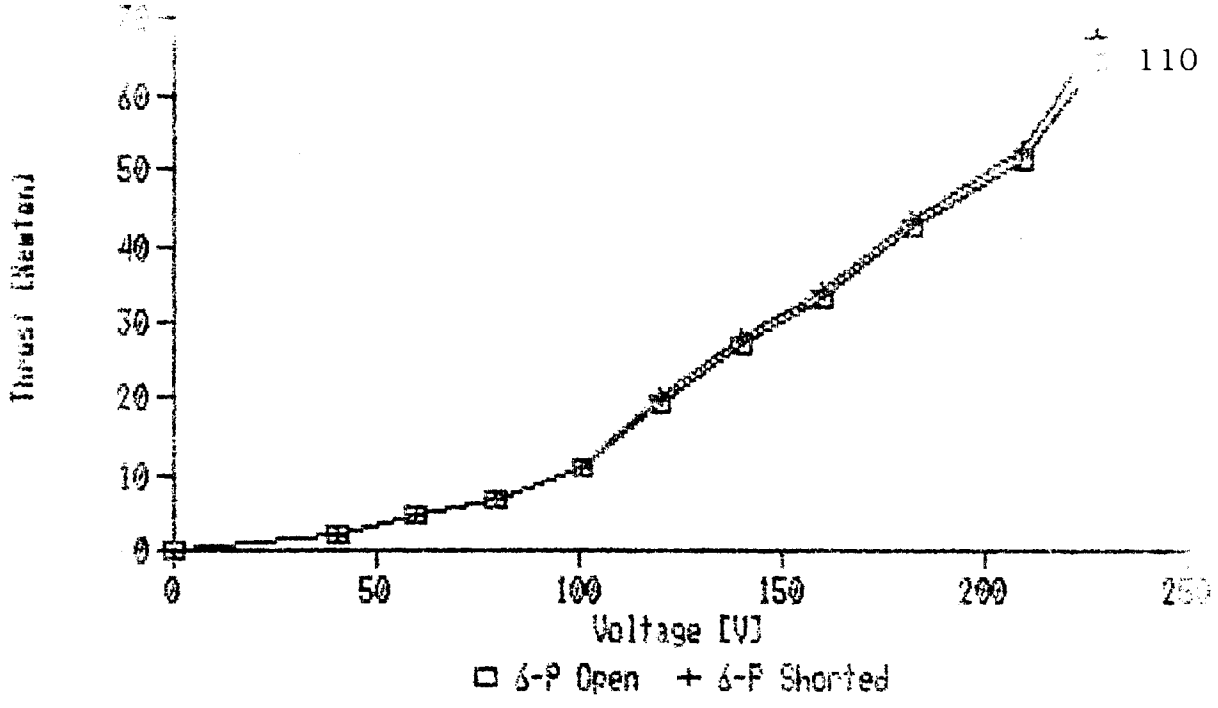

Fig. 7.2.2 Thrust versus voltage of the 2-pole at 60 Hz.

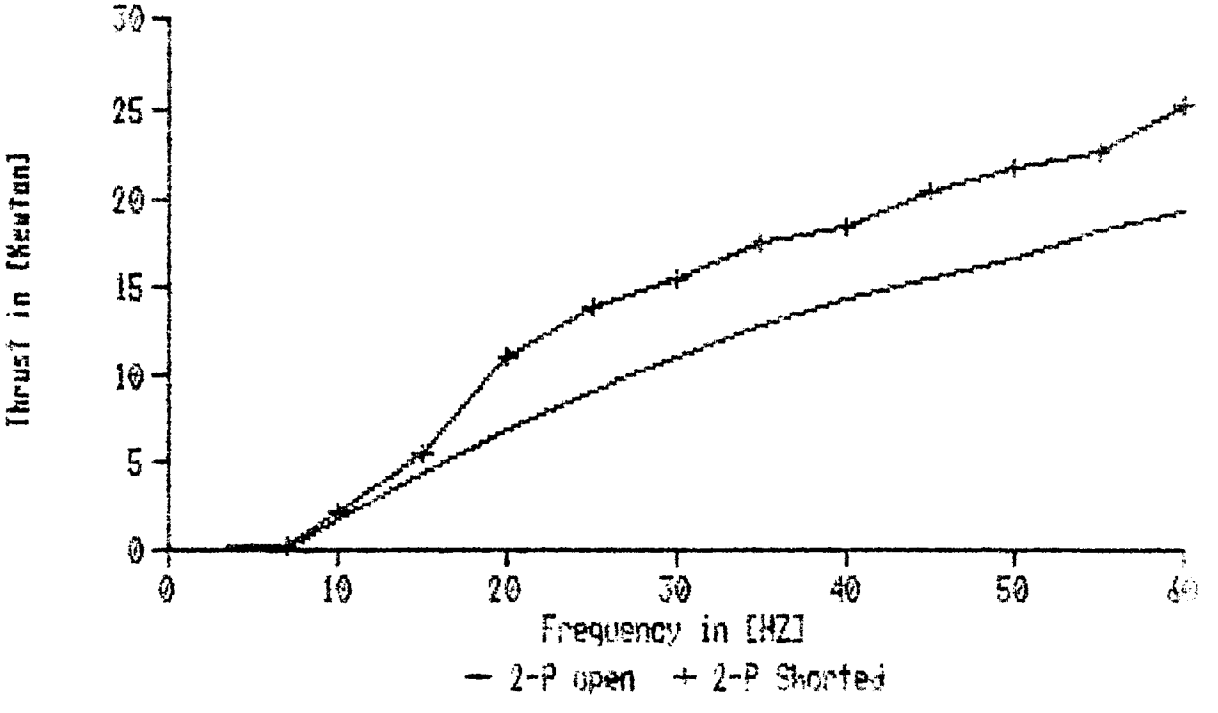

Fig. 7.2.3 Thrust versus frequency of the 6-pole at constant V/Hz.

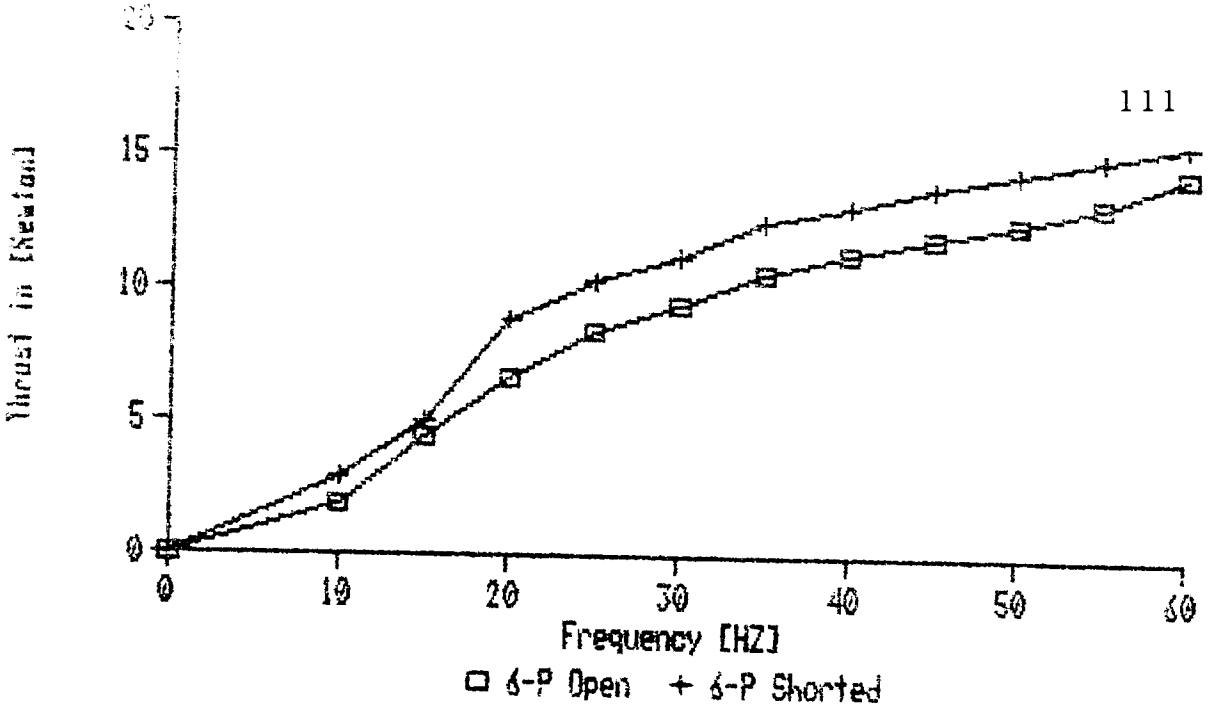

Fig 7.2.4 Thrust versus frequency of the 2-pole at constant V/Hz.

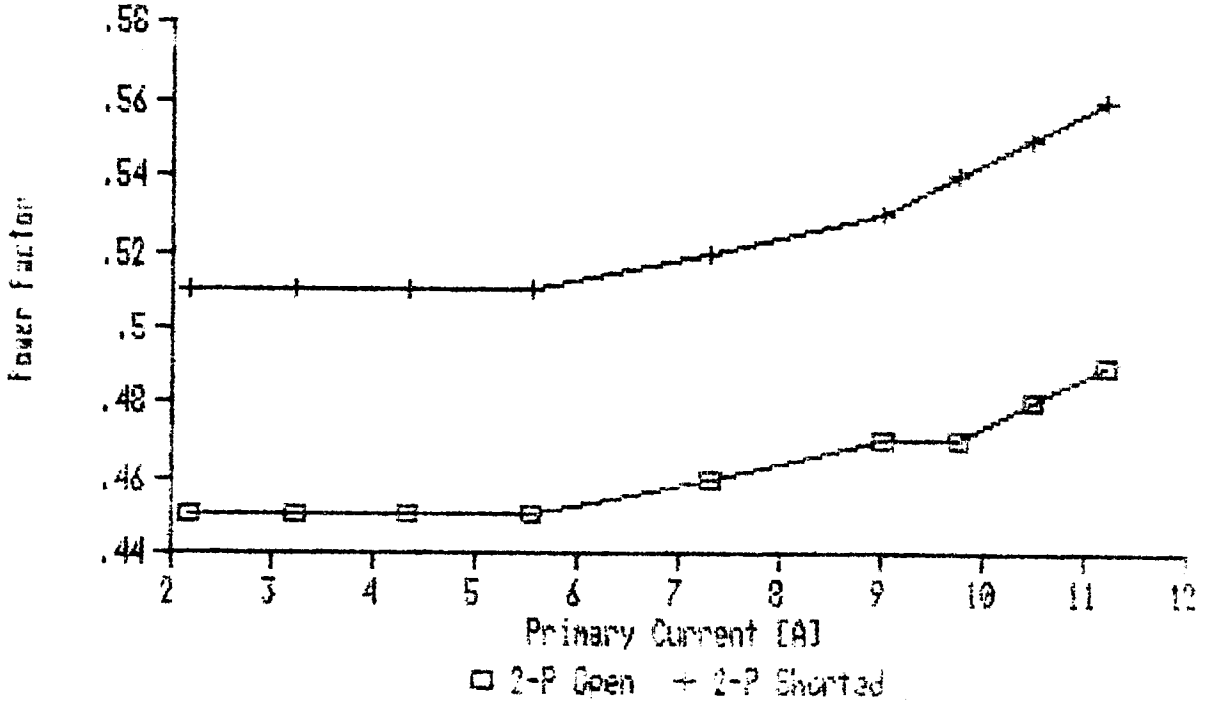

Fig 7.2.5 Power factor versus primary current of the 6-pole.

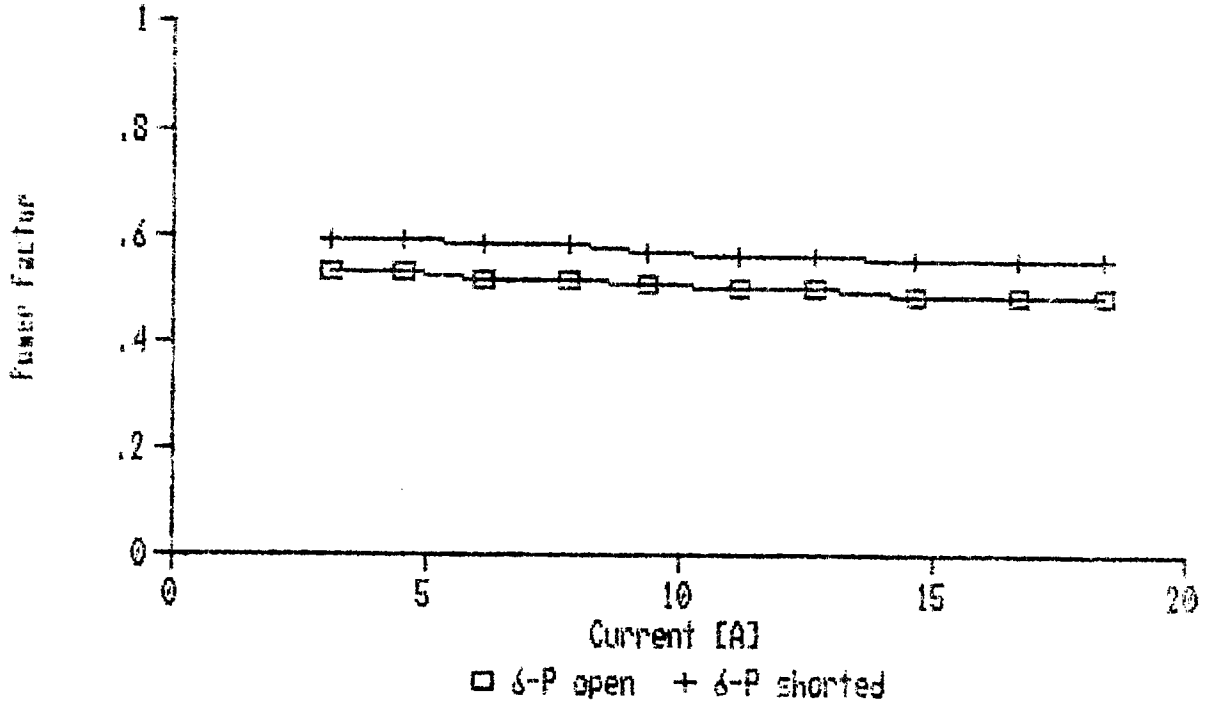

Fig 7.2.6 Power factor vs input current of the 2-pole.

Finally input current versus applied voltage shown in Figures 7.2.7 and 7.2.8 for both 6-pole and 2-pole sets, displays a linear relationship between voltage and current in the singly-fed mode of operation.

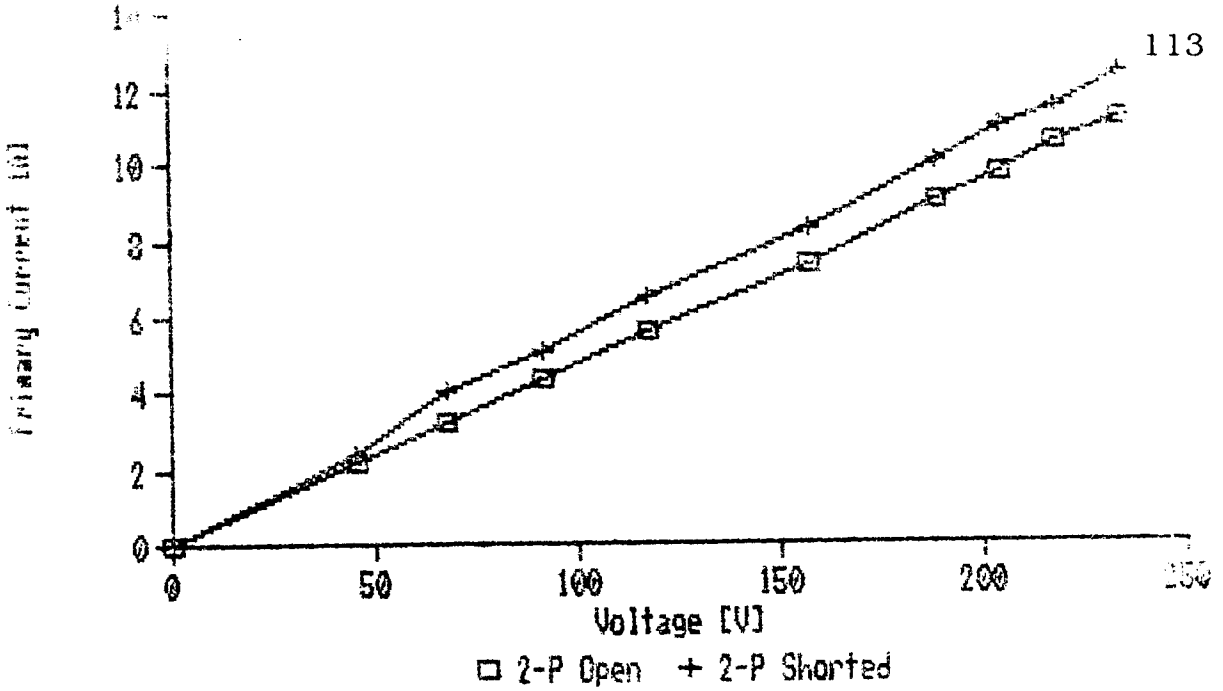

Fig. 7.2.7 Primary current vs voltage of the 6-pole.

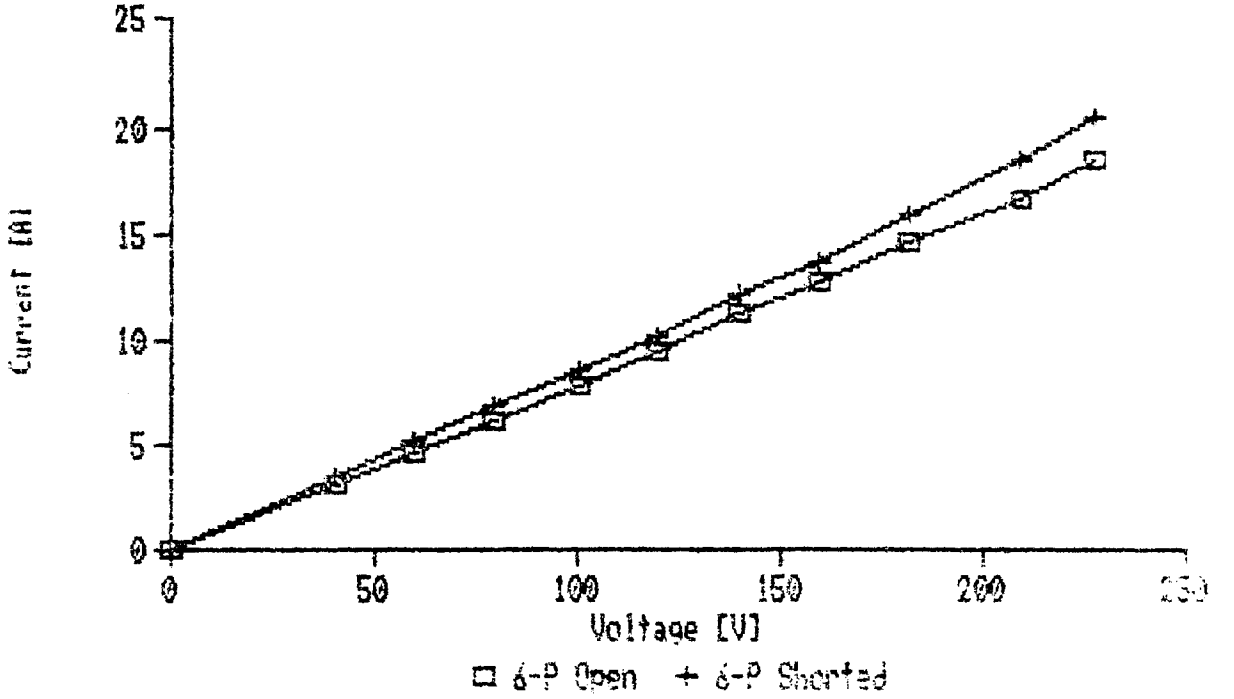

Fig. 7.2.8 Primary current vs voltage of the 2-pole.

7.2.2 Doubly-Fed Mode of Operation

To obtain the characteristics of the doubly-fed mode of operation, both 3-phase systems of the machine must be fed accordingly. The 6-pole set is fed by a 3-phase transformer with variable voltage capability, and 2-pole set is fed by a converter unit capable of providing adjustable frequency/voltage. By applying fixed voltage on the 6-pole side with frequency of 60 Hz, and varying the frequency of the 2-pole side, the doubly-fed thrust-frequency characteristic is obtained as shown in Figure 7.2.9. As it can be observed from this characteristic by projecting this curve down to 60 Hz on the 2-pole side, it should give zero thrust if synchronism is obtained. To obtain this characteristic, first 6-pole system of the machine was excited via a 115V supply from the grid while the 2-pole system was not energized. By increasing the 2-pole frequency and voltage, the overall thrust started to decrease. As the frequency of the 2-pole reached close to 20 Hz, secondary of the machine had some vibration. However, around 22 Hz the machine was stabilized all the way up to 55 Hz. After this frequency the primary had oscillating motion, going backward and forward. At frequencies above 55 Hz due to the instability no measurement of thrust, currents, voltages, power factor, etc could be made. The point by point

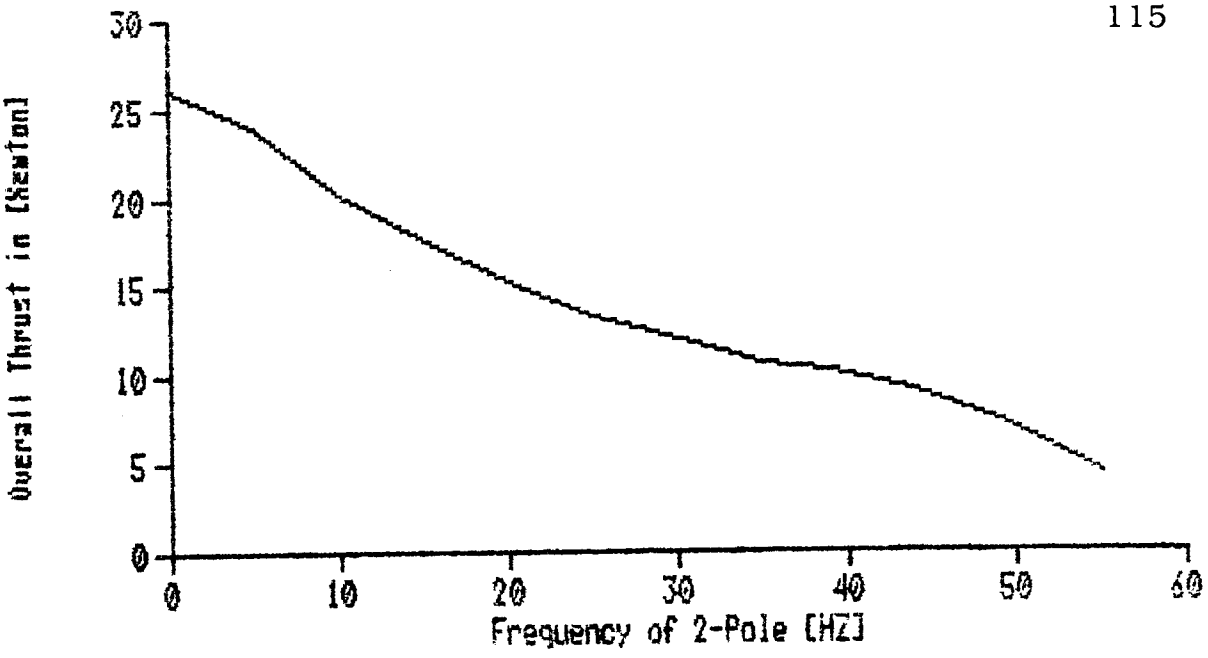

Fig. 7.2.9 The doubly-fed thrust-frequency characteristic.

measurement of the thrust and frequency indicate decrease in thrust while the 2-pole frequency and voltage were increasing. The 6-pole current, voltage, and power were virtually constant during this period. Snapshots of currents and voltages of the 6-pole shown in

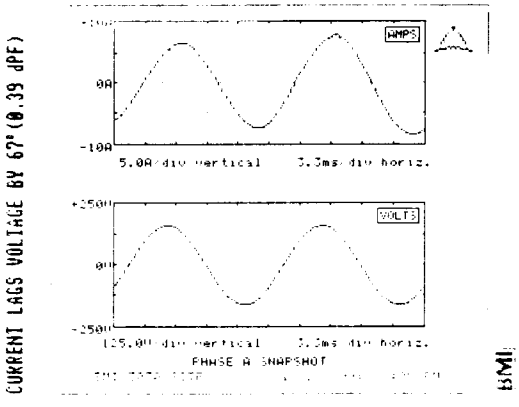

Fig. 7.2.10 Snapshot of current and voltage

Figure 7.2.10 indicates small harmonic distortion in current and voltage. The 2-pole voltage and current however, had much higher harmonic distortion due to their source, the PWM converter.

8. POSSIBLE APPLICATIONS OF THE LBDFM

Prior to the invention of linear motors, rotary motors with rotary to linear converter mechanisms were utilized. A very significant advantage of linear motors is the elimination of gears and other required mechanisms. Therefore, in that aspect linear motors are more reliable.

Potentially, LBDFM may be applicable in most applications that linear induction motors are capable of, such as: conveyor systems, accelerators and launchers, low & medium speed trains, etc. LBDFM is in the very early stage of development. However, one of the most promising applications of the LBDFM is for propulsion systems.

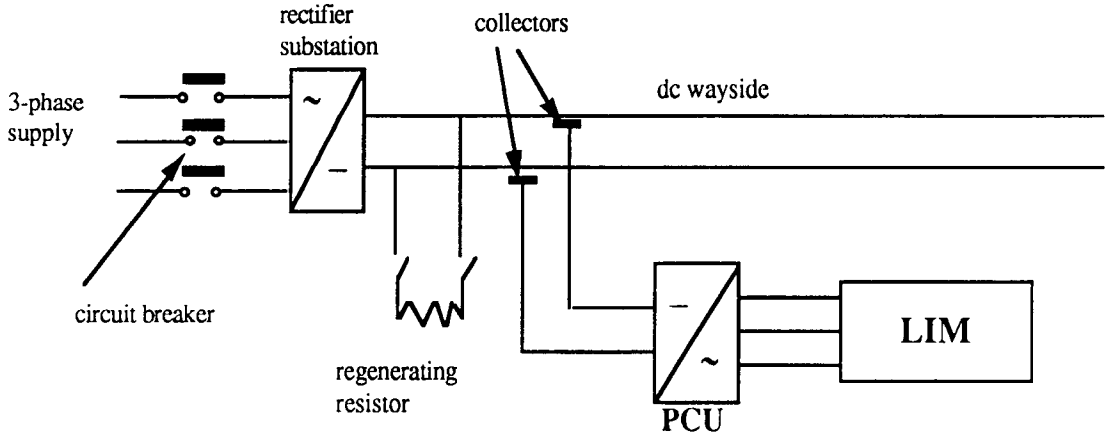

Fig. 8.1.1 An ordinary LIM system for transit applications.

Figure 8.1.1 displays an ordinary linear induction motor for transit system applications. As it is seen in the figure, the three-phase rectifier system is needed to convert ac power to dc for supplying the dc transmission system. PCU system is a power electronic converter unit which converts the dc power to ac with adjustable frequency and current, to supply the ordinary LIM for variable speed capability. In comparison, Figure 8.1.2 proposes an

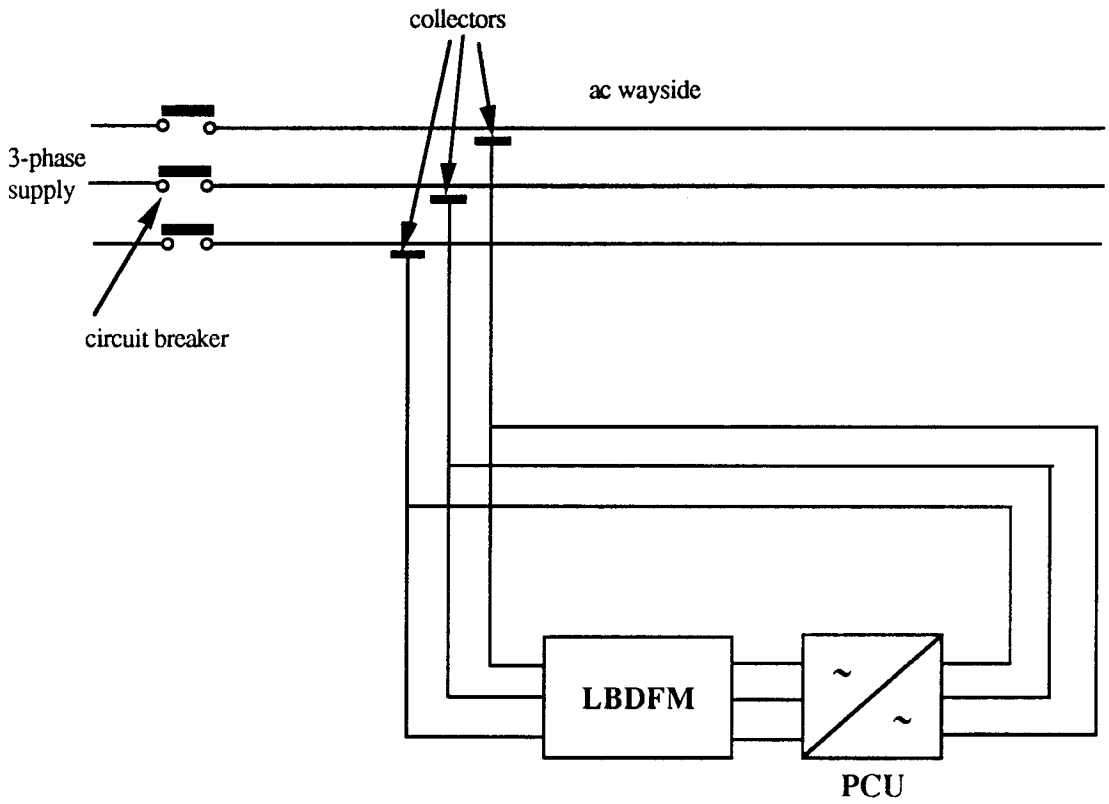

Fig. 8.1.2 Proposed LBDFM system for transit applications.

proposes an LBDFM system for the same purpose. In this model, rectifier substation system is eliminated and three-phase ac supply which can be installed on the opposite side of the passenger access along the track, directly feeds the primary of the machine through collectors. In the proposed system however, dc wayside with two lines would have to be converted to a three line system with three collectors which will result in higher cost for construction of the transmission line. However, a significant advantage of the proposed system over the conventional model is the substantial reduction of the PCU power rating, therefore, smaller in size and cheaper in cost. The proposed model is also capable of operating under possible PCU failures by simply operating in the singly-fed mode. This reliability can not be achieved in LIM systems. Moreover, in the conventional model if the train is operating and running at the speed greater than its synchronous speed, regenerated power must be dissipated through resistor banks to maintain the appropriate level of voltage on the line. In the LBDFM system however, this produced power can be utilized by injecting it to the grid through the ac to ac inverter. Due to those specific constructional properties of the LBDFM system, the primary with two three-phase system may be larger. Furthermore, secondary system which in this application is the reaction rail, would require more developments compared with the secondary system of the LIM's.

9. CONCLUSIONS AND FUTURE WORK

9.1 Conclusions

The objective of the work in this thesis was to design and construct a proof of concept LBDFM, which would be used to investigate the possibility of operation of this type of machine in a variable-speed transportation systems. The effort towards this task has been carried out both theoretically and experimentally. This chapter summarizes the conclusions of the research, the difficulties, and gives recommendations for future work on the LBDFM technology.

A brief literature review and background about the linear machines and their constructional and topological differences in terms of field equation compared to their rotary counterparts were given. The specifications and requirements of the LBDFM for a successful design and construction were also discussed. There are several major differences between linear and rotary machines which make the design criteria and analysis of the linear machines more complicated than rotary machines. Openness of the magnetic path in linear machines has a significant influence on analysis and

mathematical model of the machine. Larger air gap in linear machines makes them to operate in lower efficiency compared to rotary machines. In linear machines we are no longer dealing with a balanced system as we can make that assumption, which make the analysis much easier, for the rotary machines.

Design, development, and the specifications of the windings layout for both 3-phase sets of the primary were achieved. Due to the openness of the primary core, the design of the windings to provide the desired number of poles had to be investigated. The proposed design for the prototype machine was implemented to obtain a proof of concept LBDFM. The requirements for the secondary design and construction were also addressed. Due to more complexity in the primary design, it is not appropriate to utilize a ladder type of secondary, as it is used in LIM systems, for the LBDFM. In order to interact with the combined field produced in the air gap by the primary windings, a secondary with special design is needed. Plots of the phase mmf's of each of the 3-phase systems and overall mmf of each 3-phase system are presented in chapter 3. The overall mmf in the the air gap which is a point by point summation of both the 2-pole and the 6-pole mmf's, shows a non-sinosoidal nature which could increase harmonic distortion compared to LIM systems.

Preliminary estimates for the primary core and designed windings to establish the most optimized and adequate number of turns for each coil group of both systems, suitable size of windings, and estimation of copper losses under normal loading, which are presented in chapter 4, were achieved. The design and estimation procedure had to be modified to derive more appropriate criteria for our linear machine.

At this stage of the LBDFM development, all the parameters of the machine must have been identified. Chapter 5 describes the derivation of all the necessary equations for parameter calculations as well as the results of all calculations for both primary and secondary systems. The initial purpose of detailed calculation for the LBDFM was to develop an equivalent circuit for this device. In this chapter step by step procedure to achieve this task is described. After processing all the required initial work, the conclusion was drawn that deriving an equivalent circuit for the LBDFM is a complicated task due to the unbalance which exists in the 3-phase model of the machine and may not be achieved by the approach that has been utilized for the equivalent circuit development of the rotary BDFM. It is likely that a simple equivalent circuit cannot be derived with mathematical rigor. However, approximate forms may be appropriate

or, alternatively, multiple time variant coil models may be necessary.

The obtained theoretical calculations of the mathematical model must correlate with the actual parameters that physical model contains. Therefore, in chapter 6 an appropriate measurement technique is developed to identify the parameters of the actual device. The limitation on this task was the fact that merely the parameters of the primary systems can be obtained by measurement techniques. It is shown that both measured and calculated quantities were matched and consistent which confirmed the work devoted to the calculation of the parameters of the machine.

Static tests were accomplished in the research laboratory to obtain and study the initial characteristics of the machine. In chapter 7 a test strategy arrangement is suggested and based on that, some of the performance characteristics of the device both in singly-fed and doubly-fed modes of operations were obtained and discussed. Due to our limited facilities and resources in the lab, some of the important characteristics of the device such as: thrust-speed curve in the induction and synchronous mode of operations couldn't be performed.

Finally in chapter 8 the most promising application that LBDFM is believed to be capable of, is briefly described and advantages of using LBDFM in propulsion system applications over the ordinary LIM systems are addressed.

9.2 Future Work

The subject matter of this thesis was to verify the potential and function of the LBDFM and its performance as an alternative for variable speed trains and come up with an equivalent circuit for the steady state condition for the device. More analysis and investigations are needed to be applied, to first be convinced that derivation of an equivalent circuit for this device can be achieved. One possible approach to investigate this task is to apply symmetrical components theory. Since the impedance matrix of the 3-phase systems of both sets of the primary are unbalanced, it may be possible to derive three symmetrical components for an unbalanced system. Then, by applying 3-phase to two-axis transformation technique to each one of the obtained balanced systems, d-q-o model for each component could be obtained and possibly equivalent circuit for each of the positive, negative and zero sequence of the unbalanced system may result.

The other possible approach to attack unbalance problem and derive an equivalent circuit for this device could be based on compensation windings. Since we are dealing with unbalanced 3-phase systems in the primary of the LBDFM, it is possible to change the design of the windings by adding or subtracting number of turns to particular coils to artificially make a balance system out of an unbalance 3-phase system. As it was discussed in chapter 5, the mutual inductance between phases "A" and "B" of the 6-pole and "a" and "b" of the 2-pole are not identical to mutual inductance of phases "A"-"C" and "B"-"C" of the 6-pole and "a"-"c" and "b"-"c" of the 2-pole. Therefore, by having this significant information a particular design could be implemented to get rid of the unbalanced system, and apply the transformation technique to this new balanced 3-phase system to derive d-q-o model and finally single-phase equivalent circuit.

The other significant step in developing LBDFM is to investigate other possibilities to simulate the dynamic test to possibly be able to study the synchronous mode of operation under different loading conditions. Moreover, it is obvious that further experimental work in needed to study the effect of the harmonics of the converter on the performance of the system.

REFERENCES

[1] I. Boldea and S. A. Nasar, Linear Motion Electromagnetic Systems, John Wiley, New York, 1985, pp. 79-95.

[2] S. Yamamura and H. Ito, "Three-Dimensional Analysis of Linear Induction Motors," 1976 IEEE-IAS Annual Meeting Conference Record, pp. 1180-1187.

[3] J. Dukowitz, " Analysis of Linear Induction Machines with Discrete Windings and Finite Iron Length," 1973 IEEE-IAS Annual Meeting Conference Record, pp. 311-319.

[4] Syed A. Nasar, and I. Boldea, Linear Electric Motors, Prentice-Hall, New Jersey, 1987, pp. 56-71.

[5] H.K. Lauw, " Characteristics and Analysis of the Brushless Doubly-Fed Machine, " report for Bonneville Power Administration, Contract # 79-85BP24332-Mod4, June 1989.

[6] A. R. W. Broadway and L. Burbridge, "High-Frequency Brushless Alternator," Proceedings IEE, 1970, Vol. 117, pp. 1277-1290.

[7] F. Creedy, " Development in Multi-Speed Cascade Induction Motors," Journal IEE, Vol. 59, 1927, pp. 511-532.

[8] A. K. Wallace, R. Spee, H. K. Lauw, " The Potential of Brushless Doubly-Fed Machines for Adjustable Speed Drives," 1990 IEEE-IAS Pulp & Paper Annual Conference Record, pp. 45-50.

[9] A. K. Wallace, P. Rochelle, and R. Spee, " Rotor Modeling And Development for Brushless Doubly-Fed Machines," 1990 International Conference on Electric Machines, Cambridge, MA, Vol. 1, pp. 54-59.

[10] P. Rochelle, R. Spee, and A. K. Wallace, " The Effects of Stator Winding Configuration on the Performance of Brushless Doubly-Fed Machines in Adjustable Speed Drives," 1990 IEEE-IAS Annual Meeting, Seattle, WA.

[11] A.K. Wallace, "The Function of The Reaction Rail in Development of a LIM Propulsion System f or Urban Transit," 1984 IEEE Transaction on Industrial Applications, Vol. IA-20, pp. 942-947.

[12] R. Li, A. K. Wallace, R. Spee, and Y. Wang, " Two-Axis Model Development of Cage-Rotor Brushless Doubly-Fed Machines," IEEE-PES Winter Meeting, New York, 1991.

[13] R. Li, A. K. Wallace, and R. Spee, "Dynamic Simulation of Cage Rotor Brushless Boubly-Fed Machines," IEEE-PES Winter Meeting, New York, 1991.

[14] A. K. Wallace, R. Spee, and H. K. Lauw, "Dynamic Modeling of Brushless Doubly-Fed Machines," 1989 IEEE-IAS Annual Meeting, pp. 329-334.

[15] R. Spee, A. K. Wallace, and H. K. Lauw, "Performance Simulation of Brushless Doubly-Fed adjustable Speed Drives,"1989 IEEE-IAS Annual Meeting, pp. 738-743.

[16] Alexander Kusko, and Clement B. Somuah, "Speed Control of a single-Frame Cascade Induction Motor with Slip-Power Pump Back," IEEE Transactions on Industrial Applications, Vol. IA-14, No. 2, March/April 1978.

[17] Masoud Soltani, Design and Estimation of Induction Motors, Atrak Inc., Mashhad, Khorasan, 1988.

[18] M. G. Say, The Performance and Design of Alternating Current Machines, Sir Isaac Pitman & Sons, LTD., London, 1961, pp. 179-195.

[19] Khosro Georjani, Electrical Machines Design, Class Note, University of Science & Technology, Narmak, Tehran, 1986.

[20] Paul C. Krause, Analysis of Electric Machinery, McGraw-Hill Book Company, New York, 1986, pp. 133-178.

[21] A. K. Wallace, Electromechanical Energy Conversion Devices, Class Note, Oregon State University, Corvallis, Oregon, 1990.